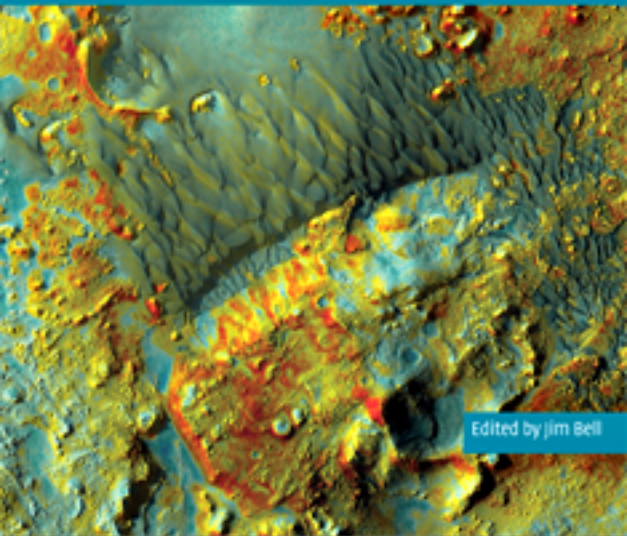


CAMBRIDGE PLANETARY SCIENCE

The Martian Surface

Composition, Mineralogy, and Physical Properties



Edited by Jim Bell

CAMBRIDGE

www.cambridge.org/9780521866989

This page intentionally left blank

The Martian Surface

Composition, Mineralogy, and Physical Properties

Phenomenal new observations from Earth-based telescopes and Mars-based orbiters, landers, and rovers have dramatically advanced our understanding of the past environments on Mars. These include the first global-scale infrared and reflectance spectroscopic maps of the surface, leading to the discovery of key minerals indicative of specific past climate conditions; the discovery of large reservoirs of subsurface water ice; and the detailed *in situ* roving investigations of three new landing sites, which give us firm evidence for the presence of liquid water on the surface or in the shallow subsurface in the distant past.

This important, comprehensive book provides an overview of the latest Mars compositional and mineralogic discoveries since the last major review of this topic was published in 1992. It is an essential resource for researchers and students in planetary science, astronomy, space exploration, planetary geology, and planetary geochemistry. Specialized terms are defined throughout, so the material will be easily understood by researchers entering this field. Color figures can be found at www.cambridge.org/9780521866989.

JIM BELL is Associate Professor in the Department of Astronomy at Cornell University. He is the Lead Scientist for the Pancam color imaging system on the NASA Mars Exploration Rovers *Spirit* and *Opportunity*, and is also a member of the science teams of the NASA Mars Pathfinder, Near Earth Asteroid Rendezvous (NEAR), Mars 2001 Odyssey Orbiter, Mars 2005 Reconnaissance Orbiter, and 2009 Mars Science Laboratory rover mission teams. He has authored or co-authored more than 150 peer-reviewed scientific papers on Mars, is an editor for *Icarus*, and has an asteroid named after him (8146 Jimbell) by the International Astronomical Union.

Cambridge Planetary Science

Series Editors:

Fran Bagenal, David Jewitt, Carl Murray, Jim Bell, Ralph Lorenz,
Francis Nimmo, Sara Russell

Books in the series:

- 1 Jupiter: The Planet, Satellites and Magnetosphere*
Edited by Bagenal, Dowling and McKinnon
9780521035453
- 2 Meteorites: A Petrologic, Chemical and Isotopic Synthesis*
Hutchison
9780521035392
- 3 The Origin of Chondrules and Chondrites
Sears
9780521836036
- 4 Planetary Rings
Esposito
9780521362221
- 5 The Geology of Mars
Edited by Chapman
9780521832922
- 6 The Surface of Mars
Carr
9780521872010
- 7 Volcanism on Io: A Comparison with Earth
Davies
9780521850032
- 8 Mars: An Introduction to its Interior, Surface and Atmosphere
Barlow
9780521852265
- 9 The Martian Surface: Composition, Mineralogy, and Physical Properties
Edited by Bell
9780521866989

*Issued as a paperback

THE MARTIAN SURFACE

Composition, Mineralogy, and Physical Properties

Edited by

JIM BELL



CAMBRIDGE UNIVERSITY PRESS

Cambridge, New York, Melbourne, Madrid, Cape Town, Singapore, São Paulo

Cambridge University Press

The Edinburgh Building, Cambridge CB2 8RU, UK

Published in the United States of America by Cambridge University Press, New York

www.cambridge.org

Information on this title: www.cambridge.org/9780521866989

© Cambridge University Press 2008

This publication is in copyright. Subject to statutory exception and to the provision of relevant collective licensing agreements, no reproduction of any part may take place without the written permission of Cambridge University Press.

First published in print format 2008

ISBN-13 978-0-511-41047-5 eBook (Adobe Reader)

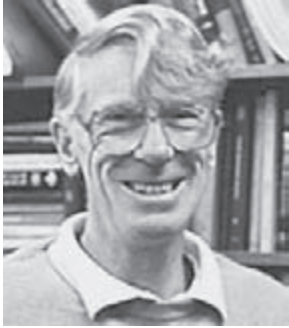
ISBN-13 978-0-521-86698-9 hardback

Cambridge University Press has no responsibility for the persistence or accuracy of urls for external or third-party internet websites referred to in this publication, and does not guarantee that any content on such websites is, or will remain, accurate or appropriate.

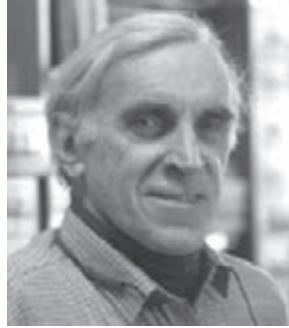
DEDICATION

There is a relatively small community of “Martians” living here on Earth who study the Red Planet from afar, using images and other data acquired from telescopes or sent back by robotic orbiters, landers, and rovers. Because we are a small community, the loss of a colleague is keenly and sadly felt in our field. This book is dedicated to those colleagues whom we have lost during the past 15 years or so, since the last major review book on this topic was published. Among the most prominent, prolific, and respected of these departed friends are the gentlemen pictured here in the following page: Roger G. Burns, Robert B. (“Rob”) Hargraves, Larry A. Haskin, Norman H. Horowitz, Harold P. (“Chuck”) Klein, Jens Martin Knudsen, Leonard J. Martin, Harold (“Hal”) Masursky, Henry J. (“Hank”) Moore, Vassily I. Moroz, James B. Pollack, David J. Roddy, Carl Sagan, David H. Scott, Eugene M. (“Gene”) Shoemaker, and Gerald A. Soffen.

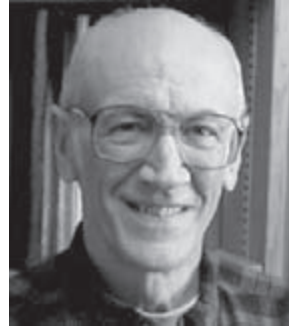
These colleagues played critical roles in the fundamental scientific, engineering, educational, and managerial work that led directly to today’s spectacularly successful era of Mars exploration. The results, interpretations, and speculations about Mars described here in this book are a tribute to their pioneering work, and we honor their memories and accomplishments by continuing to try to unlock the mysteries of the Red Planet.



Roger G. Burns



Robert B. Hargraves



Larry A. Haskin



Norman H. Horowitz



Harold P. Klein



Jens Martin Knudsen



Leonard J. Martin



Harold Masursky



Henry J. Moore



Vassily I. Moroz



James B. Pollack



David J. Roddy



Carl Sagan



David H. Scott



Eugene M. Shoemaker



Gerald A. Soffen

CONTENTS

<i>List of contributors</i>	page x
<i>Foreword</i>	xv
JAMES B. GARVIN	
<i>Acknowledgments</i>	xvii
Part I Introduction and historical perspective	1
1 Exploration of the Martian surface: 1992–2007	3
L. A. SODERBLOM AND J. F. BELL III	
2 Historical context: the pre-MGS view of Mars’ surface composition	20
W. M. CALVIN AND J. F. BELL III	
Part II Elemental Composition: Orbital and <i>in situ</i> Surface Measurements	31
<i>Part II. A Results and Interpretations from New <i>in situ</i> APXS Measurements</i>	33
3 Martian surface chemistry: APXS results from the Pathfinder landing site	35
C. N. FOLEY, T. E. ECONOMOU, R. N. CLAYTON, J. BRÜCKNER, G. DREIBUS, R. RIEDER, AND H. WÄNKE	
4 Mars Exploration Rovers: chemical composition by the APXS	58
J. BRÜCKNER, G. DREIBUS, R. GELLERT, S. W. SQUYRES, H. WÄNKE, A. YEN, AND J. ZIPFEL	
<i>Part II. B Results and Interpretations from New Orbital Elemental Measurements</i>	103
5 Elemental abundances determined via the Mars Odyssey GRS	105
W. V. BOYNTON, G. J. TAYLOR, S. KARUNATILLAKE, R. C. REEDY, AND J. M. KELLER	
6 Volatiles on Mars: scientific results from the Mars Odyssey Neutron Spectrometer	125
W. C. FELDMAN, M. T. MELLON, O. GASNAULT, S. MAURICE, AND T. H. PRETTYMAN	

Part III Mineralogy and Remote Sensing of Rocks, Soil, Dust, and Ices	149
<i>Part III. A Visible to Near-IR Telescopic and Orbital Measurements</i>	151
7 Mineralogy of the Martian surface from Mars Express OMEGA observations J. -P. BIBRING AND Y. LANGEVIN	153
8 Visible to near-IR multispectral orbital observations of Mars J. F. BELL III, T. D. GLOTCH, V. E. HAMILTON, T. McCONNOCHIE, T. McCORD, A. McEWEN, P. R. CHRISTENSEN, AND R. E. ARVIDSON	169
<i>Part III. B Mid-IR and Magnetic Orbital Measurements</i>	193
9 Global mineralogy mapped from the Mars Global Surveyor Thermal Emission Spectrometer P. R. CHRISTENSEN, J. L. BANDFIELD, A. D. ROGERS, T. D. GLOTCH, V. E. HAMILTON, S. W. RUFF, AND M. B. WYATT	195
10 The compositional diversity and physical properties mapped from the Mars Odyssey Thermal Emission Imaging System P. R. CHRISTENSEN, J. L. BANDFIELD, R. L. FERGASON, V. E. HAMILTON, AND A. D. ROGERS	221
11 Mars' crustal magnetization: a window into the past M. H. ACUÑA, G. KLETETSCHKA, AND J. E. P. CONNERNEY	242
<i>Part III. C Observations from Surface Landers/Rovers</i>	263
12 Multispectral imaging from Mars Pathfinder W. H. FARRAND, J. F. BELL III, J. R. JOHNSON, J. L. BISHOP, AND R. V. MORRIS	265
13 Mars Exploration Rover Pancam multispectral imaging of rocks, soils, and dust at Gusev crater and Meridiani Planum J. F. BELL III, W. M. CALVIN, W. H. FARRAND, R. GREELEY, J. R. JOHNSON, B. JOLLIFF, R. V. MORRIS, R. J. SULLIVAN, S. THOMPSON, A. WANG, C. WEITZ, AND S. W. SQUYRES	281
14 The mineralogy of Gusev crater and Meridiani Planum derived from the Miniature Thermal Emission Spectrometers on the <i>Spirit</i> and <i>Opportunity</i> rovers S. W. RUFF, P. R. CHRISTENSEN, T. D. GLOTCH, D. L. BLANEY, J. E. MOERSCH, AND M. B. WYATT	315
15 Iron mineralogy and aqueous alteration on Mars from the MER Mössbauer spectrometers R. V. MORRIS AND G. KLINGELHÖFER	339
16 Magnetic properties of Martian surface materials W. GOETZ, S. F. HVIID, K. M. KINCH, AND M. B. MADSEN	366
<i>Part III. D Martian Meteorites as Crustal Samples</i>	381
17 Martian meteorites as crustal samples H. Y. McSWEEN JR.	383

	Part IV Physical Properties of Surface Materials	397
18	The thermal inertia of the surface of Mars M. T. MELLON, R. L. FERGASON, AND N. E. PUTZIG	399
19	Physical properties of the Martian surface from spectrophotometric observations J. R. JOHNSON, J. F. BELL III, P. GEISSLER, W. M. GRUNDY, E. A. GUINNESS, P. C. PINET, AND J. SODERBLOM	428
20	<i>In situ</i> observations of the physical properties of the Martian surface K. E. HERKENHOFF, M. P. GOLOMBEK, E. A. GUINNESS, J. B. JOHNSON, A. KUSACK, L. RICHTER, R. J. SULLIVAN, AND S. GOREVAN	451
21	Martian surface properties from joint analysis of orbital, Earth-based, and surface observations M. P. GOLOMBEK, A. F. C. HALDEMANN, R. A. SIMPSON, R. L. FERGASON, N. E. PUTZIG, R. E. ARVIDSON, J. F. BELL III, AND M. T. MELLON	468
	Part V Synthesis	499
22	Implications of observed primary lithologies G. J. TAYLOR, S. M. McLENNAN, H. Y. McSWEEN JR., M. B. WYATT, AND R. C. F. LENTZ	501
23	Aqueous alteration on Mars D. W. MING, R. V. MORRIS, AND B. C. CLARK	519
24	The sedimentary rock cycle of Mars S. M. McLENNAN AND J. P. GROTZINGER	541
25	Martian polar processes T. N. TITUS, W. M. CALVIN, H. H. KIEFFER, Y. LANGEVIN, AND T. H. PRETTYMAN	578
26	Astrobiological implications of Mars' surface composition and properties D. J. DES MARAIS, B. M. JAKOSKY, AND B. M. HYNEK	599
	Part VI Summary, Upcoming Missions, and New Measurement Needs	625
27	The future of Mars exploration J. F. BELL III	627
	<i>Index</i>	631

The color plates are between pages 302 and 303

LIST OF CONTRIBUTORS

MARIO H. ACUÑA
NASA Goddard Space Flight Center
Laboratory for Extraterrestrial Physics
Code 695
Greenbelt, MD 20771
USA

RAY E. ARVIDSON
Earth & Planetary Science
Washington University
St Louis, MO 63130
USA

JOSHUA L. BANDFIELD
Arizona State University
MC 6305
Mars Space Flight Facility
Tempe, AZ
USA

JAMES F. BELL III
Cornell University
Department of Astronomy
402 Space Sciences Building
Ithaca, NY 14853-6801
USA

JEAN-PIERRE BIBRING
Institut d'Astrophysique Spatiale
Universite Paris Sud
Bat. 121
Orsay Cedex, F-91405
France

JANICE L. BISHOP
SETI Institute
515 N. Whisman Road
Mountain View, CA 94034
USA

DIANA L. BLANEY
JPL
MS 183-501
4800 Oak Grove Drive
Pasadena, CA 91109
USA

WILLIAM V. BOYNTON
Lunar and Planetary Laboratory
University of Arizona
Tuscon, AZ 85721
USA

JOHANNES BRÜCKNER
Geochemistry Department
Max Planck Institut für Chemie
PO Box 3060
Mainz D-55020
Germany

WENDY M. CALVIN
Department of Geological Science
MS 172
University of Nevada
Reno, NV 89557-0138
USA

BENTON C. CLARK
Planetary Sciences Laboratory
Lockheed Martin Aerospce
MS 8001, PO Box 179
Denver, CO 80201
USA

ROBERT N. CLAYTON
Enrico Fermi Institute
5640 S. Ellis Avenue, RI 440
Chicago, IL 60637
USA

PHILIP R. CHRISTENSEN
Planetary Exploration Laboratory
Arizona State University
Moeur Building 110D
Tempe, AZ 85287
USA

JOHN E. P. CONNERNEY
NASA Goddard Space Flight Center
Code 691
Greenbelt, MD
USA

DAVID J. DES MARAIS
NASA Ames Research Center
MS 239-4
Moffett Field, CA 94035-1000
USA

GERLIND DREIBUS
Cosmochemistry Department
Max Planck Institut für Chemie
PO Box 3060
Mainz D-55020
Germany

THANASIS E. ECONOMOU
Laboratory for Astrophysics & Space Res.
University of Chicago
933 East 56th Street
Chicago, IL 60637
USA

WILLIAM H. FARRAND
Space Science Institute
4750 Walnut Street, # 205
Boulder, CO 80301
USA

WILLIAM C. FELDMAN
Los Alamos National Laboratory
MS D466
Space & Atmospheric Science
Los Alamos, NM 87545
USA

ROBIN L. FERGASON
School of Earth & Space Exploration
Arizona State University
PO Box 876305
Tempe, AZ 85287-6305
USA

C. NICOLE FOLEY
Department of Terrestrial Magnetism
Carnegie Institute of Washington
5241 Broad Branch Road, NW
Washington, DC 20015-1305
USA

OLIVIER GASNAULT
Laboratoire d'Astrophysique
14 Avenue Belin
Toulouse, 31400
France

PAUL GEISSLER
US Geological Survey
2255 N. Gemini Drive
Flagstaff, AZ 86001
USA

RALF GELLERT
Department of Physics
University of Guelph
Guelph, ON
N1G 2W1
Canada

TIMOTHY D. GLOTCH
Department of Geosciences
SUNY at Stony Brook
Stony Brook, NY 11794
USA

WALTER GOETZ
Max Planck Institute for Solar System Research
Max Planck Str. 2
Katlenburg-Lindau, 37191
Germany

MATT P. GOLOMBEK
JPL
MS 183-501
4800 Oak Grove Drive
Pasadena, CA 91109
USA

STEVEN GOREVAN
Honeybee Robotics Spacecraft Mechanisms Corporation
460 W. 34th Street
New York, NY 10001
USA

RONALD GREELEY
Planetary Geology Group
Arizona State University
Tempe, AZ 85287-1404
USA

JOHN P. GROTZINGER
Geology & Planetary Sciences
California Institute of Technology
MC 170-25
1200 E. California Blvd.
Pasadena, CA 91125
USA

WILLIAM M. GRUNDY
Lowell Observatory
1400 W. Mars Hill Road
Flagstaff, AZ 86001
USA

EDWARD A. GUINNESS
Washington University
Campus Box 1169
St Louis, MO 63130
USA

ALBERT F. C. HALDEMANN

JPL
4800 Oak Grove Drive
Pasadena, CA 91109
USA

VICTORIA E. HAMILTON

Hawaii Institute of Geophysics & Planetology
University of Hawaii
1680 East-West Road
Honolulu, HI 96822
USA

KEN E. HERKENHOFF

U.S. Geological Survey
Astrogeology Team
2255 N. Gemini Drive
Flagstaff, AZ 86001-1698
USA

STUBBE F. HVIID

Max Planck Institute for Solar System Research
Max Planck Str. 2
Katlenburg-Lindau, 37191
Germany

BRIAN M. HYNEK

Department of Geological Sciences
Laboratory for Atmospheric and Space Physics
392 UCB
University of Colorado
Boulder, CO 80309
USA

BRUCE M. JAKOSKY

University of Colorado, Boulder
LASP/Campus Box 392
Boulder, CO 80309-0392
USA

JEROME B. JOHNSON

USACE ERDC – Cold Regions Research and Engineering
Laboratory Alaska Projects Office
PO Box 35170
Ft. Wainwright, AK 99703
USA

JEFFREY R. JOHNSON

US Geological Survey
Astrogeology Team
2255 N. Gemini Drive
Flagstaff, AZ 86001-1698
USA

BRADLEY JOLLIFF

Washington University
Campus Box 1169
One Bookings Drive
St Louis, MO 63130
USA

SUNITI KARUNATILAKE

Cornell University
514 Space Sciences Building
Ithaca, NY 14853-6801
USA

JOHN M. KELLER

University of Arizona
1629 E. University Blvd.
Tucson, AZ 85721
USA

HUGH H. KIEFFER

Celestial Reasonings
2256 Christmas Tree Lane
Carson City, NV 89703
USA

KJARTAN M. KINCH

CRSR Cornell University
408 Space Sciences Building
Ithaca, NY 13853
USA

GUNTHER KLETETSCHKA

NASA Goddard Space Flight Center
Code 691
Greenbelt, MD
USA

GÖSTAR KLINGELHÖFER

Institut für Anorganische Chemie und Analytische Chemie
University of Mainz
Mainz, 55099
Germany

ALASTAIR KUSACK

Honeybee Robotics Spacecraft Mechanisms Corporation
460 W. 34th Street
New York, NY 10001
USA

YVES LANGEVIN

Institut d'Astrophysique Spatiale
91405 Orsay
France

RACHEL C. F. LENTZ

University of Hawai'i at Manoa
Hawai'i Institute of Geophysics and Planetology
1680 East-West Road, POST 602
Honolulu, HI 96822
USA

MORTEN B. MADSEN

Niels Bohr Institute for Astronomy
University of Copenhagen
Universitetsparken 5
Copenhagen, DK-2100
Denmark

SYLVESTRE MAURICE
Centre d'Etude Spatiale des Rayonnements
9 Avenue du Colonel Roche
BP 24346
Toulouse Cedex 4
France

TIMOTHY McCONNOCHIE
NASA Goddard Space Flight Center
Mailstop 693.0
Greenbelt, MD 20771
USA

TOM McCORD
Space Science Institute
4750 Walnut Street, Suite 205
Boulder
Colorado 80301
USA

ALFRED McEWEN
Lunar & Planetary Laboratory
University of Arizona
1541 E. University Blvd.
Tucson, AZ 85721-0063
USA

SCOTT M. McLENNAN
Department of Geosciences
SUNY Stony Brook
Stony Brook, NY 11794-2100
USA

HARRY Y. McSWEEN JR.
Department of Earth & Planetary Science
University of Tennessee
Knoxville, TN 37996-1410
USA

MICHAEL T. MELLON
Laboratory for Atmospheric & Space Physics
University of Colorado
Boulder, CO 80309-0392
USA

DOUGLAS W. MING
NASA/JSC
Code KX, Building 31, Room 120
2101 NASA Road 1
Houston, TX 77058
USA

JEFFREY E. MOERSCH
Department of Earth & Planetary Science
University of Tennessee
1412 Circle Drive, Room 306
Knoxville, TN 37996
USA

RICHARD V. MORRIS
NASA/JSC
Code KR, Building 31, Room 120
2101 NASA Road 1
Houston, TX 77058
USA

PATRICK C. PINET
UMR 5562/CNRS
Observatoire Midi-Pyrenees
14 Avenue Edouard Belin
Toulouse, 31400
France

THOMAS H. PRETTYMAN
Los Alamos National Laboratory
MS D466
Space and Atmospheric Science
Los Alamos, NM 87545
USA

NATHANIEL E. PUTZIG
Laboratory for Atmospheric & Space Physics
University of Colorado
Campus Box 392
Boulder, CO 80309
USA

ROBERT C. REEDY
Institute of Meteoritics
University of New Mexico
MSC03-2050
Albuquerque, NM 87131
USA

L. RICHTER
German Aerospace Center (DLR)
Institute of Space Simulation
Linder Hoehe
Cologne, D-51170
Germany

RUDOLF RIEDER
Cosmochemistry Department
Max Planck Institut für Chemie
PO Box 3060
Mainz D-55020
Germany

A. DEANNE ROGERS
Department of Geosciences
SUNY at Stony Brook
Stony Brook, NY 11794
USA

STEVEN W. RUFF
Mars Space Flight Facility
Arizona State University
Moeur Building, Room 131
Tempe, AZ 85287-6305
USA

RICHARD A. SIMPSON
Stanford University
David Packard #332
350 Serra Mall
Stanford, CA 94305-9515
USA

JASON SODERBLOM
Lunar and Planetary Laboratory
University of Arizona
1629 E. University Blvd.
Tucson, AZ 85721
USA

LAURENCE A. SODERBLOM
US Geological Survey
2255 North Gemini Drive
Flagstaff, AZ 86001
USA

STEVE W. SQUYRES
Department of Astronomy
Cornell University
428 Space Sciences Building
Ithaca, NY 14853
USA

ROBERT J. SULLIVAN
CRSR
Cornell University
308 Space Sciences Building
Ithaca, NY 14853
USA

G. JEFFREY TAYLOR
Hawaii Institute of Geophysics & Planetology
1680 East-West Road
Post 504
Honolulu, HI 96822
USA

SHANE THOMPSON
Arizona State University
School of Earth and Space Exploration
Box 871404
Tempe, AZ 85287
USA

TIMOTHY N. TITUS
US Geological Survey
Astrogeology Team
2255 N. Gemini Drive
Flagstaff, AZ 86001-1698
USA

ALIAN WANG
Department of Earth & Planetary Sciences
Washington University
Campus Box 1196
1 Bookings Drive
St Louis, MO 63130-4862
USA

HEINRICH WÄNKE
Abteilung Kosmochemie
Max Planck Institut für Chemie
PO Box 3060
Mainz D-55020
Germany

CATHY WEITZ
Planetary Science Institute
NASA
1700 East Fort Lowell
Suite 106
Tucson, AZ 85719
USA

MICHAEL B. WYATT
Brown University
Department of Geological Science
324 Brook Street
Providence, RI 02912-1846
USA

ALBERT YEN
JPL/Caltech
4800 Oak Grove Road
M/S 183-501
Pasadena, CA 91109-8099
USA

JUTTA ZIPFEL
Forschungsinstitut und Naturmuseum
Senckenberg
Frankfurt/Main, D-60325
Germany

FOREWORD

The concept of a *frontier* is a commonplace metaphor in the physical sciences, as well as in the history of exploration. Today, one of the most tangible and alluring of all such frontiers is represented by the surface of Mars. This is because of the literally phenomenal scientific progress that has resulted from the intensified robotic exploration of the Red Planet since 1996. In little more than a decade (1996–2007), scientific viewpoints have been altered more profoundly than in the previous 30+ years. Some would describe this radical alteration in thinking as a *scientific revolution*. A case for this perspective is made in a convincing fashion here in *The Martian Surface: Composition, Mineralogy, and Physical Properties*, edited by Jim Bell and written by him and 82 other colleagues who study Mars for a living. Indeed, since the dawn of the Space Age, now in its 50th year (1957–2007), thoughts have often drifted to the so-called “Martian frontier,” with an ever-changing and sometimes disappointing scientific appreciation of what it might offer. This book puts the emerging “new Mars” into a modern scientific context on the basis of an ensemble of up-to-date scientific hypotheses and viewpoints. It brings Mars alive and promotes prospects for future scientific exploration that are certain to continue the revolution at hand.

The Mars that scientific exploration has come to witness today is vastly more dynamic and scientifically interesting than that which the Viking missions of the 1970s revealed. When the last full compilation of scientific thinking about Mars was captured in the early 1990s (The 1992 University of Arizona Press book *Mars*, edited by Hugh Kieffer, Bruce Jakosky, Conway Snyder, and Mildred Matthews), the planet was effectively viewed as a nearly static geological world with intriguing but enigmatic climate cycles and little prospect for what we describe today as “habitability” or “biological potential.” In the post-Viking view of Mars, all the dynamics of the planet and its hydrologic cycles were relegated to the most distant past, with only lurking and ephemeral signatures in the geology and atmosphere visible today. While interesting as one variety of silicate planet, Mars was not viewed as a scientific “holy grail,” with revolutionary potential. NASA’s only plans post-Viking converged upon a mission initially described as the “Mars Geosciences and Climatology Orbiter” (MGCO), which was later renamed *Mars Observer* in the latter part of the 1980s. This comprehensive mission was to have investigated the Martian “system” in a fashion more akin to an Earth Observing System (EOS) than any traditional planetary

remote-sensing mission, in order to understand what scientific steps were justifiable in the competitive scientific landscape of the time.

When Mars Observer failed in the early 1990s, the development of a more agile and distributed approach to Mars exploration was put in place, resulting in the reconnaissance observations of the Mars Global Surveyor (MGS). The MGS catalyzed the scientific revolution that began in 1996 when the ALH 84001 meteorite shocked the scientific and public communities into the renewed possibilities of life, or at least of primitive biological activity, on Mars. The measurements of MGS, however, provided the framework for quantifying and understanding a “new Mars.” This framework, and the scientific impact of MGS as our views of the surface of Mars evolved from relative unknowns to well-measured systems, is articulated here by the authors of this book. For example, in June 2000 Mike Malin and Ken Edgett rocked the scientific community when they presented evidence for geologically recent runoff of liquid water on Mars, despite the current understanding of its stability. This explosive discovery was a first glimmer of the revolution that was at hand. In the words of Steven Jay Gould, the mainstream thinking of this exciting time had its equilibrium punctuated by revolutionary discoveries that allowed a new set of theories about the role of water and potentially life on Mars to take root. *The Martian Surface: Composition, Mineralogy, and Physical Properties* paints for the reader a first-hand impression of the impact of such discoveries on the web of geological, geochemical, and climatological processes that shape any planet’s surface.

Perhaps most catalytic in the unfolding Martian scientific revolution has been the interplay of measurements from the armada of reconnaissance-oriented orbiters (MGS, Mars Odyssey, and ESA’s Mars Express) and landed exploration via the Mars Exploration Rovers *Spirit* and *Opportunity*. Indeed, the authors of this missive bring to light, for the first time, the emerging view of Mars that has been gleaned from the ongoing “voyages” of the rovers. This new view challenges the old post-Viking thinking by bringing the role of water into focus in ways that were somewhat unimagined just 30 years ago. While Mars may appear to have been a static, forever-desiccated world, the discoveries that the *Spirit* and *Opportunity* rovers have made in their surface reconnaissance of the geochemical systems accessible on Mars today have painted a far different picture. From the ongoing work of the twin rovers to the just-commencing surveys of the Mars Reconnaissance Orbiter (MRO), it

now appears as if Mars is indeed a “water planet,” or at least a silicate planet in which the impact of water has manifested itself in a broad variety of scales and signatures. Understanding the many roles water has played in the evolution of the surface of Mars and its relation ultimately to the habitability of the Red Planet is elegantly portrayed in this book. Yet there is so much more to be learned.

Mars has become a tangible scientific frontier, thanks to the integrated measurements, experiments, and syntheses of the past decade. Fitting the story together is fraught with challenges, but the colleagues who have contributed to this timely summary and review of the field manage to succeed in a dramatic fashion. Their concluding arguments present a

case for continuing the scientific conquest of the Martian frontier in this new era of NASA’s Vision for Space Exploration (VSE). Indeed, thanks to the pioneering efforts of the women and men around the world who are exploring Mars robotically (many of whom are coauthors of the chapters in this book), the path toward human exploration of Mars has been clarified and even accelerated. Mars is indeed a compelling scientific frontier; via the scientific framework presented here, we are closer to being there ourselves!

James B. Garvin
NASA Chief Scientist for Mars Exploration, 2000–2005
Goddard Space Flight Center, Greenbelt, MD

ACKNOWLEDGMENTS

Someone once said that editing a multiauthor academic treatise is like herding cats. That is probably an understatement; it is at least insulting to cats (who would never lower themselves to being “herded”). Anyway, I have no idea why anyone would have said that.

In 2004 I asked a number of colleagues who had been instrumental in pulling together the important and extremely useful 1992 University of Arizona Press *Mars* book if they knew if anyone was planning to update the part of that tome dealing with the composition, mineralogy, and physical properties of the Martian surface, given the major advances in those areas that had occurred in the decade-plus since then. No one knew of any such plans, but everyone acknowledged that it would be a challenge, given the continual arrival of new datasets and discoveries and the resulting rapid expansion and evolution of our state of knowledge. Still, perhaps foolishly, I decided that it would be better to at least gather a snapshot of our current view of this topic rather than wait for some “lull” in Mars exploration that would allow us all to catch our breath and just spend our time writing papers about what it all means. Indeed, many of us hope that such a lull (like the one from about 1982 through to 1997) never happens again (and thus we tacitly accept the challenge of having to write those papers breathlessly).

In that spirit, my first major acknowledgment is to the more than hundred colleagues who gave me early advice and encouragement or who are the lead authors or coauthors of the chapters in this book. These people are a sample of the community of planetary scientists who are on the “front lines” of Mars exploration, having conducted – and in many cases still actively conducting – the investigations, calibrations, experiments, and analyses that are daily modifying our understanding of the Red Planet. Most of these folks (indeed, most scientists nowadays) have frenetic schedules and have to balance huge responsibilities on many levels – mission operations, major laboratories, teaching, management, student mentoring, family. I am indebted to these colleagues for agreeing to take some precious time out of their busy lives to summarize and review recent major results in their areas of specialization. I am also grateful for their indelible patience in the face of what must often have seemed like incessant nagging from a pesky editor.

Secondly, all of us – editor, authors, readers – are indebted to the dozens of colleagues who provided independent external reviews for all of the chapters of this book. These people also are among the leading experts in Mars studies, and they, too, sacrificed significant time to perform an important community service: making sure that the results and other information in these chapters are accurate (or at least appropriately acknowledged as speculative), complete, and balanced. Specifically, I would like to thank Dave Agresti, Janice Bishop, Bonnie Buratti, David Catling, Ben Clark, Claude d’Uston, Vicky Hamilton, Jim Garvin, Gary Hansen, Lon Hood, Bruce Jakosky, Jeff Johnson, Hugh Kieffer, Melissa Lane, Scott McClennan, Hap McSween, Mike Mischna, Jeff Moersch, Jeff Moore, Dick Morris, Jack Mustard, Horton Newsom, Mike Ramsey, Ken Tanaka, Timothy Titus, Alan Treiman, Deanne Rogers, and Ted Roush for reviewing one or more chapters in this book. Your time and effort have substantially improved this summary and review, and will have hopefully made it a much more useful future resource for students and other researchers new to this field.

Many other people helped to pull this project together at many stages. I thank Karla Consroe at Cornell University for providing an enormous amount of administrative and editorial assistance. I am also grateful to Bobby Fogel and Marilyn Lindstrom at NASA Headquarters for their initial encouragement of this project, and for helping to secure a small NASA grant (NNX06AH45G) to support some of the administrative costs associated with editing this book. I also thank Helen Goldrein (Morris), Vince Higgs, and Susan Francis at Cambridge University Press for their constant helpful advice and patience, and for their support for including this book in Cambridge’s prestigious Planetary Science series.

Finally, I would like to acknowledge the love and support from my wife Maureen and my children Erin and Dustin. This has been one of my “Sunday afternoon projects” for several years now, and it could not have been done without their indulgence and patience with my incessant tippity-tapping at the keyboard during random free moments at home.

On to Mars!

*Jim Bell
Cornell University
Ithaca, NY*

PART I

INTRODUCTION AND HISTORICAL
PERSPECTIVE

Exploration of the Martian surface: 1992–2007

L. A. SODERBLOM AND J. F. BELL III

ABSTRACT

Following the demise of the 1992 Mars Observer mission, NASA and the planetary science community completely redefined the Mars exploration program. “Follow the Water” became the overarching scientific theme. The history and distribution of water is fundamental to an understanding of climate history, formation of the atmosphere, geologic evolution, and Mars’ modern state. The strategy was to search for past or present, surface or subsurface, environments where liquid water, the fundamental prerequisite for life, existed or exists today. During the 1996–2007 time frame, seven richly successful orbital and landed missions have explored the Martian surface, including NASA’s Mars Global Surveyor (MGS), Mars Pathfinder Lander and Sojourner Rover, Mars Odyssey Orbiter, Mars Exploration Rovers (*Spirit* and *Opportunity*), Mars Reconnaissance Orbiter, and ESA’s Mars Express (MEx) orbiter. “Follow the Water” has borne fruit. Although the Martian surface is largely composed of unaltered basaltic rocks and sand, the Rovers discovered water-lain sediments, some minerals only formed in water, and aqueous alteration of chemically fragile igneous minerals. The geological records of early water-rich environment have shown hints of profuse and neutral-to-alkaline water that later evolved to sulfurous acidic conditions as aqueous activity waned. We now have a global inventory of near-surface water occurring as hydrated minerals and possibly ice and liquid in equatorial and mid latitudes and as masses of water ice making up an unknown but potentially large fraction of the polar regolith. Martian meteorites have provided new insights into the early formation of Mars’ core and mantle. We now know that Mars possessed a magnetic dynamo early after its core formed and that the magnetic field disappeared very early, leaving the early atmosphere unprotected to erosion by the solar wind. Our view of Mars’ geological evolution has been dramatically enriched by a wealth of new mineralogical and chemical information and new ideas. We stand well poised to pursue the major new scientific questions that have emerged.

1.1 MARS EXPLORATION PROGRAM, THE NEW ERA: 1992–2007

At the time of publication of the last comprehensive scientific compilation on Mars (Kieffer *et al.*, 1992), the exploration of

the Red Planet by robotic spacecraft had been largely suspended for over a decade since the completion of the Viking project in 1982. Phobos-2 had achieved Mars orbit in 1988, contributed important new information, but survived only a few months. The next major successful missions, MGS and Mars Pathfinder (MPF), were not launched until 21 years after Viking. Even so, during this hiatus our understanding of Mars continued to expand rapidly owing to (a) continued analysis of the wealth of data returned by Mariners 4, 6, 7, and 9, Phobos-2, the two Viking orbiters, and the two Viking Landers (Kieffer *et al.*, 1992); (b) a rich collection of new Earth-based spectroscopic observations of Mars that capitalized on major advances in telescopic instrumentation (Chapter 2); and (c) laboratory analysis of the growing suite of Mars meteorites, many collected on the Antarctic blue-ice fields, that had an enormous impact on Mars science (Chapter 17).

In 1992 NASA had restarted the robotic Mars exploration program with the launch of the Mars Observer mission (Table 1.1). As an experiment to save money, NASA had elected to base the Mars Observer spacecraft, with its rich, ambitious scientific payload, on a line of earth-orbital communications satellites. Unfortunately, Mars Observer was lost just before reaching Mars orbit; the cause was surmised to be a rupture of the monomethyl hydrazine fuel pressurization system. Faced with the rapidly growing and renewed interest in Mars exploration by the scientific and public communities and the loss of Mars Observer, NASA, the National Academy of Sciences (NAS), and the scientific community were compelled to completely rethink the approach to Mars exploration.

In the 1993–6 time frame, NASA’s Mars Expeditions Strategy Group (later evolved to become NASA’s Mars Exploration Program Analysis Group or MEPAG), consisting of planetary scientists, mission managers, and program administrators, formulated a new Mars robotic exploration program that would include launches every 26 months (the cycle by which favorable, low-energy launch opportunities to Mars repeat). Ideally, at least two spacecraft would be launched in each opportunity to enhance program resilience to mission failure (see Table 1.1). This group also laid out a new set of scientific goals and rationale for Mars exploration (discussed in the [next section](#)) that formed the basis for planning the next decade. The explosion of new knowledge and scientific discoveries that resulted from the Mars exploration missions that followed, including both NASA and ESA Mars missions listed in Table 1.1, forms, in large part, the basis for this book.

The new NASA plan that emerged saw the launch of both the Mars Global Surveyor Orbiter and the Mars

Table 1.1. *Missions and investigations relevant to Mars surface science: 1988–2007*

Launch/status	Mission	Nation/ agency	Mission outcome/science investigations described in this volume ^a
1988	Phobos-1, Phobos-2	USSR	Phobos-1 failed; Phobos-2 reached Mars orbit and survived for several months; ISM
1992	Mars Observer	NASA	Failed: lost prior to Mars arrival
1996, mission ended 2006	Mars Global Surveyor (MGS)	NASA	MOC, TES, MAG/ER, MOLA
1996	Mars 96	USSR	Launch vehicle failed
1996, mission ended 1997	Mars Pathfinder (MPF)	NASA	IMP, Mars Pathfinder APXS, Magnetic Properties
1998	Nozomi	Japan	Failed: no orbit insertion
1998	Mars Climate Orbiter	NASA	Lost on arrival (human navigation error)
1999	Mars Polar Lander	NASA	Lost on arrival (crashed into Mars)
1999	Deep Space 2 Probes	NASA	Carried by MPL – failed; no signal after release
2001–current	Mars Odyssey Orbiter	NASA	GRS, NS, HEND, THEMIS
2003–current	Mars Express Orbiter	ESA	HRSC, MARSIS, OMEGA
2003	Beagle 2 Lander	ESA	Carried by Mars Express – failed landing
2003–current	Mars Exploration Rovers (MER)	NASA	Two Rovers (<i>Spirit</i> and <i>Opportunity</i>), each carrying Pancam, Mini-TES, MER APXS, MB, MI, RAT, Magnetic Properties
2005–current	Mars Reconnaissance Orbiter (MRO)	NASA	CRISM, HiRISE, CTX, MARCI, MCS, SHARAD

Note: ^aInvestigations discussed in this book: CRISM (Compact Reconnaissance Imaging Spectrometer for Mars), CTX (Context Camera); GRS (Gamma Ray Spectrometer); HEND (High-Energy Neutron Detector); HiRISE (High Resolution Imaging Science Experiment); HRSC (High Resolution Stereo Camera); IMP (Imager for Mars Pathfinder); ISM (Imaging Spectrometer for Mars); MAG/ER (Magnetometer and Electron Reflection); Mars Pathfinder APXS (Alpha Proton X-ray Spectrometer); MARCI (Mars Color Imager); MARSIS (Subsurface Sounding Radar/Altimeter), MB (Mössbauer Spectrometer); MCS (Mars Climate Sounder), MER APXS (Mars Exploration Rover Alpha Particle X-ray Spectrometer); MI (Microscopic Imager); Mini-TES (Miniature Thermal Emission Spectrometer); MOC (Mars Orbiter Camera); MOLA (Mars Orbiter Laser Altimeter); NS (Neutron Spectrometer); OMEGA (Observatoire pour la Minéralogie, l'Eau, les Glaces et l'Activité, Visible and Near-IR Imaging Spectrometer); Pancam (Panoramic Camera); RAT (Rock Abrasion Tool); SHARAD (Shallow Radar), TES (Thermal Emission Spectrometer); THEMIS (Thermal Emission Imaging System).

Pathfinder Lander/Sojourner Rover in the 1996 launch opportunity. Mars Global Surveyor re-flew much of the lost Mars Observer scientific payload (Magnetometer and Electron Reflection [MAG/ER], Mars Orbiter Camera [MOC], Mars Orbiter Laser Altimeter [MOLA], Thermal Emission Spectrometer [TES], Radio Science); two other key instruments (Gamma Ray Spectrometer [GRS] and Pressure Modulator Infrared Radiometer [PMIRR]) were reserved for subsequent opportunities. Mars Global Surveyor was tremendously productive, operating in orbit for about 10 years. It generated a wealth of new global datasets including an unprecedented global map of surface topography from MOLA that has had widespread scientific impact; extremely high-resolution MOC images (down to ~ 0.5 m/pixel) of a plethora of fluvial, polar, volcanic, and eolian features; TES global mineralogical maps using thermal infrared emission spectroscopy; MAG/ER discovery of an ancient magnetic dynamo, and high-order gravity maps from Radio Science (Chapters 9, 11, 21, 25). Today's active missions and the missions in development have all relied heavily on this rich collection of MGS data for their design and planning.

Mars Pathfinder had both strong scientific and engineering motives. EDL (Entry, Descent, and Landing) at Mars is quite a

difficult feat (see Muirhead and Simon, 1999; Mishkin, 2003). Unlike the atmospheres of the Earth, Venus, or Titan, the Martian atmosphere is too thin for use of a parachute alone as the final stage in descent and landing. Pathfinder engineered and demonstrated a novel approach: after descending by parachute to ~ 50 m above the surface, a cluster of rocket motors was fired to stop the descent, airbags were inflated to encase the vehicle, and it then did a free-fall and bounced to rest at the surface. This approach allows safe landing on rough rock-strewn sites, like the flood plain that Pathfinder was sent to in the hope of accessing a broad collection of rock types. Soon after landing, Pathfinder deployed its second major engineering achievement: the Sojourner rover, the first successful rover on the Martian surface. A modification of this proven air-bag approach was later adopted for the two Mars Exploration Rovers. Mars Pathfinder made key scientific findings, including characterizing the chemical and physical properties of soils and rocks (see Chapters 3, 12, 17, 19, 20, and 21).

A series of other missions was launched by several nations in the 1996 and 1998 Mars opportunities; all of these met failure in different forms (Table 1.1), reinforcing the historic difficulty in successfully conducting Mars missions (of 38 Mars missions attempted since 1960, only 17 were fully

or partially successful; see <http://mars.jpl.nasa.gov/missions/log/>). In 2000 NASA commissioned an external committee (the Mars Program Independent Assessment Team, chaired by A. Thomas Young) to conduct a major review of the failures of Mars Polar Lander (MPL), Mars Climate Orbiter (MCO), and Deep Space 2 (DS2); the general conclusion was that the projects had been under-funded and had lacked sufficient resources for adequate testing and quality control. The committee tied the low-funding levels to excessive zeal for NASA's new "faster, better, cheaper" philosophy. It strongly urged NASA to restore funding for high-risk planetary exploration missions to an appropriate level, to insure a more realistic chance of success. It also recommended cancellation of the soon-to-be-launched Mars Surveyor 2001 Lander, a derivative of the failed 1998 MPL. As a result, only one mission, the Mars Odyssey Orbiter, was launched in the 2001 opportunity. NASA did ultimately follow many of the Assessment Team's recommendations, including requesting increased levels of funding and invoking requirements for increased mission robustness for the restructured Mars exploration program that we enjoy today.

Mars Global Surveyor had re-flown all but two of the key instruments that were on the original Mars Observer science payload. The PMIRR was re-flown on Mars Climate Orbiter and thus was lost a second time. Owing to obsolescence and unavailability of parts, the PMIRR design was discontinued as a further flight option. In its place, NASA eventually selected Mars Climate Sounder (MCS, a modern version of PMIRR) for flight on the current Mars Reconnaissance Orbiter. For Mars Odyssey 2001, the final remnant of the Mars Observer payload, the GRS package, was upgraded to include the Neutron Spectrometer (NS) and Russian High-Energy Neutron Detector (HEND). With the addition of a newly selected visible and thermal-emission imager Thermal Emission Imaging System (THEMIS-VIS and THEMIS-IR), the continuing Mars Odyssey Mission has been extremely productive, making major advances in global mapping of the physical and chemical properties of the Martian surface (Chapters 5, 6, 10, 18) and also serving as a relay satellite for more than 95% of the down-linked data from the *Spirit* and *Opportunity* rovers. Noteworthy among the many Mars Odyssey results are the discovery and mapping of near-surface reservoirs of hydrogen, most likely occurring as water ice at the poles and as hydrated minerals near the equator (Chapters 5, 6).

Four more spacecraft were launched to Mars in the 2003 opportunity: two by ESA (Mars Express/Beagle 2) and two by NASA (the Mars Exploration Rovers *Spirit*, MER-A, and *Opportunity*, MER-B). The MEx Orbiter approached Mars in late December 2003, released the Beagle 2 Lander, and successfully entered orbit. For reasons unknown, Beagle failed during landing as radio communication was never established. Mars Express has now been operating in orbit for over three years and has produced a wealth of scientific data, including stereo and color images from HRSC and global maps of composition from OMEGA, a French-led visible-to-near-IR imaging spectrometer (Chapters 7, 8). Noteworthy among the MEx results is the suggestion from OMEGA data that alteration of surface materials changed

from neutral-pH or slightly alkaline conditions (e.g., phyllosilicates as a dominant weathering product) early in Mars' history to acidic alteration (e.g., sulfates as a dominant weathering product) in a later era (Chapter 7).

The two NASA Mars Exploration Rovers landed on Mars in early 2004: *Spirit* in Gusev crater on January 4 and *Opportunity* in Meridiani Planum on January 24. These robotic field geologists have enjoyed more than 3 years of successful operation on Mars at the time of this writing, roving and exploring the Martian surface over a combined distance >16 km. They have exceeded their nominal mission lifetimes and distance goals by more than tenfold. Each rover carries a potent payload of remote sensing instruments (Pancam and MiniTES) and a suite of *in situ* instruments mounted on a robotic arm (Microscopic Imager [MI], Alpha Particle X-ray Spectrometer [APXS], Mössbauer Spectrometer [MB], and Rock Abrasion Tool [RAT]). The scientific results and achievements of these prolific missions in exploring and characterizing the geology, geochemistry, and mineralogy of the Martian surface are a major feature of this book and the principal subjects of Chapters 4, 13, 15, 16, 18, 19, 20, 21, 22, 23, 24, and 26.

In 2005, NASA launched the Mars Reconnaissance Orbiter, and the spacecraft successfully achieved orbit and commenced mapping the surface in 2006. At the time of this writing, MRO results from Compact Reconnaissance Imaging Spectrometer for Mars (CRISM), MCS, and Shallow Radar (SHARAD) are just emerging; early results from the High Resolution Imaging Science Experiment (HiRISE) instrument, which has begun spectral imaging in the visible with an unprecedented aerial-photo-scale resolution of 30 cm/pixel, are discussed in Chapter 8.

As a final note, during the bountiful 1996–2007 period of Mars spacecraft missions and resultant new knowledge about Mars, Earth-based telescopic observations and continuing analysis of pre-1992 mission imaging and spectroscopy datasets continued to add valuable new information about the Martian surface chemistry, mineralogy, physical properties, weather systems, dust storms, and migration of atmospheric volatiles. These include new observations from ground-based telescopes and the Earth-orbiting Hubble Space Telescope (Chapters 2, 8); new analyses of Phobos-2 Imaging Spectrometer for Mars (ISM) visible-to-near-IR reflectance spectra of the part of the Martian surface covered before that mission failed (Chapters 2, 7); new analyses of Mariner 6 and 7 Infrared Spectrometer (IRS) measurements of small regions of Mars studied during those 1969 flyby missions (Chapter 2); and a broad spectrum of new insights gained from continued investigation of the growing collection of Martian meteorites (Chapters 17, 22).

1.2 SCIENTIFIC RATIONALE AND GOALS FOR MARS EXPLORATION: FOLLOW THE WATER

The US Planetary Exploration Program has been traditionally recommended, reviewed, and evaluated for NASA

by two sets of science advisory bodies: (1) one internal to NASA that includes standing committees of the NASA Advisory Council (NAC) and ad hoc committees such as the MEPAG that was set up to advise the NASA Mars Program Office; and (2) an independent set of National Academy of Science committees (e.g., the Space Studies Board or SSB, the Committee on Lunar and Planetary Exploration or COMPLEX). All of these committees rely heavily on participation of the planetary research community. The severely felt loss of the ambitious Mars Observer Mission in 1993, after such a long hiatus in Martian exploration after the Viking missions, caused NASA and these advisory bodies to lay out an aggressive new exploration program with launches to Mars every 26 months.

Throughout Mars exploration a recurrent theme has been the search for evidence of past or present life: Did life ever evolve on Mars and if not, why not? A goal of the Viking Program was to search for extant life, a task that proved to be extremely difficult. Although there was general consensus that the combined results of Viking's life-detection experiments were negative (e.g., Klein *et al.*, 1992; Chapter 26), the results of one of those experiments (Viking Labeled Release Experiment) remain in debate with continuing claims that the data are consistent with extant Martian life (see Levin, 2004). The NASA Mars Expeditions Strategy Group (precursor to MEPAG) laid out a new crosscutting theme for the program – focus on the role, history, and occurrence of water (McCleese *et al.*, 1996). Considered to be the fundamental prerequisite for life as we know it, the strategy was to search for past or present, surface or subsurface, environments where liquid water existed or exists today. This approach would then yield a set of sites on Mars for detailed *in situ* study and the eventual return of samples to the Earth that would have the best chance of confirming the presence or absence of past or present life. This early 1996 strategy was cast into a set of goals centered on *Life, Climate, and Resources* with the crosscutting theme of “follow the water.”

In its review of the new plan, COMPLEX (1996) was highly supportive but felt that the strategy needed to be more clearly spelled out as relating to understanding the geology of Mars (in which water has played a major role throughout Martian evolution) and the search for resources (water, extractable oxygen, minerals) to support eventual human exploration. MEPAG (2006) broadened this set of goals to be *Life, Climate, Geology, and Preparation for Human Exploration*. Water, as the crosscutting core of the scientific goals and objectives of the program, was and remains a key feature of the Mars program, and is an important part of planning future missions. A strong component in the evaluation of missions and science payloads for selection became their ability to search for the evidence of current or past water. The NASA Mars Phoenix Mission, scheduled for launch in August 2007, continues to “follow the water”; it is intended to land at a high northern latitude site where water ice is presumed to be close enough to the surface to be probed and analyzed.

Mars Sample Return (MSR) to Earth has remained among the highest scientific priorities in the Mars Exploration Program, dating back to the Viking era. The long-term

Mars exploration strategies laid out by the NASA and NAS committees in the late 1990s included ambitious plans to begin MSR missions during the decade to follow. As Mars exploration unfolded over the next few years, however, it became clear that sample return before 2010 was programmatically unrealistic, given the pace and funding of the program and the occurrences of dramatic failures that caused significant program restructuring. Although congressional funding for NASA's Mars program was increased (based partly on the recommendations of the Mars Program Independent Assessment Team's analysis of the MCO, MPL, and DS2 failures), any potential increases that could be funneled into MSR were largely consumed in restoring the recommended program robustness. The estimated costs for MSR itself also rose, not only because of its inherent complexity and difficulty, but also from increasing requirements on higher mission reliability.

In 2002 the National Academy of Sciences Space Studies Board published a landmark set of recommended priorities for NASA's planetary science program from 2003 to 2013 that was based on a comprehensive decadal survey conducted within the planetary science community (NAS Space Studies Board, 2003). The report reinforced MSR as of highest priority for Mars exploration and called for NASA to begin preparations for sample return in the 2013 time frame or soon thereafter. COMPLEX (2003), in assessment of NASA's Mars program plan, recommended that MSR be launched in 2011. However NASA's current Mars plan recognizes the prudence of conducting more extensive surface and orbital investigations to identify optimum sample return sites before the costly investment of MSR is made. Recently published Mars exploration strategic planning documents that cover the period from 2007 to 2016 now call for the first MSR mission sometime in the time frame beyond 2020 (Beatty *et al.*, 2006; McCleese *et al.*, 2006; MEPAG, 2006). To move MSR earlier, as the scientific community has repeatedly urged, will require a national imperative and a much greater level of funding than NASA's Mars Exploration Program now enjoys. In the meantime, NASA's next robotic Mars rover mission, the Mars Science Laboratory (MSL), is now being built for launch in September–October 2009 (<http://mars.jpl.nasa.gov/missions/future/msl.html>). MSL will take the *in situ* search for chemical clues of life to a new level with its capabilities to detect multiple organic compounds, study isotopic chemistry, and search for traces of subsurface water.

The Mars missions of the last decade listed in Table 1.1 (that are largely the subjects covered in this book) have made enormous strides in our understanding of the composition, mineralogy, and physical properties of the surface and in the crosscutting theme of understanding the evolution, role, and current disposition of water on Mars. Every chapter in this book touches on (most of them very directly) the role of water in the planet's early evolution and its subsequent geologic processes and history. Each chapter also helps to reveal that “follow the water” has been a remarkably effective strategy for further expanding on the Viking-era discovery that Mars has undergone significant climatic changes over the course of time.

1.3 SCOPE, ORGANIZATION, AUDIENCE, AND GOALS OF THE BOOK

It has been 15 years since the last major research-level summary book about Mars was written (Kieffer *et al.*, 1992), and more than 14 years since the last major research-level book containing a few chapters summarizing what was known of Mars composition and mineralogy was published (Pieters and Englert, 1993). Those works summarized the Viking and telescopic-era view of Mars at the time. As described above, since then, however, our view of the composition, mineralogy, and physical properties of the surface of Mars has changed dramatically because of new data from Hubble Space Telescope and other telescopes, and the Phobos-2, MGS, Mars Odyssey, Mars Pathfinder, MEx, the twin Mars Exploration Rover missions, and Mars Reconnaissance Orbiter missions. Magnificent new datasets are now available that have, in some cases, completely changed our worldview of the Red Planet. These new missions have provided quantitative, unambiguous evidence for the presence of liquid water on the Martian surface in the distant past, and for the presence of water ice in the subsurface of the polar regions today. Water has played a more important role in the geologic and geochemical evolution of the surface than many scientists thought based on previously available data. Even though new data are still streaming in and new discoveries are still being made, it is time for a scholarly update of the state of knowledge of this important and exciting field. This book is intended to be that update.

However, it is important to point out that this book is not intended to be a complete review and summary of all of Mars science, as the University of Arizona *Mars* book was in 1992. The explosion in data and knowledge about Mars during the last decade has made it impossible to adequately write such a book again as a single volume work (even the 1992 *Mars* book was nearly 1500 pages long, after all). Therefore, this book concentrates on just one aspect of this far-reaching field: the composition, mineralogy, and physical properties of the Martian surface. The intention is to treat that topic thoroughly using contributions from some of the leading active researchers working in this area. Other recent books have been written that focus on our expanded understanding of Martian geology (e.g., Carr, 2007; Chapman, 2007), and other excellent book chapters and review papers have been written covering new data and results in Martian geology and geophysics (e.g., Head *et al.*, 2001; Nimmo and Tanaka, 2005; Solomon *et al.*, 2005) and atmospheric sciences (Encrenaz, 2001; Greeley *et al.*, 2001). This book should complement, not duplicate, those other works, for researchers looking to get a more complete and current “snapshot” of the state of Mars science.

This book is part of the Cambridge University Press *Planetary Science* series, and as such is intended to be a thorough reference for researchers and teachers covering this field. The intended audience for this book is researchers, upper-level undergraduates, and graduate students in planetary science, astronomy, space exploration, planetary geology, and planetary geochemistry. Contributed chapters are

primarily technical in nature, at a reading and content level comparable to research articles in journals like the *Journal of Geophysical Research* or *Icarus*, where many planetary science peer-reviewed results are published. However, throughout the book, there has been a concerted effort to minimize (and at least define and where possible, reference) esoteric terms, acronyms, and other jargon to make sure that the information presented here is accessible to students, new researchers, and other novices just entering this field. The hope is that this book will become the definitive resource and review of Mars surface composition, mineralogy, and physical properties issues for students and researchers for the next decade, just as the *Arizona Mars* book was for the previous decade. In addition, it is hoped that the book will be used as the basis for or as a resource in university courses being taught on Mars, planetary remote sensing, or planetary geochemistry.

1.4 INTRODUCING MARS' GLOBAL GEOLOGICAL EVOLUTION

To provide context for the discussions that follow in this and other chapters, we give a general description of Mars' physiographic provinces, their nomenclature, the geological sequence of their formation, and our best understanding of their ages. Mars exhibits a global dichotomy in its crustal structure and ages of geologic units (see Nimmo and Tanaka, 2005) whose origin is still largely a mystery. This is dramatically exhibited in one of the premier MGS datasets, a map of global topography (Figure 1.1) acquired by the Mars Orbiter Laser Altimeter (MOLA) carried by the Mars Global Surveyor (Zuber *et al.*, 2000).

The boundary dividing the dichotomy in Mars' global physiography follows approximately a great circle that is tilted $\sim 30^\circ$ to the equator and with highest and lowest latitudes at $\sim 50^\circ$ E and $\sim 230^\circ$ E. (Note: Planetary scientists studying Mars use both West [$^\circ$ W]- and East [$^\circ$ E]-based longitude definition systems to describe the cartographic locations of features on the surface. West longitude is preferred by those who favor a convention of increasing sub-solar longitude as the planet rotates. East longitude is preferred by those more comfortable with right-handed spherical coordinate systems. Both systems are recognized by the International Astronomical Union as valid.) South of this boundary are heavily cratered ancient terrains of higher-than-average elevation; the large impact basins, Hellas and Argyre, stand out in the topographic map from their depressed floors. To the north of the boundary are younger units that vary in elevation. They consist of (1) vast, smooth, mixed sedimentary and volcanic plains that are generally lower than average Mars; and (2) the Tharsis volcanic region of high plateaus and ridges centered near 240° E, where several enormous volcanoes including the largest, Olympus Mons, are found. A tectonic rift valley, the 4000-km-long Valles Marineris, opens to the east of Tharsis and ends in channels and flow features reaching to the north into the low plains. Superposed on these two global units are a plethora of younger erosional and

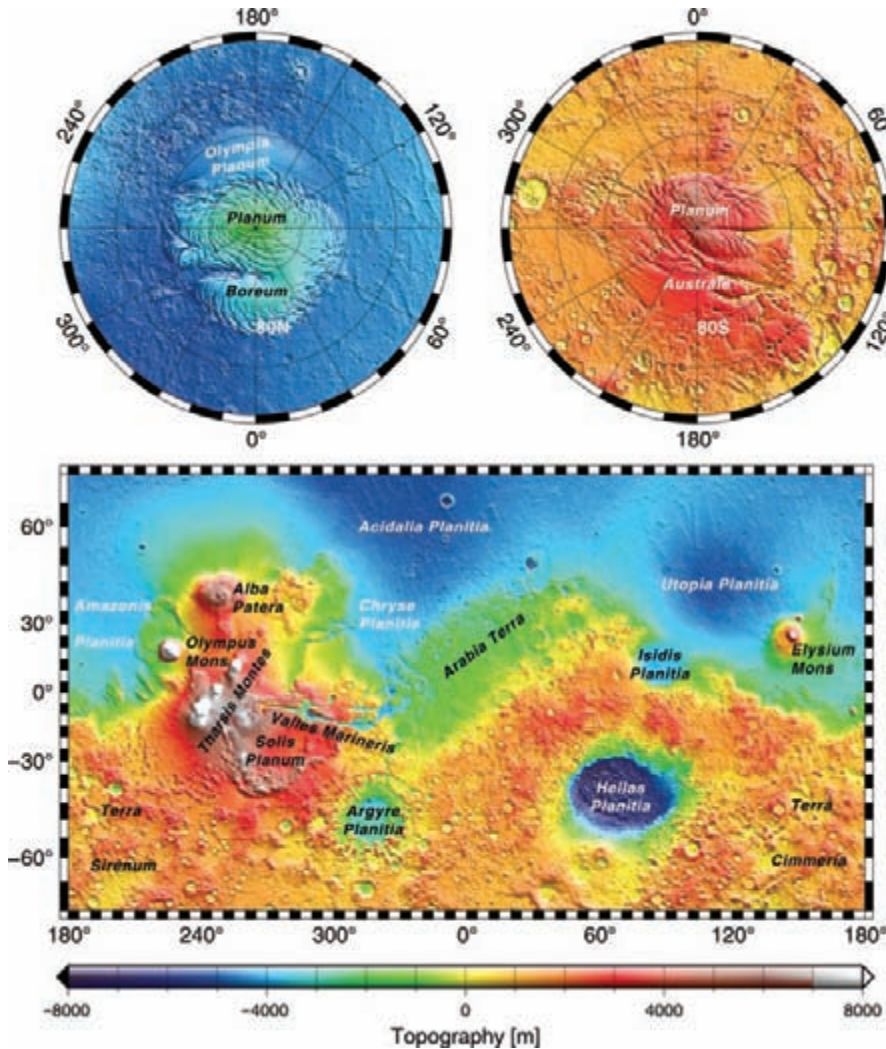


Figure 1.1. Global topography of Mars from the MGS MOLA experiment. (Credit: NASA and the Mars Global Surveyor Mars Orbiter Laser Altimeter Team.) (For a color version of this figure, please refer to the color plate section or to the e-Book version of this chapter.)

depositional features of volcanic, fluvial, lacustrine, glacial, and eolian origin. At both poles, geologically young sequences of layered strata consisting of water ice, carbon dioxide ice, and dust are covered by active veneers of perennial and seasonal water and carbon dioxide ice caps.

Beginning with Scott and Carr (1978), the distribution and sequence of Mars' global geologic units has been extensively worked out using photogeological methods applied to the now vast collection of images acquired by cameras aboard orbital spacecraft (see Scott *et al.*, 1986–7; Tanaka, 1986; Chapters 8, 10). Terrain units are mapped based on geomorphic textures, depositional or stratigraphic superposition relationships, crosscutting relationships (tectonic patterns, erosive features, impact craters), and the relative abundance of superposed impact crater populations. Chronological order is deduced from a combination of the superposition and transection relationships and the number-density of superposed impact craters. Three major geologic periods have been defined, from oldest to youngest: Noachian, Hesperian, and Amazonian. Their general distribution and the type localities for the major periods (Noachis Terra, Hesperia Planum, and Amazonis Planitia) are shown in the geologic map of Figure 1.2. This map further illustrates the global dichotomy.

The ancient Noachian units reside primarily in the higher elevation, heavily cratered southern highlands. The Amazonian units are mostly located in the lower northern plains, in the Tharsis and Elysium volcanic plateaus, and in the polar layered complexes. The Hesperian units lie mostly along the margins between the Noachian and the Amazonian, although numerous occurrences of Hesperian terrains are found within both the older and younger units.

The sequence of evolution of the geologic features and units in Figure 1.2, based on superposition, crosscutting features, and the relative numbers of impact craters formed on exposed surfaces, provides a relative chronological sequence. A next major step in understanding Mars' geologic evolution is to develop an absolute timescale. We know that the terrestrial planets accreted about 4.5 Ga (billion years ago). We know from studies of the lunar highlands and analyses of lunar samples that a period of intense late heavy bombardment, accompanying the last stages of accretion, ended ~ 3.85 Ga (Strom *et al.*, 2005). There is a reasonably firm basis that the Martian crust and the heavily cratered earliest Noachian terrains date to the cessation of heavy bombardment estimated for the Moon. Consequently, the age of Mars' earliest crust is reasonably well constrained.

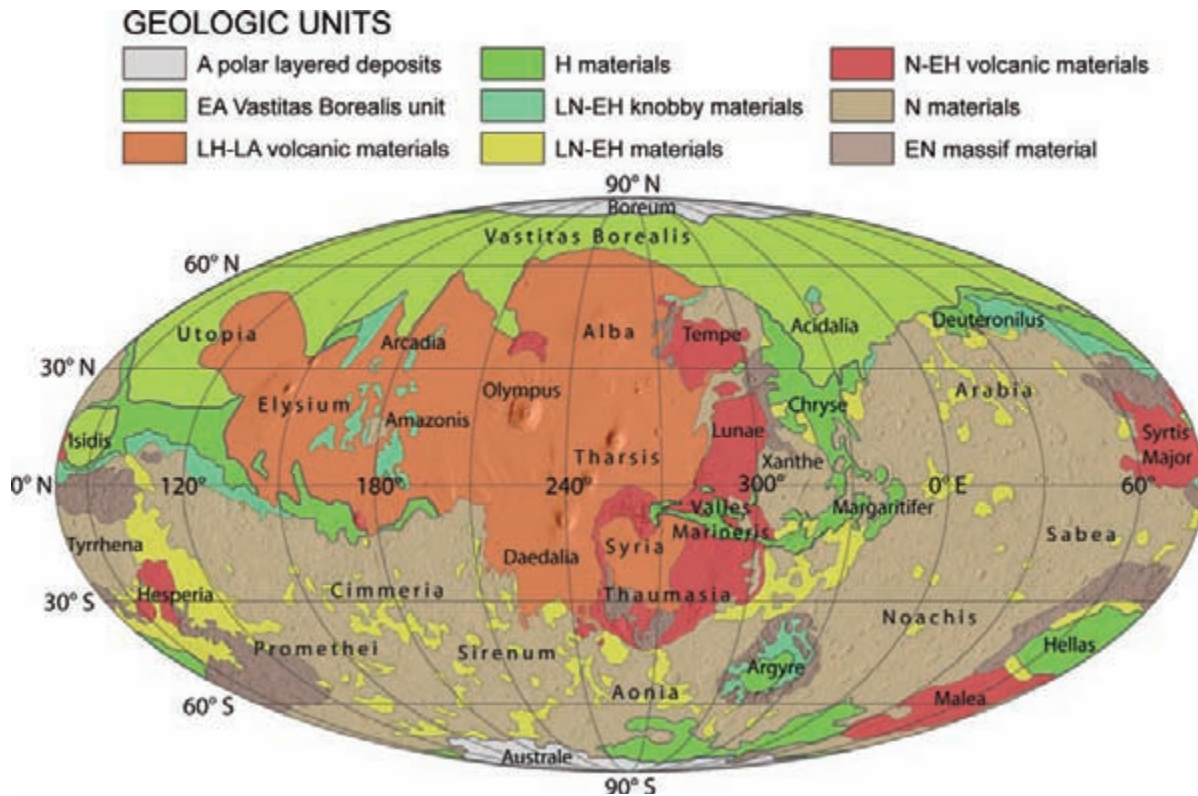


Figure 1.2. Generalized global geologic map. Symbols: Early and Late (E and L) Noachian, Hesperian, and Amazonian (N, H, and A). (Credit: Nimmo and Tanaka, 2005, Reprinted, with permission, from the *Annual Review of Earth and Planetary Sciences*, Volume 33; © 2005 by Annual Reviews; www.annualreviews.org.) (For a color version of this figure, please refer to the color plate section or to the e-Book version of this chapter.)

To model absolute ages of younger terrains requires knowledge of the production rate of impact craters through time. One model in wide use today was derived largely from extrapolation of the lunar cratering rate to Mars and from the observed populations of Mars-crossing asteroids (Hartmann and Neukum, 2001; Hartmann, 2005). Table 1.2 summarizes Hartmann's recent absolute timescale for Martian evolution. Our knowledge of the fluxes of impacting bodies through time is likely inaccurate by a factor of 2 or more (Hartmann and Neukum, 2001; Nimmo and Tanaka, 2005). Still, because the age of the accretion and formation of the Martian core and mantle (~4.5 Ga) are well documented from isotopic studies of Martian meteorites (see Chapters 17 and 22), the earliest part of the timescale is reasonably well-constrained. However, the time of the end of the Hesperian and onset of the Amazonian is uncertain by 1–2 Ga.

Based on this timescale, the Noachian covered roughly the first Ga after Mars accreted. When the crust formed, early in this period, the enigmatic global dichotomy of lowlands–highlands was created. This is evidenced by relics of large ancient impact craters and basins that can be identified in the MGS MOLA topography throughout the northern plains (e.g., Frey, 2004). Younger volcanics later filled these plains and largely masked the old structures. The origin of the

dichotomy remains a mystery, but formation of lowlands by enormous impact basins (see Wilhelms and Squyres, 1984) and long-wavelength mantle convection (see Zuber *et al.*, 2000; Nimmo and Tanaka, 2005) have been suggested. The Hellas and Argyre impact basins were formed as heavy bombardment tapered off in the middle of the Noachian. Throughout this era, rates of volcanism appear to have been 10–100 times higher than in the Amazonian (Hartmann and Neukum, 2001). Such volcanism pervasively flooded the inter-crater areas and crater floors in the ancient highlands. Mars' atmosphere was apparently exsolved in the early Noachian during magmatic overturn of the mantle. An early warm water–rich environment is evidenced by pervasive dendritic channels formed in the Middle-to-Late Noachian (see Carr, 1996, 2007; Head *et al.*, 2001).

By the onset of the Hesperian, impact bombardment had dramatically slowed. Although rates of volcanism began to fall as well, large towering volcanic constructs were built on the Tharsis and Elysium plateaus as the crust cooled and strengthened. Major tectonic activity continued as well, opening the vast extensional rift in Valles Marineris. Large outflow channels developed in many locales, along the margins of the highland–lowland boundary, and winding northward out of Valles Marineris (Figures 1.1 and 1.2). This history of the Hesperian is supported by recent geologic mapping by Tanaka *et al.* (2003, 2005), who used MOLA topography (Figure 1.1) and meter-scale-resolution MOC images to identify the Vastitas Borealis formation (Figure 1.2), interpreted to be sediments debouched by outflow channels into vast regions of the low northern plains that extend as far as the north polar basin (Figure 1.2).

Table 1.2. *Toward a Martian chronology, generalized from Hartmann (2005)*

Estimated age, 10 ⁶ yrs.	Geomorphic feature, Martian period or geological process
<10–50	Youngest lava flows, Elysium–Cerberus, Amazonis, Olympus Mons
170	Basaltic lava flows, unknown locations; 5 basaltic shergottites
100–1000	Background lava flows in Elysium, Amazonis, Cerberus, Olympus Mons
300–500	Basaltic lava flows, unknown locations; 2 basaltic shergottites
200–600	<i>Late/Mid Amazonian boundary</i>
≤670	Transient water exposure in the nakhlite Lafayette, unknown location
~1000–2000	<i>Mid/Early Amazonian boundary</i>
1300	Igneous rock-forming episodes, unknown locations from the Nakhilites
2000–3200	<i>Amazonian/Hesperian boundary</i>
3000–3500	Many outflow channels
~3200–3600?	<i>Late/Early Hesperian boundary</i>
3000–3500	Oldest <2 km-scale craters
~3500–3700?	<i>Hesperian/Noachian boundary</i>
3700–4500	Resurfacing rates 10X–100X higher than in Amazonian
3700–4500	Oldest >20 km craters
~3600–3900?	<i>Late/Mid Noachian boundary</i>
~3800–4100?	<i>Mid/Early Noachian boundary</i>
~3970	Carbonates in ALH 84001
~4510	Formation of Martian crust and ALH 84001

During the Amazonian period, volcanic, tectonic, and fluvial processes rapidly waned (e.g., Head *et al.*, 2001; Hartmann, 2005). Evidence for channeling of the surface by water or glacial ice is only rarely found in Middle and Late Amazonian terrains. By the Middle Amazonian, tectonism had virtually ceased even in the active Tharsis and Elysium volcanic regions. Although volcanic eruption rates also fell dramatically, extremely young volcanic flows (ages <50 million years old (50 Ma) based on sparse impact craters) do occur in a few regions (e.g., near Olympus Mons). It is likely that active volcanism continues to this day at a quiescent level; it is improbable that Martian volcanism ended 98% of the way through geologic time. The polar layered deposits (PLD) are of Late Amazonian age; the exposed layers may record Mars' climatic history as far back as 10–100 Ma. Active polar processes continue today, as the polar deposits are continually formed and eroded by dust and volatiles migrating in and out of the polar regions over timescales ranging from seasonal to long-term (10⁶–10⁷ yrs) and driven by changes in obliquity (e.g., Touma and Wisdom, 1993; Laskar *et al.*, 2004). By the Late Amazonian, Mars became the arctic desert planet that we see today. Eolian processes came to dominate, scouring the surface, moving massive dune fields like the north circumpolar erg, and stirring storms of bright reddish-brown dust across the globe.

1.5 OUR CURRENT UNDERSTANDING OF THE MARTIAN SURFACE

Since 1992 when the comprehensive work *Mars* (Kieffer *et al.*, 1992) was published, our understanding of the nature and evolution of the Martian surface has undergone a revolutionary expansion. The dictum “follow the water” has truly paid off scientifically. We have examined the geological processes and chemical details of Mars' watery past both from orbit and at the surface. We have followed the chemical evolution of Mars' water through time to learn how its surface environment changed. Although the bulk of the surface materials consists of weakly altered basaltic minerals, we see extensive alteration in local environments. We have direct evidence for water-lain sediments and extensive interaction of subsurface water with chemically-fragile igneous minerals. We see suggestions of early more profuse and more alkaline waters, later evolving to become highly acidic as aqueous activity waned. Martian meteorites have given up many isotopic secrets about the early formation of Mars' core, mantle and crust, and the varieties of magma sources from which they were derived. We now know Mars possessed an early magnetic dynamo and think that it disappeared very early, leaving the atmosphere unprotected to loss by the scavenging processes of the solar wind. We have an inventory of near-surface water, occurring as ice or in hydrated minerals across the globe and as high concentrations of water ice in the polar regolith. Our view of Mars' geological evolution has been dramatically enriched by a wealth of new mineralogical and chemical information and new ideas. Here we summarize the current understanding of the physical character, chemistry, mineralogy, and evolution of the Martian surface that is expanded in detail in the chapters that follow.

1.5.1 Fundamentally a basaltic planet

Mars' dark regions have long been inferred to be basaltic from telescopic observations, reinforced by Phobos-2 ISM's identification of LCP (low-Ca) and HCP (high-Ca) pyroxenes (Chapter 2). MGS/TES (Chapter 9), Mars Odyssey THEMIS (Chapter 10), and MEX OMEGA (Chapter 7) provide global maps of many mineralogical components and have confirmed the general basaltic nature of Mars' surface. Collectively, they reveal a great variety in the igneous lithologies exposed in the dark regions that are mostly unaltered or only weakly so. Thus, even with the wide variety of secondary minerals and phases (e.g., oxides, glasses, sulfates, and clays) discovered on Mars and described throughout this volume, the fundamental makeup of the surface is still basaltic, with typically only a weak degree of alteration (Chapters 22, 23, 24, 26).

TES, THEMIS, and OMEGA are highly complementary investigations. For example, TES and THEMIS data provide evidence for plagioclase feldspar, silica glasses, quartz-rich phases, and dacite, none of which could be detected by OMEGA. In contrast, TES and THEMIS are not particularly sensitive to sulfates or phyllosilicates like those that OMEGA has identified. Olivine is a key

rock-forming mineral on terrestrial planets that is very vulnerable to aqueous alteration. TES, THEMIS, and OMEGA all confirm olivine-bearing basalts to be common throughout dark regions, and all have identified local areas of high-olivine concentration (Chapters 7, 9, 10). These investigations have also extensively mapped pyroxenes, another class of key rock-forming minerals, showing them to be diverse and widespread on Mars. TES finds highly variable HCP/LCP ratios throughout Hesperian and Noachian units, pointing to great diversity in magma chemistry. OMEGA results suggest LCP is enriched in some Noachian areas and HCP is more abundant in younger volcanic shields. One interpretation is that because enstatite (LCP) melts at higher temperature than diopside (HCP), the increased LCP concentration might signal higher temperatures in the early magmas (Chapter 7).

TES distinguished two global-scale volcanic units (TES Surface Type 1 [or ST1] and Surface Type 2 [or ST2]; Chapters 5, 9, 17, 22). ST1 is older, is concentrated in Noachian regions, and consists of unaltered plagioclase-rich and clinopyroxene-rich basalt (Chapter 9). Surface Type 2 occurs in Amazonian-Hesperian northern plains, is higher in silica-rich phases, and has been suggested to be more andesitic (Chapter 9). Mars Pathfinder APXS measurements also suggested the presence of soil-free rocks (SFR) similar in composition to andesitic basalts (Chapter 3). Alternatively, ST2 and SFR surfaces may be coated with secondary phases (silica glass, zeolites, clays) and/or dust (Chapters 3, 9, 12, 17, 19, 22). Interestingly, Mars Odyssey GRS measurements found no detectable difference in Si content or K/Th ratio between TES Types 1 and 2, although it did show K to be ~30% higher in Type 2 (Chapter 5). Regardless, it is still possible that ST1 and ST2 represent different magma sources. Adding to the diversity, TES and THEMIS data suggest local exposures of high-silica rocks, possibly quartz- and plagioclase-rich granitoids and dacites (Chapters 9, 10), and GRS detected very low-Si rocks west of Tharsis. In summary, orbital data have revealed diverse igneous rocks ranging from ultramafic high-olivine basalts to silicic dacites and granitoids, rivaling the diversity found in the Earth's crust.

The mafic components of typical Martian soils studied at the landing sites also reveal the presence of weakly altered basalts. The elemental composition of the sandy-to-cloddy soils at all sites was found to be chemically similar (Chapters 3, 4, 12) and MER Mössbauer (MB) observations directly characterized the soil mineralogy (Chapter 15). Mössbauer shows that soils on the Meridiani and Gusev plains and within the geologically complex Columbia Hills are virtually identical in terms of their iron-bearing mineralogy, with the exception of the unique sulfur-rich “Paso Robles” soil in Gusev. It is remarkable that in almost all of these soils, from diverse geologic settings on opposite hemispheres, MB analyses show 33%–34% olivine, 6%–8% magnetite, and 33%–37% pyroxene; the mafic component of average Martian soil is clearly olivine basalt (Chapter 15). Further, the observed APXS correlation between Ti and Fe in the soils implies that the magnetite is most likely titanium bearing (titanomagnetite; Chapter 4). Mössbauer measurements

and the results of the MER and MPF Magnetic Properties experiments (Chapter 16) indicate that almost all fine-grained dust and soil particles on Mars are magnetic, and that the magnetic component of the soil is a relatively unaltered igneous mineral rather than an alteration product such as maghemite. Clearly, the globally uniform “Laguna Class” soils do not appear to have been exposed to significant aqueous alteration (Chapters 15, 16). This finding represents a significant paradigm shift from a decade ago, when it was widely assumed that the presence of fine-grained ferric oxides and oxyhydroxides indicated that typical Martian dust and soil was a heavily weathered secondary alteration product. Apparently, the altered (ferric) phases in the dust and soil represent only a minor weathered veneer and are not representative of the bulk volumetric properties of Martian soil grains.

Analyses of Martian meteorites (shergottites, nakhlites, and chassignites; SNCs) further point to the principally basaltic nature of the Martian crust (Chapters 17, 22). All SNCs are lavas or cumulates derived from a wide variety of basaltic magmas. As representative members of these classes contain gases matching the atmosphere isotopic chemistry measured by Viking, the evidence is convincing that they are from Mars (Chapter 17). Their ejection ages cluster, indicating that groups were ejected in single impacts. Some groups exhibit wide ranges in crystallization age (up to 400 Ma), indicating long-lived local volcanic activity. It is not understood why the crystallization ages of most meteorites are extremely young (95% ≤ 1.3 Gyr). This is apparently inconsistent with chronological models that suggest that half of the surface is >2 Gyr old and raises a serious open issue. Nevertheless, even with the young crystallization ages, the SNC isotopic chemistry shows that the magma sources from which they were derived are ancient; these magmas formed very early (~ 4.5 Ga), around the time of formation of the core, mantle, and crust, and have remained unchanged and intact for billions of years (Chapters 17, 22).

SNC meteorites were evidently derived from heterogeneous mantle magma sources (Chapters 17, 22), consistent with the variable igneous mineralogies mapped by TES, THEMIS, OMEGA, and GRS. Although SNCs and rocks analyzed at the surface and from orbit are somewhat different (Chapters 4, 5, 14, 15, 17, 22), all exhibit a common mineralogic inventory (ferroan olivine and pyroxenes and sodic plagioclase) that distinguishes them from terrestrial basalts. For example, the pristine Gusev basalts are similar to olivine-phyric shergottites, and Bounce Rock, believed to be a Meridani erratic derived from the subsurface by a distant impact, is virtually identical to basaltic shergottite meteorites (Chapters 4, 17, 22). With the exception of the single ancient meteorite ALH 84001 that exhibits significant secondary carbonate minerals (Chapters 17, 22, 23, 26), aqueous alteration of SNC meteorites is very mild, although ubiquitous. Evidently, subsurface aqueous alteration on Mars, at least in the regions sampled by the SNC meteorites, was limited in intensity and duration.

In summary, the bulk of the Martian surface and crust consists of minimally altered igneous rocks. This seems inconsistent with ample evidence presented throughout this

volume (and summarized in the next section) that a variety of styles of aqueous alteration have occurred in many locales. The picture that emerges is that the globally integrated intensity, duration, available water, and other factors controlling the degree of aqueous alteration must have been far less than that required to affect a significant fraction of Mars' igneous crust and mantle overall.

1.5.2 Mars' altered surface, dominated by acid-sulfate processes

It is important to ask, to what degree have the basaltic surface materials on Mars been altered? Sulfur-containing soils and sulfate-bearing rocks were found at the Viking, Pathfinder, and MER landing sites and point to possible low-pH aqueous conditions resulting from acid-sulfate alteration. However, most of the observed altered materials are still fundamentally basaltic in their overall chemistry (see Figure 23.2 in Chapter 23 and Figure 24.4 in Chapter 24). In contrast to the apparent ubiquity of S-bearing soils and rocks, no surface exposures of carbonates (beyond traces seen in dust by TES and Miniature Thermal Emission Spectrometer [Mini-TES], see Chapters 9, 14) have been found by *in situ* or orbital techniques, and only minor amounts are found in many young (≤ 1.3 Ga) SNC meteorites (Chapters 17, 22). The only direct evidence for the presence of ancient carbonates is from the single old (~ 4.5 Ga crystallization age) meteorite ALH 84001. The carbonates in ALH 84001 appear to have been formed around 3.9 Ga. Evidence for other rare alteration products (clays and aluminous phases) that form under near-neutral pH conditions have also been found by OMEGA and MER (Chapters 7, 23, 26). Along with the carbonates in ALH 84001, these secondary minerals may be much older than the sulfates, possibly recording earlier ancient non-acidic aqueous conditions.

As far back as the 1930s the reddish-brown color of the dust in bright regions and dust storms was conjectured to arise from iron oxide (Chapter 2). By the 1960s, oxidized basalt became the leading candidate for the origin of the dust. Viking soils were estimated to contain $\sim 18\%$ FeO, and subsequent telescopic work suggested that the dust contained extremely fine-grained (nm-sized grains or nanophase) crystalline "red" hematite (Fe_2O_3) and/or other poorly crystalline iron oxides/oxyhydroxides (Chapters 2, 23). OMEGA has mapped the ubiquitous ferric oxides but has only revealed the presence of anhydrous ferric phases (Chapter 7).

Discovery by TES of small concentrations of coarse-grained, crystalline "gray" hematite, potentially formed in liquid water, was a key new finding in the search for alteration minerals on Mars; eventually, it led to the decision to land the *Opportunity* rover in Meridiani Planum. In one scenario for the formation of gray hematite, goethite (FeOOH) precipitates in water, is buried, and re-crystallizes to hematite. MER data have provided conclusive evidence that liquid water was involved in forming the Meridiani hematite (Chapters 4, 13, 14, 15, 23, 24, 26). MER mineralogical analyses (MB, Mini-TES, Pancam)

have confirmed the existence of coarse-grained anhydrous ferric oxide (hematite) and oxyhydroxide (goethite) in specific locations and samples at the landing sites. MER data also confirm the presence of the ubiquitous nanophase ferric oxide and/or oxyhydroxide phase inferred from earlier telescopic and orbital observations, although the MER data cannot distinguish between hematite, goethite, ferrihydrite, or perhaps other minerals as the nanophase material (Chapters 2, 13, 14, 15, 16).

Viking soils exhibited surprisingly high levels of S and Cl, and similarly high levels were also found in Pathfinder and MER soils (Chapters 3, 4, 23). GRS also mapped high levels of Cl in some regions (Chapter 5). The observed correlation between Mg and S abundances in APXS data and the high concentration of S in soil clods have been interpreted to indicate the presence of Mg-sulfate cements. Such high-relative abundances of S and Cl in the soils led to the realization that low-pH acid-sulfate weathering was a major alteration pathway on Mars (Chapters 3, 4, 23, 24, 26). In Eagle crater on Meridiani Planum, *Opportunity* discovered sedimentary outcrops (the Burns formation) made up of jarosite [$(\text{K}, \text{Na}, \text{H}_3\text{O})\text{Fe}_3(\text{SO}_4)_2(\text{OH})_6$], hematite, Mg- and Ca-sulfates, and siliciclastic materials derived from altered basaltic sand (Chapters 4, 14, 15, 23, 24). The hematite occurs in spherules (and their weathered lags); evidently, these now-famous "blueberries" are concretions (hard, compact aggregates of mineral matter formed by precipitation from an aqueous solution) formed by later stage fluids (Chapter 24). Some strata in the Noachian-Hesperian Burns formation appear to be eolian but others exhibit textural features strongly indicative of formation in shallow flowing surface water. These observations have led to the interpretation of Meridiani Planum outcrops as "dirty" evaporites (Chapters 23, 24, 26). This interpretation has been challenged by suggestions that base surges from impact events or volcanic explosion could produce the observed textures and chemical observations (Chapters 24, 26). Identification of jarosite in the sedimentary rock is of signal importance, however, as this mineral only forms by aqueous processes under low-pH conditions; clearly, aqueous acid-sulfate alteration was involved. Although telescopic and OMEGA observations have not detected jarosite (Chapters 7, 8), OMEGA has mapped a variety of other hydrated sulfates in stratified terrains, including kieserite (monohydrated MgSO_4), gypsum (dihydrated CaSO_4), and polyhydrated sulfates of unknown mineralogy (Chapter 7).

Spirit landed in Gusev, a 150-km Noachian crater, whose rim was breached by Ma'adim Vallis, an ancient channel system that left sediments on the crater floor resembling deltas (Chapter 26). The landing site is on a Hesperian plain, mantled by typical soil (basalt sand mixed with ferric oxide dust, ubiquitous at all sites) and with minimally altered basalts scattered about. Only minor evidence for aqueous activity was found on the Gusev plains: small, possibly mineralized veins in some rocks; light-toned, possibly cemented dust coatings on other rocks. However, after *Spirit* drove ~ 3 km to the Columbia Hills, highly altered soils and rocks emerged. While scrambling uphill, *Spirit* excavated bright reddish and yellowish soils at a location

known as Paso Robles (Chapter 13); these soils exhibit the highest sulfur content (~30 wt.%) measured so far by APXS (Chapter 4). The mineralogy of these soils has been modeled as containing Fe-, Mg-, and Ca- sulfates, Ca-phosphates, hematite, halite, allophane, and amorphous silica (Chapters 4, 13, 23). Mössbauer measurements showed Paso Robles to be rich in ferric-sulfates that Mini-TES data showed to be hydrated (perhaps ferrihydrite; Chapters 14, 15). Acid-sulfate aqueous alteration is again implicated, as Paso Robles soil might be an evaporite deposit formed from solutions rich in Fe, Mg, Ca, S, P, and Si (Chapters 23, 24). Unlike the weakly altered Gusev plains basalts that were difficult to grind with the MER RAT (Chapters 20, 21), most altered rocks found in the Columbia Hills were very soft – evidence (though not unique) of exposure to highly acidic sulfurous conditions. Many of the Columbia Hills rocks have rudimentary sedimentary textures; they may be of both volcanoclastic and impact derivation. Others, like the Peace outcrops, appear to be well-sorted (eolian?) mafic basaltic sand cemented by Mg- and Ca-sulfates (Chapters 23, 24). An important MB discovery is that many of these rocks contain goethite, a hydroxylated iron oxide that only forms in water (Chapter 15). As in Meridiani Planum, these kinds of discoveries provide conclusive evidence that at least some putatively Noachian rocks of the Columbia Hills may have been altered under *aqueous* acid-sulfate conditions (Chapters 4, 14, 15, 23, 24, 26).

There is some evidence for altered materials on the Martian surface that appear to have been produced in neutral-pH or slightly alkaline conditions. For example, the Independence Class rocks of the Columbia Hills are among the very few rocks that appear to have undergone substantial leaching of their original basaltic elemental character, leading to major Al-enrichment. They may well contain various aluminous phases including phyllosilicate clays such as montmorillonite or other smectite phases (such as nontronite). The evidence for the presence of clays in these rocks supports a model of their formation near-neutral pH conditions (see Figure 23.4, Chapter 23). An exciting and important discovery by OMEGA is of isolated Noachian units that exhibit spectral absorption features in the 2.2–2.4- μm region that are diagnostic of phyllosilicates and arise from Fe-OH, Mg-OH, and Al-OH vibrations in clays such as nontronite, chamosite, and montmorillonite (Chapter 7). If these observations and their interpretation are correct, they provide strong supporting evidence for an early epoch, prior to the period of pervasive acid-sulfate conditions, when an alkaline or neutral-pH water-rich environment existed on Mars.

Telescopic spectra from the 1960s and later Mariner 6 and 7 IRS and Phobos-2 ISM spectra showed the surface to contain bound water at the 1%–10% level. However, exactly how the water was bound (i.e., as ice, adsorbed water, structural hydrate or hydroxyl groups, etc.; see Chapter 2) was unknown. Odyssey GRS and NS have mapped hydrogen concentrations in the upper meter of the Martian regolith, estimating the global distribution of water-equivalent-hydrogen (WEH) with high precision (Chapters 5, 6) and OMEGA has mapped hydrated sulfates and hydrated phyllosilicates at high-spatial resolution (Chapter 7). GRS and

NS data provide an estimate of an average of 7 wt.% WEH in the upper meter at Meridiani Planum. Because the Meridiani sulfate sediments appear mantled by only a few cm of soil, this estimate may closely correspond to the water abundance in the upper meter of the Burns formation. The estimated range of crystal-bound water in these sediments is 6–22 wt.% derived from the measured mineralogy (stoichiometrically) and modeled mineralogy (range of specific candidate hydrous minerals) of the sediments (Chapter 23). Comparison with the GRS/NS value of 7 wt.% suggests that at this site the water is mostly held in hydrated and hydroxylated minerals (Chapter 23).

Where are the carbonates on Mars? This remains a mystery. Like the Earth and Venus, Mars must have outgassed significant amounts of carbon dioxide into its early atmosphere. Coupled with evidence of plentiful water in the earliest period of Martian geologic history, carbonates should have formed (Chapters 24, 26). Other than trace amounts of carbonate detected in the fine Martian surface dust by TES and Mini-TES (Chapters 9, 14), though, convincing evidence for surface carbonate deposits has yet to be found. Both TES and OMEGA should have easily detected any substantial carbonate exposures if they existed. The only evidence for *ancient* carbonates comes from the meteorite ALH 84001, which is known for the (now generally discounted) possibility that it contains relicts of ancient Martian life (Chapters 17, 26). This is the only Noachian Martian meteorite, with a crystallization age of 4.5 Ga (all other SNCs are Amazonian). Its Fe–Mg–Ca carbonate globules date to 3.9 Ga and could have formed in hydrothermal precipitation in CO₂-rich fluids (Chapters 17, 23). Perhaps crustal waters were then alkaline, allowing carbonates to precipitate, and then later when conditions became more acidic surface carbonates were destroyed (Chapters 7, 23). Alternatively, the early alkaline waters in which the ALH 84001 carbonates precipitated may have existed in the subsurface, isolated from an early contemporaneous acidic surface environment. Such a surface–subsurface isolation has been proposed for formation of the carbonates in the nakhlites during the Amazonian (see Figure 24.6, Chapter 24).

Most of the SNCs are very young by Martian standards. One-third of them have crystallization ages <0.2 Ga, two-thirds are <0.6 Ga and the remainder are ~1.3 Ga (Chapter 17). All display some degree of alteration, but none is pervasively altered. Secondary phases include sulfates, carbonates, iron oxides, sulfides, and poorly crystalline silicates or aluminosilicates. The variety of minor Fe-, Ca-, and Mg-rich carbonates that exist in these young samples of the Martian crust suggest a wide range of conditions (e.g., variable pH) in the subsurface, perhaps even today (Chapters 17, 22, 23).

1.5.3 Martian evolution: accretion through Hesperian

The accreted bulk chemistry of Mars is better constrained by recent evidence from (1) improved moment of inertia estimates (0.3662 for Mars compared to 0.3315 for Earth; Folkner *et al.*, 1997), leading to better refined core and

mantle density structure (Bertka and Fei, 1998); (2) elemental and isotopic chemistry of Martian meteorites (Chapters 17, 22); (3) GRS orbital elemental abundance data (Chapter 5); and (4) MPF and MER APXS surface elemental composition data (Chapters 3, 4). The estimated uncompressed density of Mars ($3.8\text{--}3.9\text{ g cm}^{-3}$) is lower than that of Earth ($4.4\text{--}4.5\text{ g cm}^{-3}$), whereas the Martian mantle is likely denser ($\sim 3.5\text{ g cm}^{-3}$) than Earth's (3.34 g cm^{-3}). Mars' lower bulk density is consistent with the available chemistry data in that (1) moderately volatile elements (e.g., K, P, S, Cl) are more abundant in meteorites and *in situ* measurements on the Martian surface (Chapters 4, 17) and (2) GRS measurements that show the surface K/Th ratio to be twice that of Earth's crust (Chapter 5). With respect to the higher mantle density, although the bulk Fe/Si must be lower for Mars, FeO is much more abundant ($\sim 18\%$) in both Martian meteorites and in the surface as measured by GRS and APXS. This probably arises because a larger fraction of the planet's Fe was oxidized and occurs as FeO in its mantle, with correspondingly less in the core as Fe⁰. It may be that Mars' metallic Fe was oxidized by water or as a result of its higher oxygen abundance during accretion. The relatively large difference in bulk composition between Mars and Earth suggests that thorough mixing across accretional source regions in the inner Solar System did not occur (Chapters 4, 17, 22).

The 4.5 Ga age of ALH 84001 shows that Martian igneous processes began soon after accretion. Martian meteorite isotope systematics constrain the time of differentiation of the interior into a core and mantle to have largely completed within the first few $\times 10^7$ years; the core might have existed only ~ 12 Ma after accretion (Chapter 22). Mars may have possessed a magma ocean at this early time, from which the early crust crystallized. Martian meteorites other than ALH 84001 have very young (< 1.3 Ga, Amazonian) crystallization ages; still, isotopic data show that their parent magma sources evolved early, perhaps within the first few $\times 10^7$ years after accretion. Although they are all generally basaltic, these younger meteorites exhibit substantial diversity (e.g., in Ca/Si and Mg/Si, Chapter 17). Their ancient magma sources must have remained intact and segregated for several Ga, until partial melting occurred and the young meteorites in our collection crystallized during the Amazonian (Chapters 17, 22).

MGS MAG/ER discovered regions of strong remnant magnetization concentrated in the southern Noachian highlands, showing that Mars possessed a magnetic dynamo very early in its history (Chapter 11). The younger northern Amazonian plains show only weak magnetic signatures. Earlier modeling had suggested that such a dynamo, driven by thermal convection, might have lasted for the first billion years (Chapter 11 and references therein). We now know that the dynamo ceased very early, probably < 0.5 Ga after accretion. Impacts that created the Hellas and Argyre basins demagnetized large regions of the ancient crust. Thus, by the time these impacts occurred, the dynamo had expired. The estimated age of Argyre and Hellas are 4.1 ± 0.1 Ga, near the end of heavy bombardment (Hartmann and Neukum, 2001; Frey, 2004; Strom *et al.*, 2005).

The global hemispheric dichotomy in the crust also appears to have emerged during this early period. Its origin remains a major debate, ranging between thinning of the northern crust by late basin-scale impacts and/or by short-lived early convection (Nimmo and Tanaka, 2005; Solomon *et al.*, 2005). Evidently, evolution of the dichotomy was largely completed before the end of late heavy bombardment but overlapped with the period of the planet's active magnetic dynamo. This is evidenced by (1) the lack of significant remnant magnetic signatures in the northern lowlands (Chapter 11); and (2) numerous subtle relicts of large impacts that underlie the Amazonian deposits in the northern lowlands (Chapter 22). The smooth northern plains lie ~ 5 km lower than the ancient highland terrains and the Tharsis volcanic plateau. MGS topography and gravity data are best fit by a lower density crust (typically $2.5\text{--}3.0\text{ g cm}^{-3}$) of highly variable thickness (30–100 km) overlying a denser (typically $3.0\text{--}3.5\text{ g cm}^{-3}$) mantle (see Zuber *et al.*, 2000; Neumann *et al.*, 2004). The thinner crust under the northern plains was later overlain by veneers of younger sediments and basaltic lavas (from which most of the SNC meteorites appear to have been derived). Thicker crust underlies and supports the Tharsis volcanic plateau. The petrology of the less dense crust is unknown; no samples are evident in the meteorites (including ALH 84001, with a density of 3.41 g cm^{-3}). This also remains an outstanding puzzle.

During the Noachian, volatile-rich magmas transported water, carbon dioxide, and other volatiles from the mantle to the surface, helping to form the atmosphere. There are several lines of evidence that Mars' early atmosphere was dense and wet (Chapters 9, 22, 24, 26). Foremost, the Noachian terrains exhibit ubiquitous valley networks (including Ma'adim Vallis that flowed into Gusev crater) suggesting an early fluvial, if not pluvial, environment. Compared to Earth, Mars' lower bulk density is evidence for the accretion of a higher fraction of volatiles. For example, geophysical models suggest Mars' magma ocean could have had 2 wt.% water, and recent simulations of accretion suggest abundant water could have been present from late-arriving water-rich planetary embryos (Chapter 22). If only a few percent of this inventory devolved from the interior, ample surface water would have been available to carve valley networks, produce playa evaporites, and leave layered sandstones cemented by subsurface fluids. Additionally, the early atmosphere might have contained up to several bars of CO₂ that could have generated an effective greenhouse, keeping the surface water liquid (Chapter 26). Although volcanically active up to the recent era (e.g., possible lava flows < 50 Ma; Table 1.2), the Tharsis plateau is ancient; the bulk of its development was largely completed by the end of the Noachian (Phillips *et al.*, 2001). It is generally agreed that the high levels of Tharsis volcanism and tectonism played a pivotal role in the Noachian period, with massive outgassing of CO₂ and H₂O to the atmosphere leading to a warmer and wetter early environment (Nimmo and Tanaka 2005; Solomon *et al.*, 2005).

If abundant carbonates ever did form at the Martian surface, it would have been in just such an early warmer and wetter environment, probably under a denser CO₂

atmosphere. In fact, our only sample of the early Martian crust (ALH 84001, crystallization age 4.5 Ga) contains secondary carbonate globules that formed ~ 4 Ga (Chapters 17, 23) at the time of the hypothesized Noachian warmer, wetter environment. Carbonates require a slightly alkaline environment both to form and to survive (see Figure 22.4 of Chapter 22). MER results indicate that by the Late Noachian and Early Hesperian the aqueous alteration environments had become acidic at two sites on opposite hemispheres (Chapters 23, 24). It seems straightforward, then, to speculate that most near-surface carbonates were destroyed by these later pervasive acidic fluids. A reaction product of Ca-carbonate with sulfuric acid is gypsum ($\text{CaSO}_4 \cdot 2\text{H}_2\text{O}$), a mineral that OMEGA has in fact identified in a few locations (Chapter 7). OMEGA's discovery of isolated occurrences of phyllosilicates in Noachian terrains further adds to this picture. Phyllosilicates are stable in near-neutral Eh and pH environments (see Figure 23.4 of Chapter 23). The picture that emerges is that during the latter half of the Noachian, the chemistry of near-surface waters gradually shifted from alkaline to near-neutral conditions to acidic conditions, and stable species shifted from carbonates, to phyllosilicates, to sulfates (Chapters 7, 9, 23, 24, 26).

As the thermal convection in the core tapered off and the magnetic dynamo disappeared in the Early Noachian, escape of Mars' early dense atmosphere was accelerated. No longer shielded by a magnetic field, the atmosphere was exposed to scavenging by the solar wind (Chapters 11, 26). Viking results showed that the current atmospheric D/H is 5 times that of Earth, testifying to the long-term sputtering of the atmosphere by the solar wind and the thermal escape of H (Chapter 22). The shift from early alkaline to later acidic conditions may have been the result of a combination of factors: the gradual fall in atmospheric pressure, the collapse of the greenhouse, the gradual loss of water as hydrogen escaped or ice was sequestered to the polar regions and the subsurface, and the long-term injection of sulfurous volcanic vapors into the environment by Tharsis and by other centers of early intense volcanism. The Independence Class rocks in the Columbia Hills may record the earlier slightly alkaline or neutral pH environment, but all other altered rocks and soils investigated in the Hills appear to have been altered by later acid-sulfate aqueous conditions, probably with low water-rock ratios (Chapters 23, 24). Likewise, the sulfate-rich sediments and hematite concretions of the Meridiani Planum Burns formations (cemented eolian sandstones likely derived from so-called "dirty" playa evaporites) date to the episode of Late Noachian sulfurous acidic waters (Chapters 4, 9, 14, 15, 23, 24, 26).

By the beginning of the Hesperian (estimated ~ 3.5 – 3.7 Ga; Table 1.2), the formation of valley networks by pluvial activity appears to have largely ceased. It is thought that as Mars continued to cool much of the water was trapped as ice in the upper kilometer or so. Episodic catastrophic outflow channels continued to burst forth throughout the Hesperian period (Chapter 26), possibly triggered by volcanic magmas interacting with the water ice stored in the crust. Through the Hesperian, volcanic and fluvial activity dramatically waned,

but isolated major events continued. The basaltic lava plains where the *Spirit* rover landed in the floor of Gusev crater are thought to date to the Hesperian. The Adirondack Class basalts on that plain exhibit minimal aqueous alteration (Chapters 4, 14, 15, 23) and resemble the young basaltic shergottite meteorites (Chapters 17, 22). Clearly, very little aqueous activity has occurred since these Hesperian basaltic plains were emplaced (Chapter 21).

1.5.4 The Amazonian and active processes today

The end of the Hesperian is estimated by Hartmann (2005) to be in the range 2.0–3.2 Ga (Table 1.2). By this estimate the Amazonian has lasted for $\sim 60\%$ of Mars' entire geologic history. There is some evidence for fluvial activity during the Early and Middle Amazonian but it is extremely sparse in contrast to the dense valley networks of the warmer, wetter Noachian or to the significant outflow channels of the less wet Hesperian (Chapter 26). During the Amazonian, the Martian surface appears to have evolved into the arctic desert that we see today. The Early Amazonian is marked by widespread volcanism throughout Amazonis Planitia that extends from Tharsis to Elysium (Figure 1.2). Tectonism also continued in these regions but at a lower level than in the Hesperian; by the Middle Amazonian it had effectively ceased (see Head *et al.*, 2001). Although volcanism in Amazonis Planitia declined throughout the Amazonian, what appear to be extremely young (10–50 Ma) lava flows are found near Olympus Mons and in southern Elysium Planitia. It seems improbable that Mars' volcanic lava eruptions stopped after 98% of Martian geologic time; episodic, quiescent volcanic activity in these regions probably continues through today.

With the single exception of ancient ALH 84001, all available Martian meteorites crystallized after 1.3 Ga and are Amazonian (Chapters 17, 22). As two-thirds are younger than 600 Ma and one-third are younger than 200 Ma, they appear fairly uniformly scattered throughout the Amazonian in age. Why the meteorite ages are skewed toward younger (Amazonian) ages, given that more than half of Mars' surface is Noachian and Hesperian, is largely a mystery. It has been suggested that perhaps only these young rocks are sufficiently resilient to survive the impact-driven transport to Earth (Chapter 17). Although the Amazonian meteorites are only weakly altered, they display small amounts of secondary aqueous minerals, including carbonates, clays, sulfates, and halite, indicating that subsurface aqueous fluids likely permeated these young rocks after crystallization (Chapters 17, 23). Perhaps some of these fluids came into contact with isolated subsurface deposits of ancient carbonates that had been sealed off from the surface environment and which thus survived the Late Noachian– to Early Hesperian–pervasive period of acid-sulfate alteration.

The Martian surface appears to have experienced very little aqueous activity since the Hesperian. Basaltic rocks of Hesperian age are found ubiquitously at all landing sites except at Meridiani Planum (although the Meridiani soil contains unaltered basaltic sand of unknown source;

Chapters 15, 20, 21). These basaltic rocks show minimal alteration, although many have surfaces that suggest weak leaching, silica glass coatings, eolian polish, and/or dust (Chapters 3, 4, 8, 12, 13, 14, 19). RAT grindings from the interiors of the fresh Hesperian basalts of the Gusev crater plain (Adirondack Class) show little to no trace of ferric iron (Chapter 13). The soils at all five landing sites appear quite similar. Mössbauer data show that the ubiquitous Laguna Class soils found in the Gusev crater plains, in the Columbia Hills, and on Meridiani Planum (on opposite hemispheres) are nearly identical both in content of primary igneous minerals and of the globally uniform ferric-rich clay-sized dust (Chapters 2, 4, 8, 9, 13, 14, 15). Evidently, basaltic sand has been homogenized by eons of saltation on a global scale or else the parental basalts are globally quite uniform. Unaltered olivine and magnetite show that these soils have not been exposed to liquid water for any appreciable length of time since the Hesperian (Chapters 15, 16). Eolian processes and occasional impacts dominate the Amazonian. In fact, MGS MOC observed the appearance of a number of small impact craters over the 10-year span of MGS observations (Malin *et al.*, 2006). MER made many direct observations regarding the role of current winds in mixing and shaping these deposits, including time-lapse movies of dust devils and microscopic observations of basaltic sand grain sizes that are optimal for transport by saltation (Chapter 20).

While variable amounts of H₂O and/or OH⁻ exist today in the equatorial soils and rocks, ranging from a few-to-several percent (from Odyssey GRS/NS, Chapters 5, 6) to tens of percent (for Paso Robles soil and the Meridiani outcrop; Chapter 23), most of this water is likely tied up in hydrated or hydroxylated minerals. Water ice is not stable at latitudes <45° unless buried by a largely impermeable layer (Chapter 6). However, modern gullies were discovered by MGS MOC at latitudes between 30° and 50° in both northern and southern hemispheres. Although dry landslides and discharge of subsurface liquid CO₂ have been proposed, most of the suggestions for gully formation involve liquid water in some form, either discharged from aquifers intercepting slopes or by a variety of models involving melting of ground ice or snow (Chapters 8, 9, 26). Recently, Malin *et al.* (2006) have discovered some gullies that have changed albedo (brightened) over several-year spans, which they ascribe to the action of liquid water released from subsurface aquifers or other sources. Although the evidence is inconclusive, these gullies offer the tantalizing possibility that liquid water occasionally issues from the subsurface today.

The most active processes on Mars today occur in the polar regions (Chapters 5, 6, 7, 8, 9, 10, 18, 25, 26). Roughly, a quarter of the entire atmosphere annually cycles into and out of the seasonal CO₂ polar caps; on the order of a meter of CO₂ condenses and snows onto the surface during the polar winters. After the seasonal CO₂ deposit (that extends to ~±55° latitudes) sublimates in the polar spring, Mars' permanent north polar and south polar residual caps (NPRC and SPRC) emerge. The polar regions contain most of the near-surface (upper meter) concentration of water ice, both in the permanent caps and cold-trapped in the

near-surface ice in the regolith (Chapters 5, 6, 25). Since the Viking Missions, the NPRC has been known to be composed of water ice, as it warms rapidly after the seasonal CO₂ disappears. By contrast, the surface of the SPRC was known to be CO₂ ice as its temperature remains near the CO₂ frost point after the seasonal cap is gone. Observations from recent missions show that the SPRC may actually be largely a permanent water-ice cap, but one that is covered by a 1–10 m veneer of CO₂ ice (Chapters 5, 6, 7, 25). Carved in the top of this CO₂ veneer are a series of smooth-walled, quasi-circular pits that form an exotic terrain dubbed “Swiss Cheese.” The pits bottom out on a flat resilient layer that is probably the top of the permanent residual water-ice cap. Monitoring of the size and shape of the pits with MGS MOC over periods of years reveals that they are expanding at 2–4 m/yr, indicating that they must reside in subliming layers of CO₂ ice and not of water ice (Chapter 25).

The residual ice caps (SPRC and NPRC) are stratigraphically the uppermost layers of the PLD. These vast complexes are concentrated north and south of roughly ±80° latitudes (Figure 1.1). The PLD were discovered in the 1960s with Mariner 7. They exhibit hundreds of flat-lying layers up to tens of meters thick; each PLD complex covers ~10⁶ km². In the north, the NPRC covers most of the PLD; in the south, the SPRC covers only a small central region (~10⁵ km²) of PLD. Evidently, formation of the PLD is directly coupled to the residual water-ice caps, and thus they likely contain records of past climates, perhaps extending back more than 10 Ma.

The polar CO₂ cycle exerts major control over the climate and responds to changes in orbital and obliquity (tilt of the rotation axis) variations (Chapter 26). Change in obliquity is the most important driver of climate change (e.g., Touma and Wisdom, 1993; Laskar *et al.*, 2004). During periods of low obliquity, the polar regions become colder, trap more water and CO₂, and cause the atmospheric pressure to fall. During periods of high obliquity, the poles are exposed to more insolation during polar summers and lose water to the equatorial regions. In extreme cases, most of the polar water ice could flow to lower latitudes, covering the surface globally with up to tens of meters of ice. Such ice flows could produce glaciers; evidence for their existence has indeed been observed (e.g., Lucchitta, 1981; Kargel *et al.*, 1995; Head *et al.*, 2005). At high obliquity, polar temperatures could rise to the melting point of ice, possibly generating liquid water in the polar regions (Chapter 26).

An area of anomalous behavior within the south polar seasonal CO₂ deposit has become known as the “cryptic” region (Chapters 7, 25). During retreat of the seasonal cap in the southern mid spring, this region becomes dark in visible-light images, first suggesting that the CO₂ had sublimed and that the region should begin to warm. However, thermal-IR measurements reveal that the cryptic region remains cold, near the frost temperature of CO₂. Two possible explanations are that either the CO₂ deposit is a coarse-grained slab (Chapters 9, 25) or that it is dirty CO₂ snow (Chapter 7). This anomalous region also exhibits bizarre features known as “black spiders,” seasonal albedo features appearing as dark round spots with halos and

fans. A model proposed for their formation (Kieffer *et al.*, 2006) involves CO₂ forming as a slab that may have embedded dust. As sunlight heats the dust grains, they migrate downward, effectively cleaning the slab; holes in the slab anneal behind them. Sunlight can then penetrate through the clean slab to a dark substrate, subliming CO₂ at the base. As CO₂ gas flows toward regions where it can vent, it scours the substrate and entrains dark dust that is finally jetted onto the surface. The physics of the model for this active Martian polar process is remarkably similar to a model invoked to explain active dark plumes observed erupting from the surface of Triton's nitrogen ice cap (Soderblom *et al.*, 1990).

1.6 OUTSTANDING QUESTIONS AND FUTURE CHALLENGES

As in any field of scientific exploration and research, the more we learn about the Martian surface, the deeper and more focused our questions become. Here we summarize some of the major outstanding questions relevant to the study of the composition, mineralogy, and physical properties of the Martian surface. These include old questions that have remained unanswered since the days of the Viking Missions, as well as some new ones that have emerged from the rich new knowledge gained over the last decade of Martian exploration.

1.6.1 Character of the Martian crust

The nature of the global dichotomy remains in debate, and is argued to be organized by early low-order mantle convection or by early large impacts into the northern plains. The existence of relic basin-scale impact features beneath the Amazonian sedimentary/volcanic plains suggests that the northern lowland crust may be as ancient as the southern cratered highlands. That the southern highland terrains stand several kilometers above the northern lowlands shows the crust to vary in thickness roughly between 30 km and 100 km and to be less dense than the mantle. What is the nature of this density contrast? Is it analogous to the lunar crust? Rocks of higher silica content such as andesitic basalts have been suggested as a component of the crust. If true, does this provide evidence for broad-scale early fractional crystallization of the crust? More detailed investigations of the ancient magnetized crust will certainly shed more light on the nature of the crust overall. Higher spatial resolution will help elucidate the depth of magnetization, the crustal thickness, early thermal profiles, and the basal structures of Tharsis and Elysium volcanic constructs and of large impact basins such as Hellas and Argyre.

1.6.2 Early aqueous chemistry

Did Mars' aqueous surface environment evolve from earlier alkaline or neutral-pH conditions to later very acidic conditions during the Middle-to-Late Noachian? Isolated evidence of phyllosilicates (clays) that require near-neutral pH to form appears in some older Noachian terrains; products of

sulfuric acid alteration abound in younger Noachian rocks at the MER landing sites. If this transition did occur, what caused the change from alkaline to acidic? Was early long-lived volcanism in Tharsis and Elysium a key factor? How profuse was early surface water, and when and how did it decline in abundance? Were the ephemeral shallow seas like those found in Meridiani Planum, evidenced by the acidic siliclastic evaporites and festoon cross-bedding textures of the Burns formation, ubiquitous across the Martian surface or were they rare, even unique to that region? Perhaps the high-regional concentration of hematite suggests the latter. Did an even more alkaline environment predate the phyllosilicates, and were significant abundances of carbonates ever deposited at the surface? Did subsequent highly acidic conditions then erase virtually all surface traces of carbonates and most traces of clays? Or did alkaline and acidic conditions coexist during this early epoch, with the alkaline conditions in the subsurface sealed off from the acidic conditions at the surface? Because we find both sulfate and carbonate secondary alteration minerals in young Amazonian meteorites, this latter scenario remains a realistic possibility.

1.6.3 Survival of primitive basaltic minerals

Although we have substantial evidence that acid-sulfate alteration was commonplace, perhaps even pervasive, across the Martian surface during the Late Noachian, it had to be quite limited in total effect. Other than the globally uniform bright red ferric-bearing dust, on average the surface rocks and soils are only weakly altered basalts. Chemically fragile minerals like olivine are mapped ubiquitously in low-albedo regions of the Noachian highlands. Basalt rocks on the Gusev crater floor have been exposed throughout the Amazonian and during much of the Hesperian (perhaps >3.5 Ga) and exhibit very minimal aqueous alteration. Ubiquitous runoff channels in the Late Noachian also seem inconsistent with widespread ancient exposures of olivine. How did primitive igneous minerals survive the early wet period? Clearly, surface water cannot have been around but for a fraction of time after these primitive minerals were exposed at the surface. Surface water must have been geologically short-lived, locally concentrated, and/or limited in volume. Only a small fraction of the Burns formation is consistent with deposition and evaporation of open shallow water; most of it consists of eolian dune deposits. Further, if the extent of the Burns formation is marked by the concentration of hematite mapped from orbit, it was also limited in region as well as duration. Was it simply that the combined volume and duration of liquid water at the near surface was too small to affect but a fraction of the bulk of the igneous crust? Was the limited nature and early decline of surface water tied to the loss of the atmosphere or to long-lived Tharsis/Elysium volcanism?

1.6.4 Martian meteorite enigmas

A number of major issues also remain in the interpretation of the SNCs. The first deals with their typically young crystallization ages. Given that more than half of Mars' surface terrains are Hesperian and Noachian (greater than about

3.5 Ga), why are 95% of the meteorite crystallization ages <1.3 Ga? Suggestions that this skewed age distribution arises because only young igneous rocks are sufficiently resilient to survive the cataclysmic journey to Earth or that thick debris mantles overly most of the ancient rocks are less than satisfying explanations. That a number of SNCs have very young Amazonian crystallization ages (<200 Ma) is exciting because it supports the notion that low-level, quiescent volcanism must continue through today, consistent with extremely sparse crater populations on some (estimated 10–50 Ma) volcanic flows. Where are these active volcanic regions and what are their modern eruption rates? The SNCs exhibit minor secondary alteration minerals, including carbonates and sulfates. Evidently, a variety of aqueous fluids have percolated through the subsurface in recent Amazonian time. What are these fluids and what are their sources? Distinct from terrestrial basalts, SNCs and Martian surface materials share basic characteristics (ferroan olivine and pyroxenes and sodic plagioclase) but they differ geochemically in other ways. For example, why do Gusev basalts and Bounce Rock (that closely resembles basaltic shergottites) exhibit higher K, higher Al/Si, and lower Mg/Si than do any of the SNC meteorites? Additionally, meteorites have much lower K than seen in surface materials. Have processes concentrated such volatile elements at the surface? Is the crust stratified with respect to such compositions?

1.6.5 Polar phenomena and climate change

In situ exploration of the deep polar regions remains a fundamental goal for future lander and rover missions. Observations from the surface of polar geologic processes and records, of the physics of active phenomena in the polar volatiles, and of atmospheric phenomena that control global weather systems, all offer a rich set of scientific opportunities. Direct investigation of active CO₂ ice layers, the “Swiss cheese” and “cryptic region,” are key targets for surface exploration. Most of the known inventory of water now resides in the upper meter of the polar regolith. But how much water is locked up in the upper few kilometers of the polar crust? What climatological records are held in the hundreds of strata in the polar layered terrains? How far back in time do they extend? Understanding the role of Mars’ changing eccentricity and obliquity in controlling the modern climate is of paramount importance for understanding the global migration of water. Does water episodically migrate from the polar regions to the equatorial areas where infrequent volcanism continues in Tharsis and Elysium? Is there occasional (10–100 Ma) interaction between volcanic eruptions and temporary equatorial water ice, perhaps resulting in rare aqueous environments even in the current geologic epoch? Are such events recorded in the polar layered terrains?

1.6.6 The search for life goes on

During 1996–2007, seven major NASA and ESA planetary spacecraft successfully achieved Mars orbit or landed on the surface (Table 1.1). These missions have been scientifically

prolific and, coupled with continuing analyses of Martian meteorites, have generated an enormous wealth of new information that permits us to sharpen and refocus our search for evidence of Martian life. We have “followed the water” and have begun to assemble a clearer picture of the chemical conditions in Mars’ early aqueous environment. We suspect that both slightly alkaline and extremely acidic aqueous environments existed in the Noachian. It is likely that alkaline conditions preceded acidic conditions, but perhaps they coexisted, isolated from one another regionally or as surface versus subsurface conditions. Ancient outcrops of clay minerals formed in less acidic conditions may be more likely to have harbored ancient evidence for life. Ancient carbonates were formed in ALH 84001 some 3.9 Ga. Around this time period there must have been conditions conducive for carbonate formation, but whether or not these conditions were only in the subsurface we do not yet know. Continued searches by orbiting spectrometers for clays, silica, carbonates, and other aqueous alteration minerals remain critical for potentially revealing ancient habitats. Modern habitable environments are most likely restricted to those containing subsurface liquid water. Carbonates and sulfates found in SNCs testify to the existence of subsurface briny liquids during the Middle and Late Amazonian. Climatic changes driven by oscillating obliquity could episodically generate conditions for surface water even during the current geological epoch. Search for such sites by orbiters is an essential task. Evidence suggested for liquid water in the formation of modern gullies is tantalizing. In our search for Martian life, ultimately, the return of carefully selected samples for analysis by the most sophisticated laboratory techniques will be required. Currently, an MSR mission is beyond at least the next decade in NASA’s planning horizon. But discovery of compelling surface or subsurface geological evidence of benign aqueous environments could certainly accelerate that schedule.

REFERENCES

- Beaty, D. W., M. A. Meyer, and the Mars Advance Planning Group, 2006 Update to “Robotic Mars Exploration Strategy 2007–2016,” Unpublished white paper, posted November 2006 by the Mars Exploration Program Analysis Group (MEPAG), <http://mepag.jpl.nasa.gov/reports/index.html>, 24pp., 2006.
- Bertka, C. M. and Y. Fei, Implications of Mars Pathfinder data for the accretion history of the terrestrial planets, *Science* **281**, 1838–40, 1998.
- Carr, M. H., *Water on Mars*, Oxford University Press, 1996.
- Carr, M. H., *The Surface of Mars*, Cambridge University Press, 2007.
- Chapman, M. (ed.), *The Geology of Mars: Evidence from Earth-based Analogs*, Cambridge University Press, 472pp., 2007.
- COMPLEX, *On NASA Mars Sample-Return Mission Options*, Washington, D.C.: National Academy of Sciences, 1996.
- COMPLEX, *Assessment of Mars Science and Mission Priorities*, Washington, D.C.: National Academy Press, 2003.
- Encrenaz, T., The atmosphere of Mars as constrained by remote sensing, *Space Sci. Rev.* **96**, 411–24, 2001.

- Folkner, W. M., C. F. Yoder, D. N. Yuan, E. M. Standish, and R. A. Preston, Interior structure and seasonal mass redistribution of Mars from radio tracking of Mars Pathfinder, *Science* **278**, 1749–52, 1997.
- Frey, H. V., A timescale for major events in early Mars crustal evolution. *Lunar Planet. Sci. Conf. XXXV*, Abstr. 1382, 2004.
- Greeley, R., R. O. Kuzmin, and R. M. Haberle, Aeolian processes and the effects on understanding the chronology of Mars, *Space Sci. Rev.* **96**, 393–404, 2001.
- Hartmann, W. K., Martian cratering 8: isochron refinement and the chronology of Mars, *Icarus* **174**, 294–320, 2005.
- Hartmann, W. K. and G. Neukum, Cratering chronology and evolution of Mars. In *Composition and Origin of Cometary Materials* (ed. K. Altwegg, P. Ehrenfreund, J. Geiss, and W. F. Huebner), Netherlands: Kluwer Academic, pp. 165–94, 2001.
- Head, J. W., R. Greeley, M. P. Golombek, *et al.*, Geological processes and evolution, *Space Sci. Rev.* **96**, 263–92, 2001.
- Head, J. W., G. Neukum, R. Jaumann, *et al.*, Tropical to mid-latitude snow and ice accumulation, flow and glaciation on Mars, *Nature* **434**, 346–51, 2005.
- Kargel, J. S., V. R. Baker, J. E. Beget, *et al.*, Evidence of ancient continental glaciation in the Martian northern plains, *J. Geophys. Res.* **100**, 5351–68, 1995.
- Kieffer, H. H., P. R. Christensen, and T. N. Titus, CO₂ jets formed by sublimation beneath translucent slab ice in Mars' seasonal south polar ice cap, *Nature* **442**, 793–6, 2006.
- Kieffer, H., B. Jakosky, C. Snyder, and M. Matthews (eds.), *Mars*, Tucson: University of Arizona Press, 1498pp., 1992.
- Klein, H. P., N. H. Horowitz, and K. Biemann, The search for extant life on Mars. In *Mars* (ed. H. H. Kieffer, B. M. Jakosky, C. W. Snyder, and M. S. Matthews), Tucson: University of Arizona Press, pp. 1221–33, 1992.
- Laskar, J., A. C. M. Correia, M. Gastineau, *et al.*, Long term evolution and chaotic diffusion of the insolation quantities of Mars, *Icarus* **170**, 343–54, 2004.
- Levin, G. V., Interpretation of new results from Mars with respect to life. In *Instruments, Methods, and Missions for Astrobiology VIII* (ed. R. B. Hoover, G. V. Levin, and A. Y. Rozanov), *Proc. SPIE* **5555**, pp. 126–38, 2004.
- Lucchitta, B. K., Mars and Earth: comparison of cold-climate features, *Icarus* **45**, 264–302, 1981.
- Malin, M. C., K. S. Edgett, L. V. Posiolova, S. M. McColley, and E. Z. N. Dobreá, Present-day impact cratering rate and contemporary gully activity on Mars, *Science* **314**, 1573–7, 2006.
- McCleese, D. J. and the Mars Advance Planning Group, *Mars Exploration Strategy 2007–2016*, NASA, Jet Propulsion Laboratory, Pasadena, California, <http://mepag.jpl.nasa.gov/reports/index.html>, 2006.
- McCleese, D. J. and the Mars Expeditions Strategy Group, *The Search for Life on Mars*, NASA, Jet Propulsion Laboratory, Pasadena, California, <http://mepag.jpl.nasa.gov/reports/index.html>, 2001 [written in 1996].
- MEPAG, the Mars Exploration Program Analysis Group, *Mars Scientific Goals, Objectives, Investigations, and Priorities* (ed. J. Grant), <http://mepag.jpl.nasa.gov/reports/index.html>, 31pp., 2006.
- Mishkin, A., *Sojourner: An Insider's View of the Mars Pathfinder Mission*, Berkeley, CA, 352pp., 2003.
- Muirhead, B. K. and W. L. Simon, *High Velocity Leadership*, New York: Harper Business, 1999.
- National Research Council Space Studies Board, *New Frontiers in the Solar System, An Integrated Exploration Strategy*, Washington, D.C.: National Academy of Sciences, 2003.
- Neumann, G. A., M. T. Zuber, M. A. Wicczorek, *et al.*, Crustal structure of Mars from gravity and topography, *J. Geophys. Res.* **109**, E8:E08002, pp. 1–18, 2004.
- Nimmo, F. and K. L. Tanaka, Early crustal evolution of Mars, *Ann. Rev. Earth Planet Sci.* **33**, doi:10.1146/annurev.earth.1133.092203.122637, 2005.
- Phillips, R. J., M. T. Zuber, S. C. Solomon, *et al.*, Ancient geodynamics and global-scale hydrology on Mars, *Science* **291**, 2587–91, 2001.
- Pieters, C. M. and P. A. J. Englert (eds.), *Remote Geochemical Analysis: Elemental and Mineralogical Composition*, Cambridge University Press, 594pp., 1993.
- Scott, D. H. and M. H. Carr, Geologic map of Mars. *USGS Misc. Inv. Ser. Map*, I-1083, 1978.
- Scott, D. H., K. L. Tanaka, R. Greeley, and J. E. Guest, Geologic maps of the western and eastern equatorial and polar regions of Mars. *USGS Misc. Inv. Ser. Map*, I1802-A, B, C, 1986–7.
- Soderblom, L. A., T. L. Becker, S. W. Kieffer, *et al.*, Triton's geysier-like plumes: discovery and basic characterization, *Science* **250**, 410–15, 1990.
- Solomon, S. C., O. Aharonson, J. M. Aurnou, *et al.*, New perspectives on ancient Mars, *Science* **307**, 1214–20, 2005.
- Strom, R. G., R. Malhotra, T. Ito, F. Yoshida, and D. A. Kring, The origin of planetary impactors in the inner solar system, *Science* **309**, 1847–50, 2005.
- Tanaka, K. L., The stratigraphy of Mars, *J. Geophys. Res.* **91**, E139–58, 1986.
- Tanaka, K. L., J. A. Skinner, and T. M. Hare, Geologic map of the northern plains of Mars, *USGS Sci. Inv. Map*, 2888, 2005.
- Tanaka, K. L., J. A. Skinner, T. M. Hare, T. Joyal, and A. Wenker, Resurfacing history of the northern plains of Mars based on geologic mapping of Mars global surveyor data, *J. Geophys. Res.* **108**, E4:8043, 24-1–24-32, 2003.
- Touma, J. and J. Wisdom, The chaotic obliquity of Mars, *Science* **259**, 1294–7, 1993.
- Wilhelms, D. E. and S. W. Squyres, The Martian hemispheric dichotomy may be due to a giant impact, *Nature* **309**, 138–40, 1984.
- Zuber, M. T., S. C. Solomon, R. J. Phillips, *et al.*, Internal structure and early thermal evolution of Mars from Mars global surveyor topography and gravity, *Science* **287**, 1788–93, 2000.

Historical context: the pre-MGS view of Mars' surface composition

W. M. CALVIN AND J. F. BELL III

ABSTRACT

This chapter summarizes the state of understanding of Mars surface composition in the decade before the arrival of Mars Global Surveyor and Mars Pathfinder (about 1987–1997), updating earlier historical reviews on this topic by Soderblom (1992) and Roush *et al.* (1993). Here we summarize analyses of telescopic and spacecraft spectroscopic data sets with reference to relevant terrestrial analog studies, laboratory measurements, and modeling work. The chapter is organized around a synthesis of surface mineralogy types that have been identified and searched for: unaltered mafic volcanic minerals; alteration products including oxidized iron, hydrated minerals, and phyllosilicates; the search for carbonates; early, if equivocal evidence of sulfates; and finally, polar deposits. We highlight the way that these precursor studies have influenced the design, selection, and implementation of the current generation of science investigations focused on unraveling the composition and mineralogy of the surface of Mars.

2.1 INTRODUCTION

Mars has been the object of detailed spectroscopic observations since the early 1960s. Initial telescopic work was followed by spatially resolved observations from the Mariner 6, 7 and 9 spacecraft, and multispectral optical and infrared observations with Viking both on the surface and from orbit. Early researchers were able to identify the strong bound water feature beyond $3\mu\text{m}$, the preponderance of oxidized iron contributing to the visible spectral shape, the presence of relatively unoxidized mafic, presumably volcanic minerals based on features near 1 and $2\mu\text{m}$, and that the seasonal polar cap was dominated by CO_2 ice and the residual north cap was made of water ice (e.g., Larson and Fink, 1972; Houck *et al.*, 1973; Pimentel *et al.*, 1974; Singer *et al.*, 1979; Clark and McCord, 1982). These early observations were summarized by Soderblom (1992), in the University of Arizona Press book, *Mars* (known by some as the “Mars bible”) and also by Roush *et al.* (1993). In the years preceding the launch and loss (just three days before orbit insertion) of the NASA Mars Observer orbiter in 1993, and the subsequent successes of NASA’s Mars Global Surveyor (MGS) orbiter and Mars Pathfinder (MPF) lander/rover in 1997, knowledge of the surface composition and mineralogy was advanced by acquisition and analysis of

data from the French Imaging Spectrometer for Mars (ISM) instrument on the Soviet Phobos 2 orbiter, by new ground- and space-based telescopic observations from the visible through the infrared, by new analyses of previous Mariner and Viking spacecraft data, and by theoretical modeling and laboratory studies of Mars analog materials.

This chapter briefly summarizes the progress in our understanding of surface material compositions from the late 1980s to the turn of the new millennium and prior to the advent of global mineral and compositional maps and interpretations from the MGS Thermal Emission Spectrometer (see Chapter 9), the Mars Odyssey GRS, NS, and THEMIS instruments (see Chapters 5, 6, and 10, respectively), and the European Space Agency (ESA) Mars Express orbiter OMEGA instrument (see Chapter 7), whose results are summarized elsewhere in this book. In keeping with other summaries and reviews (e.g., Soderblom, 1992; Roush *et al.*, 1993; Bell, 1996) surface composition is discussed according to mineralogical class. These classes are somewhat further subdivided by the wavelength range used to uncover their characteristics. We first present the best spectral profiles from the visible through the thermal infrared that were available at the end of this time frame, and then discuss spectral features in terms of primary mafic mineralogy, oxidative alteration products, and minerals suggesting more substantial alteration such as hydrated silicates, sulfates, and carbonates. The measured composition of polar volatiles are treated separately, followed by a brief synopsis of the state of knowledge regarding Martian surface composition and mineralogy prior to the advent of this last decade’s phenomenal explosion of new global- and regional-scale orbiter, lander, and rover compositional and mineralogic measurements.

2.2 TYPICAL SPECTRAL PROFILES

By the time of the arrival of MGS in orbit (1997), very good spectral profiles of typical Martian terrains from the visible through to the thermal infrared had been derived from the synthesis of data from multiple instruments and data sets. Mustard and Bell (1994) generated typical bright and dark region composite spectra by merging the then-best available ground-based telescopic and ISM measurements. Figure 2.1 shows spectra from Erard and Calvin (1997), who synthesized the Mustard and Bell (1994) data with that from the Mariner 6/7 Infrared Spectrometer (IRS) instruments.

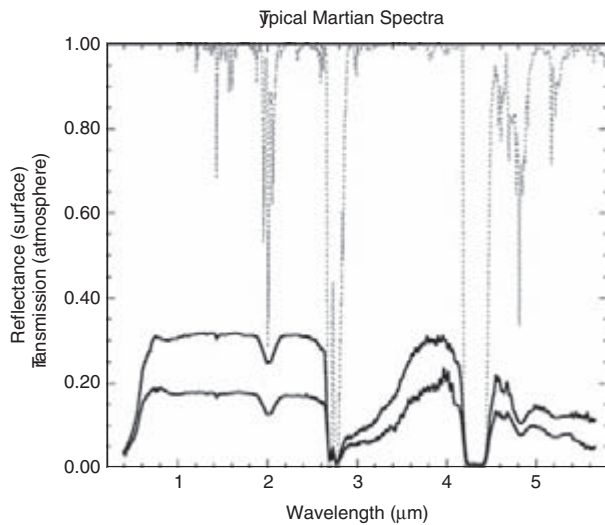


Figure 2.1. Surface reflectance spectra from 0.4 to 5.6 μm given by Erard and Calvin (1997). Data were synthesized using ground-based telescopic data from Mustard and Bell (1994) and space-based spectra from Phobos-2 ISM and Mariner 6/7 IRS data. Beyond approximately 3.5 μm , surface thermal emission begins to contribute to the measured signal; these spectra were corrected to reflectance using Kirchoff's law (reflectance = 1 – emissivity) and assuming Lambertian (cosine solar incidence angle) surface scattering behavior. A calculated transmission spectrum for the Martian atmosphere containing CO_2 , H_2O , O_3 , and CO from Crisp (1990) is shown as the gray dashed line.

Quite evident in these spectra are the strong red slope from 0.3 to 0.7 μm in both bright and dark regions, attributed to ferric minerals (likely iron oxides and hydroxides), the variable strength and position of an absorption feature near 0.9 μm caused by ferric minerals in bright regions and/or ferrous minerals in unaltered mafic materials in dark regions (likely volcanic rocks, sand, and dust high in Mg and Fe and moderately low in Si), and the strong, broad, and ubiquitous absorption feature beyond 3 μm from bound water and/or OH^- trapped in surface materials. Differences in the shape and center of the spectral peak near 0.8 μm were noted as well as variations in slope in the near-infrared (flat for bright regions, downward trending for dark regions). Weak features near 2.3 μm were observed first in telescopic data (McCord *et al.*, 1982) and subsequently explored both in ISM data (Murchie *et al.*, 2000) and higher resolution telescopic spectra (Clark *et al.*, 1990; Bell *et al.*, 1994); interpretations will be discussed later in this chapter. Early data also suggested absorption features near 1.9 μm , but these data were equivocal given the potential contribution from water in either the Martian or terrestrial atmospheres and the proximity to atmospheric CO_2 bands. In addition, scattering by atmospheric dust was found to contribute strongly to the spectral slopes of dark regions, but less so to bright regions (Erard *et al.*, 1994).

Also evident in Figure 2.1 are multiple strong absorptions by the intervening Martian atmosphere. The figure shows a calculated model of the Mars atmosphere from Crisp (1990) including nominal abundances of carbon dioxide, water, ozone, and carbon monoxide. The strongest CO_2 features

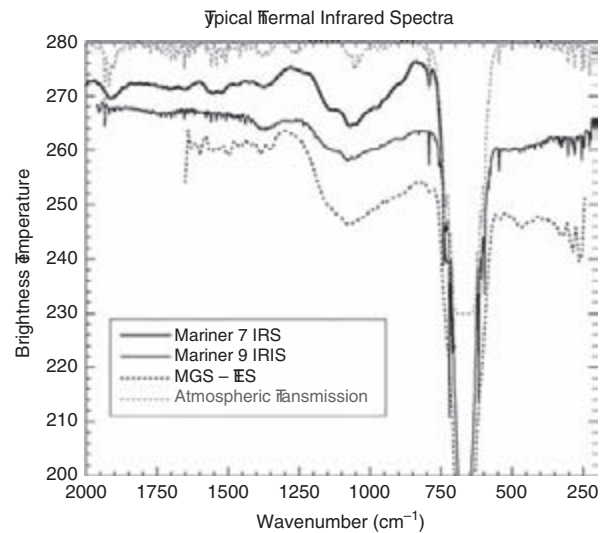


Figure 2.2. Typical thermal infrared spectra of Mars. The Mariner 7 IRS spectrum is an average of five spectra over Meridiani Sinus (M7 99:104). The Mariner 9 IRIS spectrum is an average of 1700 spectra acquired after orbit 100 (largely clear atmosphere). A typical TES spectrum from early in the mission is also shown. A calculated transmission spectrum for the Martian atmosphere multiplied by 50 and offset by 230 K is shown as the gray dashed line (Crisp, 1990).

occur near 1.4, 2.0, 2.7, from 4.2 to 4.4, from 4.6 to 5, and at 5.2 μm . Numerous other weak features occur from other minor constituents, as described in detail by Crisp (1990).

Figure 2.2 shows typical thermal-infrared spectra of Mars from the Mariner 7 IRS, the Mariner 9 Infrared Imaging Spectrometer (IRIS), and MGS/IES in the spectral range from 2000 to 200 cm^{-1} (5 to 50 μm) (Cimino and Calvin, 1997; Christensen *et al.*, 2000). When Mariner 9 arrived at Mars in 1971, the planet was in the midst of a large global dust storm. The spectral profile exhibited a strong 10- μm silicate signature and occasional structure from water ice in clouds, and water vapor (e.g., Hanel *et al.*, 1992). The Mariner 9 spectrum in Figure 2.2 is an average from IRIS data having emission angles $<60^\circ$, brightness temperature at 1300 $\text{cm}^{-1} > 260$ K, and orbit numbers >100 (meaning that the dust had largely settled from the atmosphere).

Clear atmosphere Mariner 9 spectra were combined with broadband emissivity from the Infrared Thermal Mapper (IRTM) of the Viking to show that there were spatial variations in surface infrared emissions (Christensen, 1998), a fact exploited successfully in follow-on observations from later Mars orbital infrared instrumentation. Mariner 7 IRS data were acquired during a clear atmospheric period at higher spatial resolution than IRIS, but with limited spatial coverage and with unavoidably strong variation in emission angle among the spectra, because the mission was a flyby not an orbiter. Those spectra were acquired only up to the strong atmospheric absorption at 700 cm^{-1} (14 μm) and show a broad and strong silicate envelope from 1250 to 850 cm^{-1} , and CO_2 “hot bands” at 1050 cm^{-1} , also seen with IRIS (Maguire, 1977; and Figure 2.2). Due to the strongly varying atmospheric component, only limited surface interpretations

of these IRS thermal-infrared spectra were attempted. However, the silicate band strength was shown to correlate at least in part with atmospheric pathlength, consistent with a contribution from atmospheric dust (Cimino and Calvin, 1997) and some IRS spectra were interpreted to be consistent with the presence of goethite (α -FeOOH), particularly in the Hellas region (Kirkland and Herr, 2000). Figure 2.2 again shows that numerous absorptions due to the Martian atmosphere contribute to observed spectra in the thermal infrared.

2.3 MAFIC MINERALOGY

Early in the history of Martian observations it was recognized that low-albedo regions had spectral shapes consistent with basaltic compositions, with some contribution from oxidized materials mixed at large spatial scales or as surface coatings (see reviews by Soderblom, 1992; and Roush *et al.*, 1993). In Martian dark region spectra the location of the reflectance peak at $0.75\ \mu\text{m}$ is more distinct than in bright regions, there is a well-defined absorption centered near $1.0\ \mu\text{m}$, and there is a general downward slope in reflectance toward longer wavelengths. All of these characteristics are consistent with near-infrared spectra of terrestrial basalts, and the implied presence of basaltic compositions in these spectra is consistent with spacecraft morphologic evidence of volcanic landforms and analysis of the basaltic SNC meteorites and their varying compositions (see Chapter 17). The presence of a red spectral slope in the visible, even in the dark regions, argued that the telescopic spectra of these regions were either being mixed with spectra of bright, dusty regions or that the basaltic minerals that compose the dark regions are covered or coated by variable amounts of brighter, ferric-rich dust. The bright regions are spectrally similar to some altered basaltic materials (e.g., Singer *et al.*, 1979; Singer, 1982), further strengthening the case for the presence of relatively unaltered mafic components in the dark regions.

A number of factors conspired to make the detailed identification and mapping of mafic minerals like olivine and pyroxene on Mars difficult using telescopic or spacecraft measurements prior to the 1990s. These factors included the low-spatial resolution of many of the measurements (and the subsequent dilution of small-scale spectrally unique signatures), the difficulty in quantitatively modeling mineral abundances from visible to near-IR spectra because of the confounding effects of particle size and multiple overlapping ferric and ferrous mineral absorption features, and even the effects of subtle variations in band shape, especially on the long wavelength side of the $1\text{-}\mu\text{m}$ feature, due to temperature effects. For example, Hinrichs and Lucey (2002) have shown that band edge shifts up to $0.05\ \mu\text{m}$ can occur for 40-K variations in surface temperature, a range that is routinely encountered on the Martian surface during the daytime.

With data from the Phobos-2 ISM instrument (Bibring *et al.*, 1990), detailed spatial variability in the spectral shape between 0.76 and $3.16\ \mu\text{m}$ was observed at high-spatial resolution for the first time. In particular, detailed definition

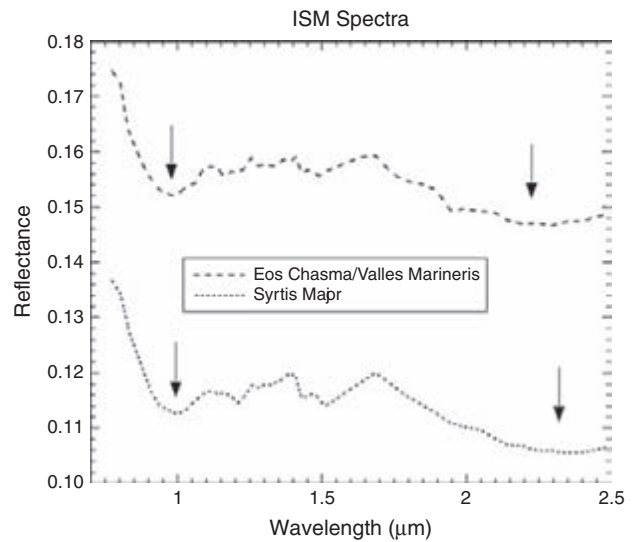


Figure 2.3. Representative Phobos-2 ISM spectra showing variations in the broad mafic absorption features near 1 and $2\ \mu\text{m}$.

of the “ $2\text{-}\mu\text{m}$ ” pyroxene feature was possible. The “ $2\text{-}\mu\text{m}$ ” band is a broad envelope centered between 2.0 and $2.3\ \mu\text{m}$ in pyroxenes, and typically occurs at longer wavelengths in ISM spectra. In addition, subtle differences in band centers near $1\ \mu\text{m}$ were observed (e.g., Mustard *et al.*, 1997; Murchie *et al.*, 2000; Figure 2.3). Models of band center shifts of both the $1\text{-}\mu\text{m}$ and the $2\text{-}\mu\text{m}$ features were used to fit these spectra with combinations of low- and high-Ca pyroxenes (e.g., Mustard and Sunshine, 1995; Mustard *et al.*, 1997). This 2-pyroxene mineralogy dominated by low-calcium pyroxene is uncommon on Earth, but characteristic of SNC meteorites and has implications both for mantle composition and evolution (see Chapter 17).

Parts of Lunae Planum and Syrtis Major were found to lack a $2\text{-}\mu\text{m}$ band (Murchie *et al.*, 2000) and Nili Patera was found to need a contribution from a feature near $1.2\ \mu\text{m}$ to best match the spectrum (Mustard and Sunshine, 1995). While the potential for olivine to contribute to the shape of the $1\text{-}\mu\text{m}$ absorption feature was suggested in the late 1970s, this interpretation was considered inconclusive given the poor spatial resolution of the data and the calibration challenges of observing through the Earth’s (and Martian) atmosphere (see the discussion in Roush *et al.*, 1993). In order to fit the ISM spectra of Nili Patera, it was noted that the additional absorption near $1.2\ \mu\text{m}$ was likely due to a combination of low- and high-Ca pyroxenes, rather than other mineral phases that have features in this region such as plagioclase or olivine. While Mustard and Sunshine (1995) considered the inclusion of olivine, it was below the detection limits of their models. In retrospect, given the identification of abundant olivine in Nili Fossae by MGS-TES (Hoefen *et al.*, 2003) and its subsequent widespread identification in higher resolution orbital and, eventually, surface rover data (e.g., Morris *et al.*, 2004; Bibring *et al.*, 2005; Hamilton and Christensen, 2005), it seems plausible that olivine may also contribute to the shape of the near-infrared spectra at this location.

SNC meteorites represent samples of the primary igneous mineralogy of Mars (see Chapter 17). During this era, a number of researchers measured the spectra of SNC meteorites in an effort to correlate remotely sensed spectra of Mars with these samples. For example, Sunshine *et al.* (1993) applied the Modified Gaussian Model (MGM) to interpret the spectrum of Elephant Moraine A79001 in terms of calcic pyroxene variations associated with two different basaltic lithologies observed in the meteorite. Additional studies of SNCs using the MGM method to assess pyroxene components include Schade and Wäsch (1999) to quantify pigeonite and augite in Zagami and Nakhl and McFadden and Cline (2005) who fit 9 SNCs for olivine, pyroxene, and augite. Bishop *et al.* (1998) measured ALH 84001, particularly for weak features from minor organics and carbonates. Hamilton *et al.* (1997) measured samples from the three major SNC lithologies in thermal emission in order to correlate with spectra from TES. All of these studies showed strong links between laboratory-derived meteorite spectra and the best available Mars remote sensing data sets, across a wide range of wavelengths, and all ultimately provided further support for what was then still a controversial hypothesis that the SNCs were from Mars.

2.4 IRON OXIDES AND HYDROXIDES

Mars is reddish brown because of the absorption of ultraviolet to blue (and to a lesser extent green) light by iron-bearing minerals on its surface. Many telescopic observations of Mars have been performed during the past century with the explicit goal of identifying and quantifying the composition of the iron-bearing minerals on the surface and in the airborne dust (see, for example, the review by Bell, 1996). Fundamental to understanding the history and evolution of Martian weathering processes is determining to what extent physical, chemical, and/or photo-oxidative weathering contribute to or control alteration of the primary basaltic materials. The amount of water involved in dissolution and hydrolysis of mafic minerals is key to determining if the surface environment was more clement at an earlier time (e.g., Gooding *et al.*, 1992). To within a few percent, the overall shape of the mean visible to near-IR spectral reflectance curve of Mars has been known since the late 1960s. More recent telescopic and spacecraft observations and reinterpretations of previous data sets have concentrated on providing more specific information on band centers, band depths, and the spatial distribution of observed spectral features, in order to further constrain the specific iron oxide and oxyhydroxide components that may contribute to the visible spectral shape.

Telescopic spectra showed that absorption band positions in most bright regions on Mars are consistent with the presence of a small amount (less than 5%) of well-crystalline “red” hematite (submicron- to several micron-sized grains of $\alpha\text{-Fe}_2\text{O}_3$) (e.g., Morris *et al.*, 1989; Bell *et al.*, 1990). Further, the relative weakness of the red hematite absorption features combined with the flat near-IR character and intense but

smooth reflectance drop-off from the visible down to the near UV in typical Mars spectra argued for the presence of a matrix of much more poorly crystalline or nanophase ferric-bearing materials (e.g., Morris *et al.*, 1989, 1993; see Bell, 1996, for a thorough review). Differences in the red hematite abundance and distribution between and among bright and dark regions have been inferred from higher resolution multispectral imaging and imaging spectroscopic observations from HST, ISM, and even Viking Orbiter measurements (e.g., Geissler *et al.*, 1993; Mustard and Bell, 1994; Bell *et al.*, 1997).

Significant effort has also been expended exploring the spectral properties of other Fe^{3+} -bearing materials that could be consistent with the available data. These minerals include palagonite, ferrihydrite, iron-substituted montmorillonites, lepidocrocite, and iron-bearing hydrated sulfates such as jarosite and schwertmannite (Singer, 1982; Burns, 1987; Banin *et al.*, 1992; Bishop *et al.*, 1993; Morris *et al.*, 1993, 1996; Bishop and Murad, 1996; Table 2.1). Exploration of these terrestrial materials supports the contribution of iron oxide and oxyhydroxide components to the visible wavelength spectral shape of Mars, even though the spatial resolution and fidelity of the available Mars data prior to the 1990s, combined with confounding effects like particle size, overlapping absorption features, and the pigmentary nature of fine-grained iron oxides, did not allow the identification of other specific ferric phases.

In the mid infrared, early studies suggested that the spectra from Mariner 9 IRIS were most consistent with at most a thin surface patina or staining of iron oxide on underlying silicates (Hunt *et al.*, 1973; Toon *et al.*, 1977). Bell *et al.* (1995) and Roush and Bell (1995) compared modern laboratory measurements of iron oxides, hydroxides, and palagonitic material with Mariner 7, Mariner 9, and telescopic mid infrared data. They showed that nanophase ferric oxide components have different spectra than crystalline forms. These components should be identified based on well-resolved features at longer wavelengths (lower wavenumbers) but they concluded identification would require both high signal-to-noise and improved spatial resolution.

Ultimately, detailed orbital studies and *in situ* studies have proven that there are indeed many diverse kinds of ferrous iron-bearing silicates (olivine, pyroxene, ilmenite, magnetite) and ferric iron-bearing oxides, oxyhydroxides, and oxyhydroxy-sulfates (hematite – both “red” and coarse-grained “gray” varieties, goethite, magnetite, nontronite, jarosite, and other as-yet unidentified ferric sulfates) that occur on Mars. These discoveries, outlined in more detail in other chapters throughout this book (see, for example, Chapters 9, 14, 15, and 16), have vindicated the original telescopic and early spacecraft searches for these climatically diagnostic mineral species. However, the isolated and sometimes rare spatial occurrence of the most interesting iron oxide and hydroxide phases amidst a virtual sea of globally homogenized nanophase ferric oxide dust grains in the surface soils and the atmospheric aerosols have also pointed out the critical need for extremely high-spatial resolution to enable their detection.

Table 2.1. *Minerals detected, inferred, or sought in historical Mars observations*

Mineral or material	Notes, results	Example references
Carbonates: e.g., Calcite (CaCO_3); Siderite (FeCO_3); Magnesite (MgCO_3); Scapolite ($\text{Ca}_4\text{Al}_6\text{Si}_6\text{O}_{24}[\text{CO}_3]$) Hydrous carbonates: e.g., Artinite ($\text{Mg}_2\text{CO}_3(\text{OH})_2 \cdot 3\text{H}_2\text{O}$); Hydromagnesite ($\text{Mg}_5(\text{CO}_3)_4(\text{OH})_2 \cdot 4\text{H}_2\text{O}$)	Simple carbonate phases not detected in significant abundances; minor amounts possible in dust and in some spectra. hydrated forms lack strong carbonate features. Telescopic evidence for surface bicarbonate anions, but specific identification uncertain.	McKay and Nedell (1988); Clark <i>et al.</i> (1990); Pollack <i>et al.</i> (1990); Bell <i>et al.</i> (1994); Calvin <i>et al.</i> (1994)
Sulfates: e.g., Kieserite ($\text{MgSO}_4 \cdot \text{H}_2\text{O}$); Gypsum ($\text{CaSO}_4 \cdot 2\text{H}_2\text{O}$); "Polyhydrated sulfate" [$(\text{Fe}, \text{Mg}, \text{Ca}) \cdot n\text{H}_2\text{O}$]; Anhydrite (CaSO_4); Jarosite [$(\text{K}, \text{Na})\text{Fe}_3(\text{SO}_4)_2(\text{OH})_6$]	Telescopic evidence for SO_4^{2-} anionic group absorptions but specific identification of any of these phases was uncertain. Specific sulfate identifications ultimately came from later MER and OMEGA measurements (see Chapters 7 and 15).	Burns (1987); Pollack <i>et al.</i> (1990); Blaney and McCord (1995); Bell (1996)
"Red" hematite: (α - Fe_2O_3 , μm -sized particles)	Identified in telescopic and ISM spectra from crystalline ferric bands near 0.65 and 0.9 μm .	Bell <i>et al.</i> (1990); Murchie <i>et al.</i> (1993)
"Nanophase" ferric oxides: e.g. (α - Fe_2O_3 , nm-sized particles)	Inferred from telescopic, spectral analog studies as the strongly pigmenting material responsible for the visible color of Mars, but lacking crystalline ferric absorptions in the near-IR.	Morris <i>et al.</i> (1989, 1990, 1993)
Goethite: (α - FeOOH)	Inferred from analysis of some Mariner IRS and Viking orbiter multispectral images; definitive identification uncertain.	Geissler <i>et al.</i> (1993); Kirkland and Herr (2000)
Palagonite	Field term for altered basaltic tephra; many are visible to near-IR spectral analogs to Mars, probably as a result of the presence of nanophase hematite.	Singer <i>et al.</i> (1979); Singer (1982); Roush <i>et al.</i> (1993); Morris <i>et al.</i> (1993); Clancy <i>et al.</i> (1995)
Phyllosilicates: e.g., Montmorillonite (Al, Mg smectite); Nontronite (Fe smectite); Greenalite, Chamosite, Cronstedtite (Fe serpentines)	Weak bands in the 2.0 to 2.5 μm range detected in some telescopic and ISM spectra, but specific layer silicate identification equivocal.	Hunt <i>et al.</i> (1973); Toon <i>et al.</i> (1977); McCord <i>et al.</i> (1978); Singer <i>et al.</i> (1979); Bell and Crisp (1993); Murchie <i>et al.</i> (1993); Calvin (1998)
Pyroxene: e.g., Low-Ca (LCP): Enstatite ($\text{Mg}_2\text{Si}_2\text{O}_6$); Pigeonite ($[\text{Mg}, \text{Fe}, \text{Ca}]\text{Si}_2\text{O}_6$); High-Ca (HCP): Diopside ($[\text{Ca}, \text{Mg}, \text{Fe}]\text{Si}_2\text{O}_6$); Augite ($[\text{Ca}, \text{Na}, \text{Mg}, \text{Fe}](\text{Si}, \text{Al})_2\text{O}_6$)	Identified in telescopic and ISM spectra from distinctive 1- and 2- μm absorption features. Both LCP and HCP detected and mapped based on band center variations tied to laboratory pyroxene spectral studies.	McCord <i>et al.</i> (1978, 1982); Roush <i>et al.</i> (1993); Mustard and Sunshine (1995); Mustard <i>et al.</i> (1997); Murchie <i>et al.</i> (2000)
Olivine: Forsterite (Mg_2SiO_4); Fayalite (Fe_2SiO_4)	Inferred from analysis of some telescopic studies from weak absorption near 1.2 to 1.5 μm , but definitive identification uncertain.	Huguenin (1987); Roush <i>et al.</i> (1993)
"Hydrated minerals"	Detected telescopically and by IRS at the 1–3 wt.% level based on ubiquitous presence of 3- μm band, but specific hydrated mineral identification uncertain.	Sinton (1967); Houck <i>et al.</i> (1973); Pimentel <i>et al.</i> (1974); Murchie <i>et al.</i> (1993, 2000); Calvin (1997); Erard and Calvin (1997)
Other ferric oxides, oxyhydroxides, or oxyhydroxysulfates: e.g., Lepidocrocite (γ - FeOOH); Ferrihydrite ($\sim\text{Fe}_2\text{O}_3 \cdot n\text{H}_2\text{O}$); Schwertmannite ($\sim\text{Fe}_8\text{O}_8(\text{OH})_6\text{SO}_4$); CO_2 ice	Inferred from analysis of some telescopic studies from visible color and ferric absorption band near 0.9 μm , but definitive identification uncertain. Detected in both seasonal polar caps.	Burns (1987); Banin <i>et al.</i> (1992); Bishop and Murad (1996); Morris <i>et al.</i> (1996)
H_2O ice	Detected in north residual polar cap and as an enhancement in the edge of the seasonal cap.	Herr and Pimentel (1969); Larson and Fink (1972) Clark and McCord (1982); Calvin and Martin (1994)

2.4.1 Aqueous alteration minerals

The first spectral indications of aqueous alteration of Martian surface materials came from the identification of bound water from a large, broad absorption feature beyond 3 μm (Sinton, 1967; Houck *et al.*, 1973). This band was observed by both IRS and ISM, and simple band ratios suggested variations in band strength with either latitude (Pimentel *et al.*, 1974) or geographic location (Murchie *et al.*, 1993). Murchie *et al.* (2000) noted that small regions of both bright and dark areas observed by ISM showed anomalous behavior with stronger 3- μm band depth. They suggested hydrated ferric minerals and/or sulfates, but the data could not provide evidence for specific phases. Both Calvin (1997) and Baldrige and Calvin (2004) found hydration increases over both Aram Chaos and Meridiani, the largest coarse-grained hematite locations identified from orbit by TES (Christensen *et al.*, 2001). This was interpreted as evidence for other hydrated minerals at these sites, and supported an aqueous formation model for the bulk hematite. Calvin (1998) proposed that low-albedo phyllosilicate minerals might be responsible for the increased hydration in dark regions. In retrospect, it appears likely that IRS was sensitive to the hydrated sulfates now known to be a substantial component of outcrop rocks in Meridiani (e.g., Squyres *et al.*, 2004). Data from IRS and ISM only overlap in Ganges and Eos Chasmae, and the spatial resolution and viewing geometry are different between the two instruments. Yet there is agreement in areas that are mapped as slightly more hydrated than average by both instruments in the region of overlap. Milliken and Mustard (2005) have developed a normalized optical path length that uses this 3- μm feature to quantify water content and which appears promising for its application on Mars, especially as hydrated minerals may make some contribution to the water-equivalent-hydrogen signal observed by the Mars Odyssey Gamma Ray and Neutron Spectrometers (e.g., Fialips *et al.*, 2005; see Chapters 5 and 6).

Weak but distinct absorption features in the spectral range from 2 to 2.5 μm were observed in the earliest telescopic data sets and subject to additional high-spectral resolution observations over time (e.g., McCord *et al.*, 1978; Singer *et al.*, 1979; Clark *et al.*, 1990; Bell and Crisp, 1993; Bell *et al.*, 1994). Initial interpretations focused on phyllosilicate minerals, which have known metal-OH overtone features in this wavelength range. Bicarbonate (HCO_3) and bisulfate (HSO_4) anions in framework silicates (i.e., scapolite) were proposed by Clark *et al.* (1990), though this was viewed skeptically at the time. High-spectral resolution observations and models clearly show contributions from carbon monoxide in the Martian atmosphere in this spectral range and some features appear to originate from telluric, Martian, or solar atmospheric absorption features (Bell *et al.*, 1994). Both Clark *et al.* (1990) and Bell *et al.* (1994) showed that at least some of the narrow, weak features seen in Mars spectra in the 2.0- to 2.5- μm region were due to surface mineralogy, however. Calvin *et al.* (1994) modeled this spectral range in IRS data with hydrous carbonate minerals and Murchie *et al.* (2000) interpreted ISM absorptions in these wavelengths

as resulting from metal-OH overtone vibrations in poorly crystalline clay minerals.

Spectroscopic observations by the Mariner 9 IRIS instrument detected spectral features near 9.0- μm in the atmospheric dust that were interpreted to be most consistent with montmorillonite (Hunt *et al.*, 1973) or a basalt-montmorillonite mixture (Toon *et al.*, 1977). More recent re-analyses of the IRIS measurements have shown that poorly crystalline weathering products like palagonite may in fact be more consistent with the data than smectite clay, however, based on improved knowledge of the optical constants of palagonites and on the scattering properties of atmospheric dust particles (e.g., Roush *et al.*, 1993; Clancy *et al.*, 1995). Modeling of Martian aerosols using Infrared Space Observatory data showed narrow features in the 2.7- μm region, suggesting a phyllosilicate composition of the dust (Fedorova *et al.*, 2002), and optical properties of dust aerosols determined from the surface by the Imager for Mars Pathfinder also suggested platy (clay) grains (Markiewicz *et al.*, 1999).

There have been many spectroscopic searches for sulfate and carbonate minerals on Mars in order to try to quantitatively substantiate numerous theoretical and indirect arguments for the occurrence of these phases. Most analyses during this era were inconclusive because of poor spatial resolution or calibration challenges related to difficult ground-based telescopic observations. The most convincing results, though still largely viewed as equivocal, are those of Blaney and McCord (1995) and Pollack *et al.* (1990). Blaney and McCord (1995) detected an absorption feature near 4.5- μm in telescopic spectra from Mauna Kea that was interpreted as an SO_4^{2-} overtone band in sulfates in the Martian surface and/or airborne dust. Careful atmospheric modeling revealed that this feature is probably not due to any known species in the Martian atmosphere; however, the specific mineralogy responsible could not be identified. Pollack *et al.* (1990) used the Kuiper Airborne Observatory to obtain high-quality spectra from 5.4 to 10.5 μm . These data showed evidence for spectral features due to carbonate (near 6.7 μm) and sulfate (near 8.7 and 9.8 μm) anionic complexes in the airborne dust. Again, however, specific mineralogies could not be identified. Lellouch *et al.* (2000) used the Infrared Space Observatory (ISO) to obtain globally averaged spectra at extremely high-spectral resolution. They identified several absorption features at 5.7, 6.3, 7.2, and 11.1 μm in addition to the silicate envelope from 8 to 12 μm . They interpreted the features at 7.2 and 11.1 μm as consistent with carbonates, but found no precise match among existing library spectra, and could not determine if the possible carbonate occurred either on the surface or in the airborne dust due to the disk-integrated nature of the observations.

2.4.2 Polar volatiles

Spectroscopic observations have established that both seasonal ice caps primarily consist of CO_2 ice (e.g., Herr and Pimentel, 1969; Larson and Fink, 1972) and that the north residual cap is primarily composed of water ice (e.g., Clark

and McCord, 1982). Summertime temperature measurements and atmospheric water vapor abundance mapping support these observations for the north residual cap (Farmer *et al.*, 1976; Kieffer *et al.*, 1976) and show that the upper surface of the southern residual cap is primarily CO₂ (Kieffer, 1979; Davis and Wanio, 1981). While small amounts of CO₂ may exist in the interior of the residual caps as ice mixed with water and dust, or in clathrate form (CO₂ molecules physically enclosed within the crystal structure of H₂O ice), thermal modeling and the rheology of CO₂ ice do not support substantial CO₂ in the interiors of either the northern or southern ice sheets (Mellon, 1996; Nye *et al.*, 2000). Extensive summaries of the relevant historical work on the polar layered deposits and volatile caps have been published by Thomas *et al.* (1992), James *et al.* (1992), and Jakosky and Haberle (1992).

A large number of polar studies occurred in the decade before the arrival of MGS, and the discussion here focuses on compositional rather than geologic, morphologic, or stratigraphic analyses. Efforts to understand the volatile content and the physical properties of the seasonal and residual ice caps emphasized new laboratory studies, particularly of carbon dioxide ices, data mining of Viking and Mariner data sets for thermal modeling, seasonal variations, and compositional constraints, and new observations with HST and other telescopes.

Hansen (1997) determined the optical constants of solid CO₂ using clear crystals. Calvin and Martin (1994) analyzed Mariner 7 data of the seasonal cap, showing an enhancement of water ice at the receding cap edge, strong spatial heterogeneity in the retreating cap spectra, and models that suggested the late seasonal cap was “more like glacier ice with cracks and bubbles” rather than a fine snow pack or frost. Figure 2.4 shows the spectrum of this late seasonal cap observed by Mariner 7 compared with models of water and carbon dioxide frosts based on Hapke (1993) and using modern optical constants (Warren, 1984; Hansen, 1997). The temperature dependence of the spectrum of water ice is well known (e.g., Fink and Sill, 1982; Grundy and Schmitt, 1998) and particularly at colder temperatures the development of a narrow feature at 1.65 μm will be observed, in addition to changes in band shapes between amorphous and crystalline water ice.

Paige *et al.* (1994) and Paige and Keegan (1994) mapped the thermal inertia (a measure of a material’s resistance to changes in temperature) and albedo of the north and south residual caps, respectively, using Viking Orbiter data. They noted that much of the north polar layered deposits appear underlain by solid ice or ice-cemented soils, in contrast to those in the south. They also noted that atmospheric conditions have a significant effect on derived albedo and thermal inertia, in particular atmospheric dust contributed to anomalously low-observed thermal emission from the southern residual cap in the Viking data. Paige *et al.* (1994) also noted frost cover variations between Mariner 9 and Viking that were further explored by Bass *et al.* (2000) and Bass and Paige (2000). Bass *et al.* (2000) modeled the northern residual cap composition and found that less dust is required for their model to match the observations if the

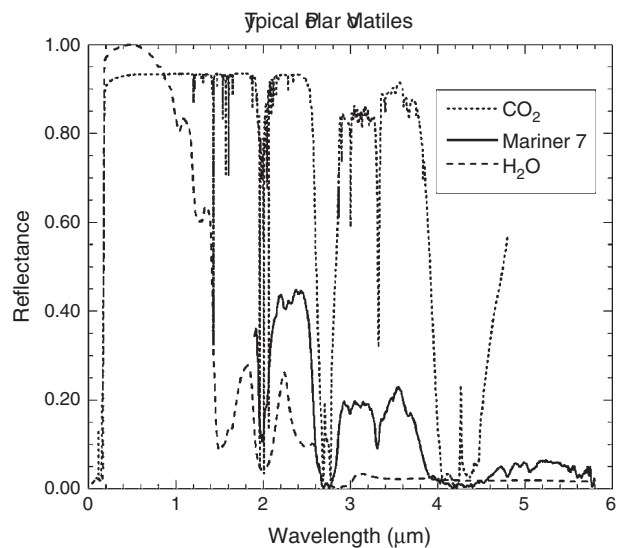


Figure 2.4. Polar volatiles. Calculated spectra for water (200 μm) and carbon dioxide (100 μm) frosts compared with a Mariner 7 spectrum of the receding seasonal cap. Strong features at 2.28 and 2.34 μm in the Mariner data are consistent with large pathlengths in ice and suppression of the level beyond 3 μm is attributed to minor amounts of water ice.

water ice is coarse-grained, and more if it is fine-grained, consistent with earlier results from Kieffer (1990). The amount of dust within the residual water ice remained largely unconstrained, however, because good estimates of the ice grain size are not possible with optical data alone.

Finally, James *et al.* (1996) and Cantor *et al.* (1998) reported on the style and rate of seasonal ice cap recession as observed by HST, in the south and north, respectively. Cantor *et al.* (1998) were able to observe and model the increase in albedo and decrease in the red/violet color ratio as the north seasonal CO₂ ice cap sublimates and exposes the residual H₂O-ice layer.

2.5 SUMMARY: POISED FOR A NEW ERA

In the decade of Mars exploration prior to the start of global high-resolution geologic and mineral mapping by the MGS mission, telescopic, laboratory, and precursor spacecraft data coupled with novel modeling approaches improved our understanding of the compositional variability of the surface of Mars, the planet’s ferric and mafic mineralogy, and the relationship between SNC meteorites and remotely sensed data. Pyroxene was known to be a major component of the low-albedo terrains from telescopic studies and Phobos-2 ISM measurements, and equivocal evidence for olivine had been found. Telescopic detection of iron oxide minerals and refined interpretations of color data from the Viking and Mars Pathfinder missions showed that crystalline iron oxides are not a major component of the soils. Rather, nanophase ferric oxides dominate the visible to near-IR spectral properties of the bright regions. While numerous models and observations suggested the possible

presence of phyllosilicates, carbonates, and sulfates, there was no consensus on the interpretation of weak spectral features and no “smoking gun” that uniquely identified specific alteration minerals. In retrospect, this appears to have been mostly a manifestation of the low-spatial resolution of the early spectroscopic searches, combined with what has turned out to be the very small-scale, spatially restricted occurrences of the most interesting mineral phases on Mars. The 3- μm water of hydration feature was found to be ubiquitous, but initial focused studies showed evidence for regional variations in hydration band strength that proved to be correlated with areas later identified as keys to the aqueous history of the planet.

Seasonal polar caps were shown to be ice “sheets” rather than frost or snow deposits, and seasonal and interannual variability were identified and characterized. Models demonstrated that the south perennial cap could not be solid CO_2 ice. Major open questions included the nature and occurrence of specific alteration minerals associated with polar volatiles and the amount of dust in the seasonal and residual ice caps.

This early work set the stage for new observations and interpretations from instruments onboard the Mars Global Surveyor, Mars Odyssey, and Mars Express orbiters. TES has now globally mapped the planet's mafic and primary silicate mineralogy at spatial scales of a few kilometers (e.g., Christensen *et al.*, 2000; Bandfield, 2002; see Chapter 9). New observations are also beginning to constrain polar deposits and alteration minerals. The residual and seasonal ice caps have shown to be host to numerous enigmatic properties and processes (Thomas *et al.*, 2000, 2005), and water ice has been observed in the south polar residual cap (Bibring *et al.*, 2004; Titus, 2005). As described in later chapters, Mars Express OMEGA spectrometer observations are found to be consistent with the presence of phyllosilicates and sulfates (Gendrin *et al.*, 2005; Langevin *et al.*, 2005; Poulet *et al.*, 2005; see Chapter 7). While no large-scale carbonate deposits have yet been identified on the surface at the scale of the available orbital (or surface lander, rover) measurements, recent models of TES data suggest a small carbonate component in the atmospheric dust (Bandfield *et al.*, 2003). Other terrestrial analog studies and focused regional studies with TES data have been interpreted as indicating evidence for hydrated sulfates, small amounts of carbonates, and possibly clays (e.g., Bishop *et al.*, 2004; Noe Dobrea *et al.*, 2006).

Evidence for specific sulfates widely distributed on Mars is convincing, thanks to *in situ* “ground truth” surface data sets from the Mars rovers *Spirit* and *Opportunity* (see Chapters 4, 13, 14, and 15 for details). Evidence for phyllosilicate minerals appears to be emerging from both surface and orbital observations (see Chapters 4, 7, and 23 for details). However, definitive identification of specific carbonate species from multiple wavelengths and instruments, and community consensus surrounding any carbonate identification, remains elusive. With evidence mounting that Mars once had warmer and wetter epochs, and presumably a thicker CO_2 -rich atmosphere, the question “Where are the carbonates?” remains as vexing today as it was when it

was first posed by the Mars community more than 25 years ago (e.g., Pollack *et al.*, 1987; Fanale *et al.*, 1982, 1992; Burns, 1993).

The decade since the arrival of Mars Pathfinder and Mars Global Surveyor has been one of tremendous growth in our knowledge of the composition and history of the Martian surface. While previous advances had been made in our understanding of the surface mineralogy and composition and their spatial distribution, the onslaught of new instruments and techniques are now allowing us to view Mars in a wholly new light.

ACKNOWLEDGMENTS

We thank John Pearl for providing the Mariner 9 IRIS spectrum in Figure 2.2, and Jack Mustard for providing the Phobos-2 ISM spectra in Figure 2.3. This work was supported by NASA's Planetary Geology and Geophysics Program and Mars Data Analysis Program in separate grants to both JFB and WMC.

REFERENCES

- Baldrige, A.M., and W.M. Calvin, Hydration state of the Martian coarse-grained hematite exposures: implications for the origin and evolution, *J. Geophys. Res., E, Planets* **109.4**, 2004.
- Bandfield, J. L., Global mineral distributions on Mars, *J. Geophys. Res.* **107**, 9–1, CiteID 5042, doi:10.1029/2001JE001510, 2002.
- Bandfield, J. L., T. D. Glotch, and P. R. Christensen, Spectroscopic identification of carbonate minerals in the Martian dust, *Science* **301**, 1084–7, 2003.
- Banin, A., B. C. Clark, and H. Wänke, Surface chemistry and mineralogy. In *Mars* (ed. H. H. Kieffer *et al.*), Tucson: University of Arizona Press, pp. 594–625, 1992.
- Bass, D. S. and D. A. Paige, Variability of Mars' north polar water ice cap – II. Analysis of Viking IRTM and MAWD data, *Icarus* **144**, 397–409, 2000.
- Bass, D. S., K. E. Herkenhoff, and D. A. Paige, Variability of Mars' north polar water ice cap – I. Analysis of Mariner 9 and Viking Orbiter imaging data, *Icarus* **144**, 382–96, 2000.
- Bell III, J. F., Iron, sulfate, carbonate, and hydrated minerals on Mars. In *Mineral Spectroscopy: A Tribute to Roger G. Burns*. (ed. M. D. Dyer, C. McCammon, and M. W. Schaefer), Geochem. Soc. Spec. Pub. No. **5**, Houston, 359–80, 1996.
- Bell III, J. F. and D. Crisp, Groundbased imaging spectroscopy of Mars in the near-infrared – Preliminary-results, *Icarus* **104**, 2–19, 1993.
- Bell III, J. F., T. B. McCord, and P. D. Owensby, Observational evidence of crystalline iron-oxides on Mars, *J. Geophys. Res.* **95**, 14447–61, 1990.
- Bell III, J. F., J. B. Pollack, T. R. Geballe, D. P. Cruikshank, and R. Freedman, Spectroscopy of Mars from 2.04 to 2.44 μm during the 1993 opposition: absolute calibration and atmospheric vs. mineralogic origin of narrow absorption features, *Icarus* **111**, 106–23, 1994.
- Bell III, J. F., T. L. Roush, and R. V. Morris, Mid-infrared transmission spectra of crystalline and nanophase iron

- oxides/oxyhydroxides and implications for remote sensing of Mars, *J. Geophys. Res.* **100**(E3), 5297–307, 1995.
- Bell III, J. F., M. J. Wolff, P. B. James, *et al.*, Mars surface mineralogy from Hubble Space Telescope imaging during 1994–1995: observations, calibration, and initial results, *J. Geophys. Res.* **102**, 9109–23, 1997.
- Bibring, J.-P., M. Combes, Y. Langevin, *et al.*, ISM observations of Mars and Phobos: first results, *Proc. Lunar Planet. Sci. Conf. 20th*, 461–71, 1990.
- Bibring, J.-P., Y. Langevin, F. Poulet, *et al.*, Perennial water ice identified in the south polar cap of Mars, *Nature* **428**, 627–30, 2004.
- Bibring, J.-P., Y. Langevin, A. Gendrin, *et al.*, Mars surface diversity as revealed by the OMEGA/Mars express observations, *Science* **307**, 1576–81, 2005.
- Bishop, J. L. and E. Murad, Schwertmannite on Mars? Spectroscopic analyses of schwertmannite, its relationship to other ferric minerals, and its possible presence in the surface materials on Mars. In *Mineral Spectroscopy: A Tribute to Roger G. Burns* (ed. M. D. Dyer, C. McCammon, and M. W. Schaefer), *Geochem. Soc. Spec. Pub. No. 5*, Houston, 337–58, 1996.
- Bishop, J. L., C. M. Pieters, and R. G. Burns, Reflectance and Mössbauer spectroscopy of ferrihydrite-montmorillonite assemblages as Mars soil analog materials, *Geochim. Cosmochim. Acta* **57**, 4583–95, 1993.
- Bishop, J. L., C. M. Pieters, T. Hiroi, and J. F. Mustard, Spectroscopic analysis of martian meteorite Allan Hills 84001 powder and applications for spectral identification of minerals and other soil components on Mars, *Meteorit. Planet. Sci.* **33**(4), 699–707, 1998.
- Bishop, J. L., M. D. Dyar, M. D. Lane, and J. F. Banfield, Spectral identification of hydrated sulfates on Mars and comparison with acidic environments on Earth, *Int. J. Astrobiol.* **3**(4), 275–85, 2004.
- Blaney, D. L. and T. B. McCord, Indications of sulfate minerals in the Martian soil from earthbased spectroscopy, *J. Geophys. Res.-Planets* **100**, 14433–41, 1995.
- Burns, R. G., Ferric sulfates on Mars, *J. Geophys. Res.* **92**(B4), E570–4, 1987.
- Burns, R. G., Rates and mechanisms of chemical weathering of ferromagnesian silicate minerals on Mars, *Geochim. Cosmochim. Acta* **57**, 4555–74, 1993.
- Calvin, W. M., Variation of the 3- μ m absorption feature on Mars: observations over eastern Valles Marineris by the Mariner 6 infrared spectrometer, *J. Geophys. Res. – Planets* **102**, 9097–107, 1997.
- Calvin, W. M., Could Mars be dark and altered? *Geophys. Res. Lett.* **25**, 1597–600, 1998.
- Calvin, W. M. and T. Z. Martin, Spatial variability in the seasonal south polar-cap of Mars, *J. Geophys. Res. – Planets* **99**, 21143–52, 1994.
- Calvin, W. M., T. V. V. King, and R. N. Clark, Hydrous carbonates on Mars: evidence from Mariner 6/7 infrared spectrometer and ground-based telescopic spectra, *J. Geophys. Res. – Planets* **99**, 14659–75, 1994.
- Cantor, B. A., M. J. Wolff, P. James, and E. Higgs, Regression of Martian north polar cap: 1990–1997 Hubble Space Telescope observations, *Icarus* **136**, 175–91, 1998.
- Christensen, P. R., Variations in Martian surface composition and cloud occurrence determined from thermal infrared spectroscopy: analysis of Viking and Mariner 9 data, *J. Geophys. Res. – Planets* **103**, 1733–46, 1998.
- Christensen, P. R., J. L. Bandfield, M. D. Smith, V. E. Hamilton, and R. N. Clark, Identification of a basaltic component on the Martian surface from thermal emission spectrometer data, *J. Geophys. Res.* **105**, 9609–22, 2000.
- Christensen, P. R., R. V. Morris, M. D. Lane, J. L. Bandfield, and M. C. Malin, Global mapping of Martian hematite mineral deposits: remnants of water-driven processes on early Mars, *J. Geophys. Res. – Planets* **106**, 23873–85, 2001.
- Cimino, G. and W. M. Calvin, The Mariner 7 infrared spectra: calibration and a preview for TES (abstract), *28th LPSC*, 231–2, 1997.
- Clancy, R. T., S. W. Lee, G. R. Gladstone, W. W. McMillan, and T. Roush, A new model for Mars atmospheric dust based upon analysis of ultraviolet through infrared observations from Mariner-9, Viking, and Phobos, *J. Geophys. Res. – Planets* **100**, 5251–63, 1995.
- Clark, R. N. and T. B. McCord, Mars residual north polar cap: Earth-based spectroscopic confirmation of water ice as a major constituent and evidence for hydrated minerals, *J. Geophys. Res.* **87**, 367–70, 1982.
- Clark, R. N., G. A. Swayze, R. B. Singer, and J. B. Pollack, High-resolution reflectance spectra of Mars in the 2.3- μ m region: evidence for the mineral scapolite, *J. Geophys. Res.* **95**, 14463–80, 1990.
- Crisp, D., Infrared radiative-transfer in the dust-free martian atmosphere, *J. Geophys. Res.* **95**, 14577–88, 1990.
- Davis, D. W. and L. A. Wanio, Measurements of water vapor in Mars' Antarctic, *Icarus* **45**, 216–30, 1981.
- Erard, S. and W. Calvin, New composite spectra of Mars, 0.4–5.7 μ m, *Icarus* **130**, 449–60, 1997.
- Erard, S., J. Mustard, S. Murchie, *et al.*, Martian aerosols: near-infrared spectral properties and effects on the observation of the surface, *Icarus* **111**, 317–37, 1994.
- Fanale, F. P., J. R. Salvail, W. B. Banerdt, and R. S. Saunders, Mars: the regolith-atmosphere-cap system and climate change, *Icarus* **50**, 381, 1982.
- Fanale, F. P., S. E. Postawko, J. B. Pollack, M. H. Carr, and R. O. Pepin, Mars: epochal climate change and volatile history. In *Mars* (ed. H. H. Kieffer, B. M. Jakosky, C. W. Snyder, and M. S. Matthews), Tucson: University of Arizona Press, pp. 1135–79, 1992.
- Farmer, C. B., D. W. Davies, and D. D. Laporte, Mars: northern summer ice cap – water-vapor observations from Viking 2, *Science* **194**, 1339–41, 1976.
- Fedorova, A. A., E. Lellouch, D. V. Titov, T. de Graauw, and H. Feuchtgruber, Remote sounding of the Martian dust from ISO spectroscopy in the 2.7 μ m CO₂ bands, *Planet. Space Sci.* **50**, 3–9, 2002.
- Fialips, C. I., J. W. Carey, D. T. Vaniman, *et al.*, Hydration state of zeolites, clays, and hydrated salts under present-day Martian surface conditions: can hydrous minerals account for Mars Odyssey observations of near-equatorial water-equivalent hydrogen?, *Icarus* **178**, 74–83, 2005.
- Fink, U. and G. T. Sill, The infrared spectral properties of frozen volatiles. In *Comets* (ed. L. L. Wilkening), Tucson: University of Arizona Press, pp. 164–202, 1982.
- Gendrin, A., N. Mangold, J.-P. Bibring, *et al.*, Sulfates in Martian layered terrains: the OMEGA/Mars Express view, *Science* **307**, 1587–91, 2005.
- Gooding, J. L., R. E. Arvidson, and M. Y. Zolotov, Physical and chemical weathering. In *Mars* (ed. H. H. Kieffer, B. M. Jakosky, C. W. Snyder, and M. S. Matthews), Tucson: University of Arizona Press, pp. 626–51, 1992.
- Geissler, P. E., R. B. Singer, G. Komatsu, S. Murchie, and J. Mustard, An unusual spectral unit in West Candor Chasma: evidence for aqueous or hydrothermal alteration in the Martian canyons, *Icarus* **106**, 380–91, 1993.

- Grundy, W. M. and B. Schmitt, The temperature-dependent near-infrared absorption spectrum of hexagonal H₂O ice, *J. Geophys. Res.* **103**(E11), 25809–22, 1998.
- Hamilton, V. E. and P. R. Christensen, Evidence for extensive, olivine-rich bedrock on Mars, *Geology* **33**, 433–6, 2005.
- Hamilton, V. E., P. R. Christensen, and H. Y. McSween, Determination of Martian meteorite lithologies and mineralogies using vibrational spectroscopy, *J. Geophys. Res. – Planets* **102**, 25593–603, 1997.
- Hanel, R. A., B. J. Conrath, D. E. Jennings, and R. E. Samuelson, The measured radiation field, Chapter 6, *Exploration of the Solar System by Infrared Remote Sensing*. Cambridge: Cambridge University Press, 1992.
- Hansen, G. B., The infrared absorption spectrum of carbon dioxide ice from 1.8 to 333 μm , *J. Geophys. Res. – Planets* **102**, 21569–87, 1997.
- Hapke, B., *Theory of Reflectance and Emittance Spectroscopy*, New York, NY: Cambridge University Press, 455pp., 1993.
- Herr, K. C. and G. C. Pimentel, Infrared absorptions near 3 microns recorded over the polar cap of Mars, *Science* **166**, 496–9, 1969.
- Hinrichs, J. L. and P. G. Lucey, Temperature-dependent near-infrared spectral properties of minerals, meteorites, and lunar soil, *Icarus* **155**, 169–80, 2002.
- Hoefen, Todd M., R. N. Clark, J. L. Bandfield, *et al.*, Discovery of olivine in the Nili Fossae region of Mars, *Science* **302**(5645), 627–30, 2003.
- Houck, J. R., J. B. Pollack, C. Sagan, D. Schaack, and J. Decker, High altitude infrared spectroscopic evidence for bound water on Mars, *Icarus* **18**, 470–80, 1973.
- Huguenin, R. L., The silicate component of martian dust, *Icarus* **70**, 162–8, 1987.
- Hunt, G. R., L. M. Logan, and J. W. Salisbury, Mars: components of infrared spectra and composition of the dust cloud, *Icarus* **18**, 459–69, 1973.
- Jakosky, B. M. and R. M. Haberle, The seasonal behavior of water on Mars. In *Mars* (ed. H. H. Kieffer, *et al.*), Tucson: University of Arizona Press, pp. 969–1016, 1992.
- James, P. B., H. H. Kieffer, and D. A. Paige, The seasonal cycle of carbon dioxide on Mars. In *Mars* (ed. H. H. Kieffer *et al.*), Tucson: University of Arizona Press, pp. 934–68, 1992.
- James, P. B., R. T. Clancy, S. W. Lee, and L. J. Martin, Seasonal recession of Martian south polar cap: 1992 HST observations, *Icarus* **123**, 87–100, 1996.
- Kieffer, H. H., Mars south polar spring and summer temperatures: residual CO₂ frost, *J. Geophys. Res.* **84**, 8263–88, 1979.
- Kieffer, H. H., H₂O grain-size and the amount of dust in Mars residual north polar-cap, *J. Geophys. Res. – Solid Earth and Planets* **95**, 1481–93, 1990.
- Kieffer, H. H., S. C. Chase, T. Z. Martin, E. D. Miner, and F. D. Palluconi, Martian north pole summer temperatures: dirty water ice, *Science* **194**, 1341–4, 1976.
- Kirkland, L. E. and K. C. Herr, Spectral anomalies in the 11 and 12 μm region from the Mariner Mars 7 infrared spectrometer, *J. Geophys. Res.* **105**(9), 22507–15, 2000.
- Langevin, Y., F. Poulet, J.-P. Bibring, and B. Gondet, Sulfates in the north polar region of Mars detected by OMEGA/Mars Express, *Science* **307**, 1584–6, 2005.
- Larson, H. P. and U. Fink, Identification of carbon dioxide on the Martian polar caps, *Astrophys. J.* **171**, L91–5, 1972.
- Lellouch, E., T. Encrenaz, T. de Graauw, *et al.*, The 2.4–45 μm spectrum of Mars observed with the infrared space observatory, *Planet. Space Sci.* **48**, 1393–405, 2000.
- Maguire, W. C., Martian isotopic ratios and upper limits for possible minor constituents as derived from Mariner 9 infrared spectrometer data, *Icarus* **32**, 85–97, 1977.
- Markiewicz, W. J., R. M. Sablotny, H. U. Keller, *et al.*, Optical properties of the Martian aerosols as derived from Imager for Mars Pathfinder midday sky brightness data, *J. Geophys. Res. – Planets* **104**, 9009–17, 1999.
- McCord, T. B., R. N. Clark, and R. L. Huguenin, Mars: near-infrared spectral reflectance and compositional implications, *J. Geophys. Res.* **83**(B11), 5433–41, 1978.
- McCord, T. B., R. N. Clark, and R. B. Singer, Mars: near-infrared spectral reflectance of surface regions and compositional implications, *J. Geophys. Res.* **87**(B4), 3021–32, 1982.
- McFadden, L. A. and T. P. Cline, Spectral reflectance of Martian meteorites: spectral signatures as a template for locating source region on Mars, *Meteorit. Planet. Sci.* **40**, 151–72, 2005.
- McKay, C. P. and S. S. Nedell, Are there carbonate deposits in the Valles Marineris, Mars?, *Icarus* **73**, 142–8, 1988.
- Mellon, M. T., Limits on the CO₂ content of the Martian polar deposits, *Icarus* **124**, 268–79, 1996.
- Milliken, R. E. and J. F. Mustard, Quantifying absolute water content of minerals using near-infrared reflectance spectroscopy, *J. Geophys. Res. – Planets* **110**, 2005.
- Morris, R. V., D. G. Agresti, H. V. Lauer Jr., *et al.*, Evidence for pigmentary hematite on Mars based on optical, magnetic, and Mössbauer studies of superparamagnetic (nanocrystalline) hematite, *J. Geophys. Res.* **94**, 2760–78, 1989.
- Morris, R. V., J. L. Gooding, H. V. Lauer Jr., and R. B. Singer, Origins of Marslike spectral and magnetic properties of a Hawaiian palagonitic soil, *J. Geophys. Res.* **95**, 14427–34, 1990.
- Morris, R. V., D. C. Golden, J. F. Bell III, H. V. Lauer Jr., and J. B. Adams, Pigmenting agents in Martian soils: inferences from spectral, Mössbauer, and magnetic properties of nanophase and other iron oxides in Hawaiian palagonitic soil PN-9, *Geochim. Cosmochim. Acta* **57**, 4597–609, 1993.
- Morris, R. V., D. W. Ming, D. C. Golden, and J. F. Bell III, An occurrence of jarositic tephra on Mauna Kea, Hawaii: implications for the ferric mineralogy of the Martian surface. In *Mineral Spectroscopy: A Tribute to Roger G. Burns* (ed. M. D. Dyer, C. McCammon, and M. W. Schaefer), Geochem. Soc. Spec. Pub. No. 5, Houston, 327–36, 1996.
- Morris, R. V., G. Klingelhöfer, B. Bernhardt, *et al.*, Mineralogy at Gusev crater from the Mössbauer spectrometer on the spirit rover, *Science* **305**, 833–6, 2004.
- Murchie, S., L. Kirkland, S. Erard, J. Mustard, and M. Robinson, Near-infrared spectral variations of Martian surface materials from ISM imaging spectrometer data, *Icarus* **147**, 444–71, 2000.
- Murchie, S., J. Mustard, J. Bishop, *et al.*, Spatial variations in the spectral properties of bright regions on Mars, *Icarus* **105**, 454–68, 1993.
- Mustard, J. F. and J. F. Bell III, New composite reflectance spectra of Mars from 0.4 to 3.14 μm , *Geophys. Res. Lett.* **21**, 353–6, 1994.
- Mustard, J. F. and J. M. Sunshine, Seeing through the dust: Martian crustal heterogeneity and links to the SNC meteorites, *Science* **267**(5204), 1623–6, 1995.
- Mustard, J. F., S. Murchie, S. Erard, and J. M. Sunshine, In situ compositions of Martian volcanics: implications for the mantle, *J. Geophys. Res.* **102**, 25605–15, 1997.
- Noe Dobrea, E. Z., J. F. Bell III, T. H. McConnochie, and M. Malin, Analysis of a spectrally unique deposit in the dissected Noachian terrain of Mars, *J. Geophys. Res.* **111**, E6, 2006.
- Nye, J. F., W. B. Durham, P. M. Schenk, and J. M. Moore, The instability of a south polar cap on Mars composed of carbon dioxide, *Icarus* **144**, 449–55, 2000.

- Paige, D. A., and K. D. Keegan, Thermal and albedo mapping of the polar-regions of Mars using Viking thermal mapper observations: 2. South polar-region, *J. Geophys. Res. – Planets* **99**, 25993–26013, 1994.
- Paige, D. A., J. E. Bachman, and K. D. Keegan, Thermal and albedo mapping of the polar-regions of Mars using Viking thermal mapper observations: 1. North polar-region, *J. Geophys. Res. – Planets* **99**, 25959–91, 1994.
- Pimentel, G. C., P. B. Forney, and K. C. Herr, Evidence about hydrate and solid water in the Martian surface from the 1969 Mariner infrared spectrometer, *J. Geophys. Res.* **79**, 1623–34, 1974.
- Pollack, J. B., J. F. Kasting, S. M. Richardson, and K. Poliakoff, The case for a wet, warm climate on Mars, *Icarus* **71**, 203–24, 1987.
- Pollack, J. B., T. Roush, F. Witteborn, *et al.*, Thermal emission-spectra of Mars (5.4–10.5- μm): evidence for sulfates, carbonates, and hydrates, *J. Geophys. Res. – Solid Earth and Planets* **95**, 14595–627, 1990.
- Poulet, F., J. P. Bibring, J. F. Mustard, *et al.*, Phyllosilicates on Mars and implications for early martian climate, *Nature* **438**, 623–7, 2005.
- Roush, T. L. and J. F. Bell III, Thermal emission measurements 2000–400 cm^{-1} (5–25 μm) of Hawaiian palagonitic soils and their implications for Mars, *J. Geophys. Res.* **100**(E3), 5309–17, 1995.
- Roush, T. L., D. L. Blaney, and R. B. Singer, The surface composition of Mars as inferred from spectroscopic observations. In *Remote Geochemical Analysis: Elemental and Mineralogical Composition* (ed. C. Pieters and P. Englert), Cambridge University Press, pp. 367–93, 1993.
- Schade, U. and R. Wäsch, Near-infrared reflectance spectra from bulk samples of the two Martian meteorites Zagami and Nakhla, *Meteorit. Planet. Sci.* **34**, 417–24, 1999.
- Singer, R. B., Spectral evidence for the mineralogy of high-albedo soils and dust on Mars, *J. Geophys. Res.* **87**(B12), 10159–68, 1982.
- Singer, R. B., T. B. McCord, R. N. Clark, J. B. Adams, and R. L. Huguenin, Mars surface composition from reflectance spectroscopy: a summary, *J. Geophys. Res.* **84**, 8415–26, 1979.
- Sinton, W. M., On the composition of Martian surface materials, *Icarus* **6**, 222–8, 1967.
- Soderblom, L. A., The composition and mineralogy of the Martian surface from spectroscopic observations: 0.3 μm to 50 μm . In *Mars* (ed. H. H. Kieffer, B. M. Jakosky, C. W. Snyder, and M. S. Matthews), Tucson: University of Arizona Press, pp. 557–97, 1992.
- Squyres, S. W., R. E. Arvidson, J. F. Bell III, *et al.*, The opportunity rover's Athena science investigation at Meridiani Planum, Mars, *Science* **306**, 1698–703, 2004.
- Sunshine, J. M., L. A. McFadden, and C. M. Pieters, Reflectance spectra of the Elephant Moraine-A79001 meteorite: implications for remote-sensing of planetary bodies, *Icarus* **105**, 79–91, 1993.
- Thomas, P., S. Squyres, K. Herkenhoff, A. Howard, and B. Murray, Polar deposits of Mars. In *Mars* (ed. H. H. Kieffer *et al.*), Tucson: University of Arizona Press, pp. 767–95, 1992.
- Thomas, P. C., M. C. Malin, K. S. Edgett, *et al.*, North-south geological differences between the residual polar caps on Mars, *Nature* **404**, 161–4, 2000.
- Thomas, P. C., M. C. Malin, P. B. James, *et al.*, South polar residual cap of Mars: features, stratigraphy, and changes, *Icarus* **174**, 535–59, 2005.
- Titus, T. N., Thermal infrared and visual observations of a water ice lag in the Mars southern summer, *Geophys. Res. Lett.* **32**, 2005.
- Toon, O. B., J. B. Pollack, and C. Sagan, Physical properties of the particles composing the martian dust storm of 1971–1972, *Icarus* **30**, 663–96, 1977.
- Warren, S. G., Optical constants of ice from the ultraviolet to the microwave, *Appl. Opt.* **23**, 1206–25, 1984.

PART II

ELEMENTAL COMPOSITION:
ORBITAL AND *IN SITU* SURFACE
MEASUREMENTS

PART II.A

Results and Interpretations from New *in situ* APXS
Measurements

Martian surface chemistry: APXS results from the Pathfinder landing site

C. N. FOLEY, T. E. ECONOMOU, R. N. CLAYTON, J. BRÜCKNER, G. DREIBUS,
R. RIEDER, AND H. WÄNKE

ABSTRACT

The Mars Pathfinder Alpha Proton X-ray Spectrometer (APXS) was utilized to determine the major and minor elemental abundances of rocks and soils at the 1997 landing site in Ares Vallis. The determined abundances suggest that: (1) the rocks are covered with various amounts of soil; (2) the Soil-Free Rock (SFR) chemistry is similar to that of an evolved SNC-like (SNC – Shergottite, Nakhilite, and Chassignite) igneous tholeiitic basalt-andesite to andesite that is minimally altered (possibly similar to Type 2 TES material); (3) the carbon content is below detection limits for all samples, implying <5% as MgCO₃ (Brückner *et al.*, 1999); (4) the α -mode oxygen abundance indicates that mineral-bound water, above the value for igneous rocks, is present in some rocks and is therefore indicative of some nonigneous alteration and therefore possibly rock-rinds that obscure the petrology of the SFR; and (5) the Pathfinder soils are similar to the Viking fines and may be composed of mafic igneous material like the SNC meteorites and of volatiles deposited from volcanic emissions, as previously suggested by Clark (1993) for the Viking soils.

3.1 INTRODUCTION

The Mars Pathfinder mission to Ares Vallis in July 1997, the first lander mission since those of the Viking missions, was the first equipped with a robotic rover to extend the chemical analyses of the Martian surface beyond that immediately proximal to the lander. While the Viking missions were the first to analyze the chemistry of soils on the Martian surface, the Pathfinder mission was the first to make *in situ* measurements of both the rocks and the soils (and in particular, to make measurements of the soils without presorting or sifting them).

The Pathfinder lander was equipped with an atmospheric structure instrument (ASI), a multispectral imager (IMP), a rover camera, and the APXS. The main scientific objective of the mission was to unveil the geochemistry of the Pathfinder landing site. In particular, the goals were to understand the role that volatiles (such as water, carbon dioxide, and sulfur) may have had, to understand the major element chemistry of the rocks, and to put these measurements into a greater context through comparison with other Martian remote-sensing measurements as well as with the Martian meteorites (SNCs; see Chapter 17). Because the Pathfinder APXS was

capable of measuring concentrations of all major and minor rock-forming elements ranging from carbon through nickel in atomic number, it was utilized to determine the geochemistry and infer the petrology of the rocks and soils at the landing site, as described in detail in Section 3.4.

3.1.1 Landing site description

The Pathfinder landing site (Figure 3.1a and b) is possibly a floodplain created from waters catastrophically emanating from southern Ares and Tiu channels (Golombek *et al.*, 1997a). Geomorphic features such as streamlined islands, undulating ground, and strewn angular boulders at the site support this floodplain hypothesis (Golombek *et al.*, 1997a). Ejecta from nearby impacts may also be present at the landing site (Golombek *et al.*, 1997a).

Ares and Tiu Valles are two of the many channels emanating from chaos regions south of the channels in the Xanthe Terra region of Mars. Chaos regions are interpreted to be potential watersheds from which groundwater was catastrophically released during the Hesperian period, between 3.1 and 1.8 Ga ago (Nelson and Greeley, 1999). Another potential watershed for flooding through the Ares and Tiu channels includes the eastern portion of Valles Marineris (Nelson and Greeley, 1999). The initiation of these flooding and channel formation events may be linked to the uplift and volcanic development of the Tharsis region in the late Noachian (~3.5 Ga), possibly concurrent with the formation of the giant rift, Valles Marineris, along with other ridged plains in the Chryse Planitia (Nelson and Greeley, 1999 and references therein). Furthermore, continued volcanism in the Tharsis region and the proximal eruption of the Lunae Planum flood basalts to Xanthe Terra may also have provided geothermal heat to release frozen groundwater during the Hesperian (Baker *et al.*, 1991). The Xanthe Terra region, through which Ares and Tiu Valles cut, is inferred to be Noachian, as old as ~4.5 Ga based on crater densities, cut by channel materials that are Hesperian, as young as ~1.8 Ga (Tanaka *et al.*, 1992). The Mars Pathfinder landing site is located approximately 800 km from the channel mouths of Ares and Tiu, within the mid fan of the channels (Nelson and Greeley, 1999 and references therein). Using terrestrial liquid water flood analogs, sand-sized particles from the channel walls are expected to have been delivered to and past the Pathfinder landing site. Larger clasts may have been delivered to the Pathfinder landing site as ice-rafted debris (Nelson and Greeley, 1999

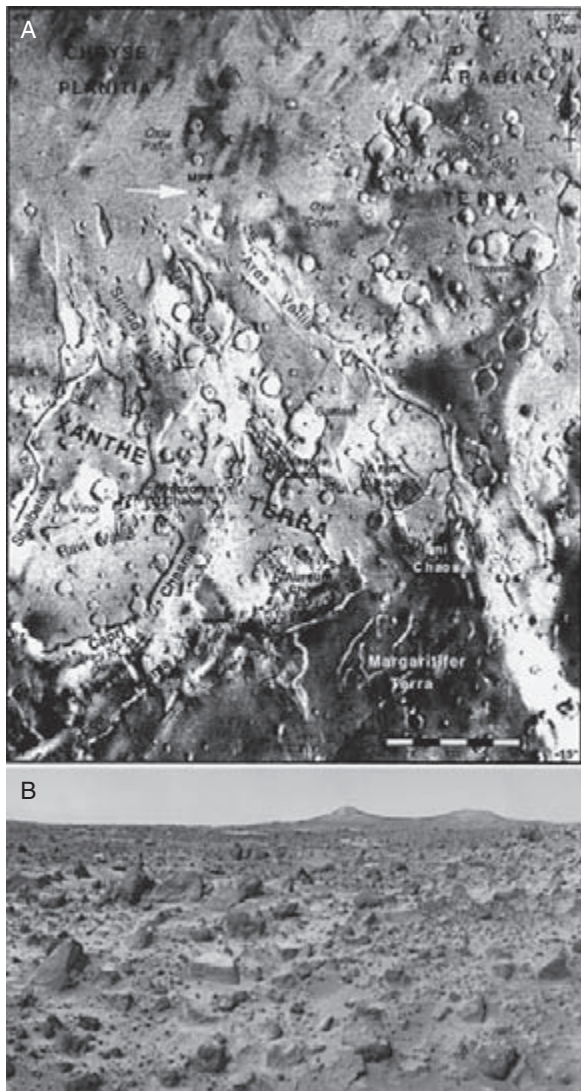


Figure 3.1. (a) The Mars Pathfinder landing site (MPF) located mid-fan from the mouths of Ares and Tiu Valles. As shown, both channels emanate from chaos regions located south of the mouths of the channels within Xanthe Terra. Figure is from Nelson and Greeley (1999). (b) Pathfinder image of the landing site.

and references therein) or by debris flows consisting of a mixture of water, ice, gas, and rock debris moving downslope (Tanaka, 1999). Thus, the surface sediments and boulders at the Mars Pathfinder landing site may therefore be Noachian- to Hesperian-aged highland plain material with reworked sediments from repeated flooding and impacting occurring over billions of years.

The scientific rationale for choosing this landing site was that, as floodplain material, it may contain a variety of rock types from the surrounding region and possibly even from the ancient southern highlands (Golombek *et al.*, 1997b). The anticipated diverse group of rocks in Ares Vallis was optimal because it had the potential to provide a plethora of information from one landing site. Igneous rocks found could reveal the type of volcanic and/or plutonic processes occurring locally and possibly more globally. Sedimentary rocks

found could reveal the magnitude of weathering involving liquid water on the surface of Mars. Metamorphic rocks, if found, would indicate a significant rock cycle occurring on Mars involving burial and exhumation of earlier igneous or sedimentary rocks.

3.1.2 Instrument description

The Pathfinder APXS design is a result of many years of development of α -scattering instruments designed for remote-sensing missions. The first such α -scattering instrument was developed at the University of Chicago by Turkevich (1961). That instrument was used to analyze lunar samples *in situ* on the Surveyor V, VI, and VII missions (Turkevich *et al.*, 1969; Franzgrote *et al.*, 1970; Patterson *et al.*, 1970). A modified α -scattering instrument, the Mini-Alpha, was designed and tested for potential Mars missions by Economou *et al.* (1973) and is further described by Economou and Turkevich (1976). This Mini-Alpha design was further modified for a potential mission to Phobos by Dieter Hovestadt at the Max-Planck-Institut für Extraterrestrische Physik in Garching, Germany (Hovestadt *et al.*, 1990). The Pathfinder APXS is a derivative of the Mini-Alpha and Phobos APXS, but was jointly redesigned to be less massive and to consume less power by Rudolf Rieder at the Max-Planck-Institut für Chemie in Mainz, Thanasis Economou at the University of Chicago, Lev Mukhin at the Space Research Institute in Moscow, and Slava Ryadchenko at the All Union Research Institute for Atomic Reactors in Dimitrovgrad. The Pathfinder APXS was originally designed and flown on the Russian Mars 1996 mission, which failed to reach Mars. The instrument is also described in further detail by Rieder *et al.* (1997a).

The instrument sensor head, which is cylindrical having dimensions of 52 mm in diameter and 70 mm in height, contains a ring of nine radioactive ^{244}Cm alpha sources surrounding a ring of six collimators for the alpha sources, a central collimator for the alpha and proton detectors, and an X-ray detector as shown in Figure 3.2a and b. The α and proton detectors are situated in a telescoping fashion at the end of these collimators because the α particles stop in the first detector while the protons, having higher energy, pass through the α detector and are stopped and detected in the proton detector behind it. The X-ray detector, a Si-PIN, is located to the side of the sensor head.

The instrument relies on the α decay of ^{244}Cm , located within the instrument sensor head, to generate sample signals. The decay of ^{244}Cm , which has a half-life of 18.1 years (Parrington *et al.*, 1996), releases α particles and ^{244}Pu X-rays. These α particles and X-rays produce α , proton, and characteristic X-ray signals from samples due to elastic α scattering, (α , p) reactions, and α -Particle Induced X-ray Emission (α -PIXE) and X-ray fluorescence (XRF), respectively. With the calibration and Martian data analyses, the α -mode was capable of independently measuring C, O, Si, Ca, and Fe abundances in Pathfinder samples. The proton-mode enabled measurement of Na, Mg, Al, Si, S, and N. The X-ray mode enabled measurement of abundances of elements which have X-ray signals ranging from 1 to

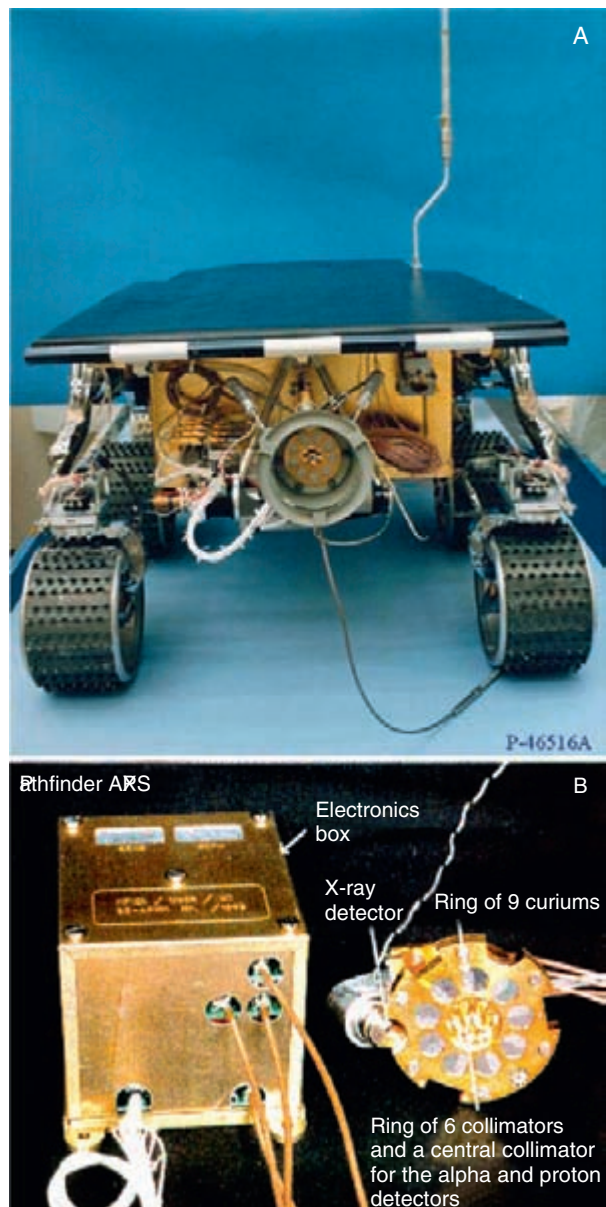


Figure 3.2. (a) The APXS on the Sojourner rover. (b) The APXS Pathfinder instrument. The sensor head consists of a ring of nine curium sources surrounding a central detector which has seven collimators for the telescoping α and proton central detectors, as shown on the right. The cylinder, which is 42 mm long and is attached to the sensor head to position the APXS against analyzed samples, is not shown here. The diameter of the circular gold-coated sensor head is 52 mm. The X-ray detector is located on the side of the instrument head. The electronics box for the APXS is also shown on the left in this figure. (For a color version of this figure, please refer to the color plate section or to the e-Book version of this chapter.)

15 KeV. Thus all major and minor rock-forming elements ranging from Na through Ni in atomic number were measured in the Pathfinder samples. The three systems can be used independently but it is the combination of all three modes, providing in some cases complementary and in other cases redundant information, that results in an accurate and complete chemical analysis.

The physics of elastic scattering from target atoms was described in detail by Rutherford *et al.* (1930), who first used α -scattering experimental data from Geiger and Marsden (1909) to determine the size of atomic nuclei (Rutherford, 1911) using Coulomb scattering principles. As derived by Rutherford from the conservation of angular momentum and energy, the energy of the scattered α depends upon both the scattering angle and the atomic mass of the target atom. Thus, with the scattering angles constrained to be near 180° , the maximal energy of the scattered α particles from the sample surface is purely a function of the atomic mass.

The intensity of elastically scattered α particles is determined by the Rutherford cross-section as well as by the sample composition. The cross-section for α backscattering, which determines the relative probability of scattering for different elements at various angles, has also been described by Rutherford *et al.* (1930). This relationship shows that elastic scattering from higher Z elements is more probable than that from lower Z elements for the same scattering angle. As a result, the α mode is more sensitive for higher Z element measurements. With the cross-sections well understood, the sample composition as a function of element intensities can be determined.

Inelastic α scattering also occurs particularly from lower Z elements, most significantly carbon and oxygen, as noted by Bittner and Moffat (1954) and Ferguson and Walker (1940), respectively. The cross-sections for inelastic scattering are more variable with scattering angle than those for elastic scattering. The intensities from inelastic scattering have been experimentally determined in order to evaluate sample compositions.

The equations relating the elastic and inelastic scattering of the α particles as well as the resulting intensity of scattered α particles are discussed in detail by Patterson *et al.* (1965) and Foley (2002). In summary, the intensity of a measured element is proportional to the abundance of that element, while the energy at which this intensity is measured is proportional to the atomic mass of the element. For an infinitely thin sample, α particles will lose no energy traversing through the sample. Therefore, the α spectrum of intensity versus energy for a measured element will look like a vertical line. For a thick target, α particles from the surface as well as from depths $\sim <10 \mu\text{m}$ backscatter to the detector. The actual maximum depth from which α particles return from can be estimated from previous experimental data compiled by Ziegler (1977). Alpha particles scattering from deeper in the sample lose energy traversing through the sample. Therefore, the α spectrum of intensity versus energy for an element within a homogeneous thick target is rectangular in shape, as shown in Figure 3.3. Equations which describe energy loss of α particles with depth are given by Patterson *et al.* (1965).

Some nuclei (particularly low-Z nuclei) will undergo (α , p) reactions upon being bombarded with the α particles from the decay of ^{244}Cm , and thus release protons and sometimes gamma rays from their nuclei. This nuclear reaction can occur when the kinetic energy of the α particle exceeds the Q value, for which the general nuclear reaction is described by Tipler (1987). Furthermore, some elements have multiple energies at which (α , p) reactions will occur. Since the α

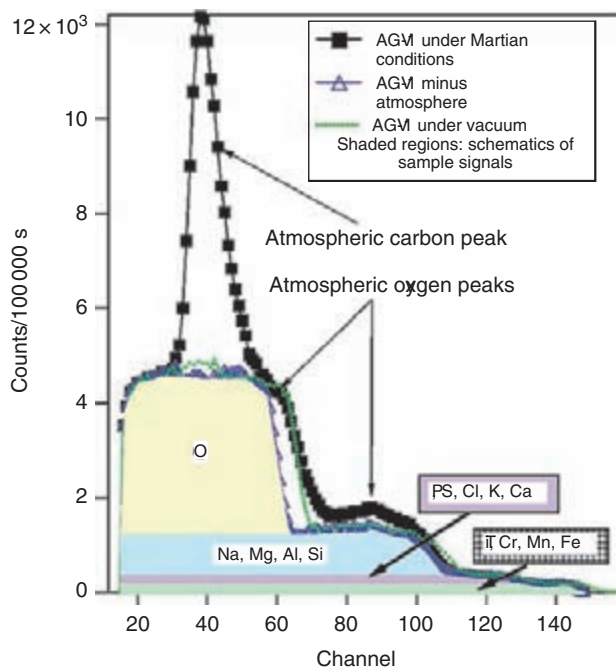


Figure 3.3. Alpha-mode laboratory spectrum of an andesite standard, AGV-1, under Martian conditions. The atmospheric signals from the carbon and oxygen of carbon dioxide form peaks within the AGV-1 sample run. The carbon atmospheric peak is centered at approximately channel 39, while the oxygen atmospheric peaks are centered at approximately channel 60 and 88. Using the atmospheric subtraction technique described within Foley *et al.* (2003a), the atmosphere-free spectrum for AGV-1 has been computed and is plotted here as well. The α spectrum for AGV-1 under vacuum is also shown for comparison. Sample signals for each element are shaded. (For a color version of this figure, please refer to the color plate section or to the e-Book version of this chapter.)

particles lose energy as they traverse through the sample, some of these proton reactions occur within the sample, rather than at the sample surface. The elements within the Pathfinder samples that produce significant proton signals for the APXS include nitrogen, sodium, magnesium, aluminum, silicon, and sulfur, whose laboratory standard spectra are shown in Figure 3.4. The intensities of the proton signals from a given element vary as a function of mean sample composition and concentration of the element with approximately the same intensity dependence as that for the α particles.

Incident α particles and X-rays from the ^{244}Cm cause sample atoms to emit characteristic X-rays. X-rays from the lower Z elements from sodium through calcium are predominantly generated by α particle bombardment, while those from the higher Z elements are predominantly generated by X-ray bombardment. Characteristic X-rays are generated from depths up to approximately 80 μm by α and XRF. However, the average sampling depth by the X-rays varies with atomic number due to absorption of outgoing X-rays within the sample. In particular, lower Z X-rays, such as those from sodium and silicon, come from the top few micrometers while higher Z X-rays, such as those from iron, come from depths of up to 18 μm for samples having approximately basaltic compositions.

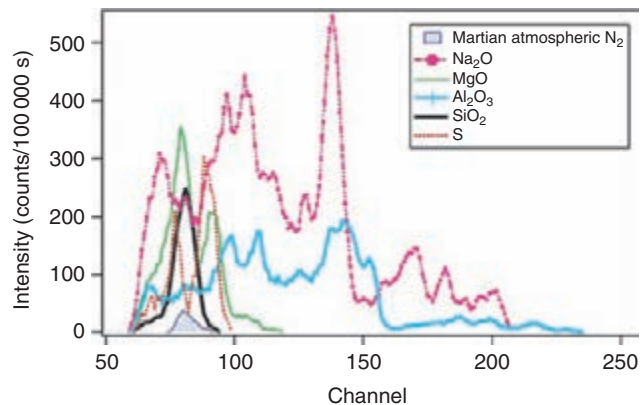


Figure 3.4. Proton-mode laboratory spectra. The multiple spectral signals at different channels, proportional to energies, are due to proton release from sample nuclei (and Martian atmosphere in the case of nitrogen) from (α , p) reactions. The Na_2O curve was calculated from measurement of NaCl . (For a color version of this figure, please refer to the color plate section or to the e-Book version of this chapter.)

3.2 APXS CALIBRATION

Due to time constraints to deliver the flight instrument for launch, the calibration of the Pathfinder APXS was accomplished by two separate calibration teams using two duplicate laboratory instruments at the University of Chicago (Foley *et al.*, 2003a,b) and at the Max-Planck-Institut für Chemie (Brückner *et al.*, 2003). During both calibrations, numerous powdered standards of oxides, pure elements, and geostandards were analyzed to derive routines to determine the compositions of the unknowns at the Pathfinder landing site. Rocks which were approximately homogeneous in surface composition on a millimeter scale, having various surface textures, were also analyzed. While Brückner *et al.* (2003) calibrated the X-ray mode of the APXS, Foley *et al.* (2003a) calibrated all three instrument modes. Both laboratories, however, utilized the α mode of the instrument to determine the concentration of sample carbon in the Pathfinder samples. The extremely similar results from the independent X-ray calibrations and carbon determinations illustrate the accuracy of both laboratories and techniques.

For each laboratory, the instrument was operated inside a stainless steel vacuum chamber that has two compartments. The upper compartment houses the APXS instrument and has an intake and exhaust valve that can regulate the pressure and introduce gas into the chamber. The lower chamber can be sealed off from the upper one providing a means to pressurize the lower chamber without affecting the upper one and hence use the lower chamber to change samples. Samples may be loaded into the lower chamber onto a sample stage that can be raised to the cylindrical base of the APXS.

3.2.1 The X-ray mode

The X-ray calibration of Brückner *et al.* (2003) utilized calibration curves derived from analyses of numerous geostandards to determine the composition of the Pathfinder samples. In contrast, the calibration of Foley *et al.* (2003a)

utilized theoretically predicted X-ray generation and matrix effects verified by analyses of laboratory geostandards to calculate the Pathfinder compositions.

The characteristic X-ray spectral peaks are nearly gaussian with small low-energy tails caused by incomplete charge collection within the X-ray detector. The X-ray peak shapes, areas, and backgrounds were analyzed using two different techniques. A least-squares fitting technique using laboratory-derived peak shapes for each element was applied by Brückner *et al.* (2003) to take into account the small non-gaussian low-energy shoulder of the peaks. Each X-ray spectrum was split in three spectral regions, which were fit separately. In contrast, Foley *et al.* (2003a) used a least-squares fitting technique with gaussian peak fitting, which deconvolves overlapping peaks and compensates for non-gaussian tails on an adjustable order polynomial background on the entire spectrum. The parameters of the peaks, such as the peak center positions and the full width at half maximum (FWHM), vary as a function of resolution and are therefore determined for each spectrum. For both techniques, care was taken to assure comparable laboratory conditions to those on the Martian surface. The Martian resolution was fairly constant as discussed by Brückner *et al.* (2003) which was important for measurement during times when temperatures varied from +9 to -75°C . Both calibration teams corrected for all escape and K_{β} peaks, as described in detail by Brückner *et al.* (2003) for laboratory and Pathfinder samples. Collected X-ray spectra were, thus, first analyzed in the ways described above to remove the spectral background and to compute the peak areas for each element. These areas were then utilized to compute the sample concentrations.

Foley *et al.* (2003a,b) determined the concentrations within samples using software written by O. F. Prilutsky, from the Space Research Institute of the Russian Academy of Sciences. This program takes into account the excitation from both the α particles and the X-rays from ^{244}Cm radioactive source as well as X-ray absorption within the sample. The program, therefore, makes ZAF (ZAF-atomic number [Z], Absorption, and Fluorescence) corrections like modern EDSs (Electron Density Systems) and electron probes. In order to calculate elemental abundances, this program needs values for X-ray intensities from standards. These intensities, normalized to the same collection time, for characteristic X-ray peaks from standards were experimentally determined during the calibration. These standards were fine-powdered oxides or fine-powdered pure elements having greater than 99.9% chemical purity and uniform grain size. The standards used to measure the respective elements within parentheses include NaCl (Na, Cl), MgCO_3 (Mg), Al_2O_3 (Al), SiO_2 (Si), CaHPO_4 (Ca, P), S (S), K_2CO_3 (K), TiO_2 (Ti), Cr (Cr), MnO_2 (Mn), and FeSO_4 (Fe). The proportionality of the count rate to the concentration of each element in the standard, instrument geometry, as well as experimentally determined outgoing X-ray matrix effects were then used to measure the composition of the samples being analyzed. A certain oxidation state for each element was assumed, and therefore oxygen was calculated using stoichiometry. As fore mentioned, this technique is very

similar to that used conventionally in analytical electron microscopy. It differs by its incorporation of the fraction of characteristic X-rays generated by α particles and X-rays within a given volume of sample, and the unique geometry parameters of the APXS described by Rieder *et al.* (1997b).

By measuring the compositions of a number of powder geostandards under Martian conditions, the accuracy of the Foley *et al.* (2003a) calibration method for the X-ray mode was determined. The geostandards analyzed include AGV-1 (andesite), BCR-1 (basalt), G-1 (granite), G-2 (granodiorite), DTS-1 (dunite), BCS-301 (iron-rich sediment), PCC-1 (dunite), and OTB-1 (basalt) (with only the first five analyzed under simulated Martian conditions). The meteorites analyzed include ALH 84001 (Martian orthopyroxenite), ALH 77005 (shergottite), EET 79001 (shergottite), Bruderheim (L6 ordinary chondrite), Murchison (CM2 carbonaceous chondrite), and Allende (CV3 carbonaceous chondrite) in vacuum. The analyses of BCS-301, PCC-1, and the meteorites were particularly useful to infer the accuracy of the calibration technique for elements such as excess O (in mineral-bound water for PCC-1 and Murchison), C, P, S, Cr, and Mn (as described further by Foley, 2002). The assigned analytical uncertainties of measurements for the Pathfinder samples are determined by combining the laboratory errors from the calibrations (Foley *et al.*, 2003a) with the statistical errors for each sample.

Rigorous calibration curves were determined for compositions within a comparable range to the Pathfinder samples through analyses of various geostandards by Brückner *et al.* (2003). Calibration geostandards include AN-G (andesite), BE-N (basalt), Mica-Fe, Millbillillie (eucrite), Murchison (CM2), and SSK1.1 (andesite) under Martian simulated conditions. Since these samples span the composition range of the Pathfinder samples, the calibration curves eliminate the need for additional corrections for matrix effects within the Pathfinder samples. Based upon the element signal as a function of atomic number for the calibration curves, only P, Cl, and Mn appear to be outliers in terms of the expected count rate for a given element. Thus, some systematic errors for these elements resulting from use of this calibration are possible (Brückner *et al.*, 2003). Average errors for each element were computed using the calibration curve and the statistical errors for each measured element. Although the average errors are not listed by Brückner *et al.* (2003), the accuracy is comparable as verified by the similar bulk chemical Pathfinder results by the two groups.

3.2.2 The alpha-proton mode

Foley *et al.* (2003a) calibrated the α -proton combined mode to measure C, N, O, Na, Mg, Al, Si, (S, P, Cl as a group), (K, Ca as a group), Ti, and (Mn, Cr, Fe, Ni as a group) for the Pathfinder analyses. The α -proton mode relied on the X-ray mode for Mg/Si, S/Si, P/Si, Cl/Si, K/Ca, Mn/Fe, and Cr/Fe ratios. With these ratios from the X-ray mode, the α -proton mode then gives the abundances of the remaining measurable elements. This results in independent α -proton mode measurements of C, N, O, Na, Al, Si, (K, Ca), Ti, and (Mn, Cr, Fe, Ni). Like the X-ray mode, the α and proton

modes rely on spectra of fine-grained oxide standards for their calibration libraries.

Unlike the X-ray mode, the α and proton spectra contain atmospheric signals from the carbon and oxygen in the Martian atmospheric CO₂ and from atmospheric nitrogen, respectively, which must first be removed before sample analyses. Once the atmospheric contributions are removed, the α and proton signals are analyzed by a least-squares fit to yield a result which is partially dependent on the X-ray mode. However, the α mode accuracy is more strongly affected by changes in measurement distance and sample texture, which is less the case for the X-ray mode. The correction for atmospheric effects, sample distance, and sample texture, as well as the resulting accuracy of the α -proton combined mode are described in detail by Foley *et al.* (2003a).

In brief, sample texture and distance differences cause some deviation from the expected rectangular shape of the α spectra for elements having resonant scattering of the α particles at some energies. Textural effects were overcome by analyzing standards having textures similar to those of the analyzed samples. Since the resonant features are in the calibration library as well as the analyzed samples, correction is not a problem if the approximate texture of the analyzed sample is known. Resonant features are subdued in powdered samples and are more pronounced in polished samples and rocks, perhaps because of increased energy scattering and loss in powdered samples which have grain sizes similar to the typical penetration depth of the α particles. These effects are minor for resonant features in sodium, aluminum, and magnesium alpha spectra. However, there is a significant effect for silicon, due to its high abundance in samples analyzed. Thus rocks are more accurately analyzed with the polished standard for silica, while soils are more accurately analyzed with the fine powder standard.

The Pathfinder measurement distance exceeded the laboratory calibration distance by 4–15 mm. This distance change affects the computed α -mode abundances alone (Foley, 2002). Distance effects were overcome by computing the sample distance utilizing the iron signal of the α mode and adjusting both the oxygen and silicon standards by an experimentally and theoretically predicted amount to compensate for the distance change (Foley, 2002). The distance change has a maximum effect on the silicon and oxygen abundances of 7 and 12 relative percent (which are smaller than the measurement errors), respectively, which were corrected for during analyses. Sample texture and distance also affect the carbon signal. However, since Pathfinder sample carbon was determined to be below the detection limit (as discussed in the following section), this is not pertinent.

The effects of the Martian atmosphere on the α and proton spectra were determined using a simulated Martian gas mix, identical to measured Martian atmosphere, of 95.32% CO₂, 2.7% N₂, and 1.6% Ar (Owen *et al.*, 1997; Owen, 1992). There are two general effects on the α spectra. The first effect is a shift in the energy of returned α particle energy from a given element due to the energy loss in the gas before and after scattering from the sample. The second effect is the

contribution to the α spectra predominantly from carbon and oxygen of the carbon dioxide gas, with only a negligible α signal from nitrogen gas and no detected α signal from argon. The atmospheric α contributions are three thin-sample peaks, due to the low density of the atmosphere, and are within the spectrum collected under Martian conditions. As shown in Figure 3.3, only the carbon atmospheric peak is clearly discernible for sample spectra. The two lowest-energy peaks are due predominantly to α particles resonantly scattered from atmospheric carbon and oxygen nuclei, respectively. The highest-energy peak is due to low-angle resonant scattering from oxygen nuclei close to the alpha detector. The amplitudes, centers, and widths of the carbon and oxygen peaks vary linearly with number density. Since the carbon peak is the only directly measurable atmospheric peak in the α spectra of laboratory geostandards as well as Pathfinder samples, it was used to infer the parameters of the other two atmospheric peaks. Most of the atmosphere parameters can be computed from the measurable parameters of the carbon peak. The high-energy oxygen width, however, is approximately constant with change in number density.

The proton spectra have several peaks due to (α , p) reactions occurring within samples at different energies for each proton-producing element. The only significant effect of the Martian atmosphere on the proton spectra is to introduce a small contribution from the atmospheric nitrogen. This nitrogen contribution was measured by pointing the APXS toward the sky to measure only atmosphere during a period of atmospheric number density comparable to that of the Pathfinder sample measurements. This modeled atmospheric contribution is shown in Figure 3.4 along with the computed and/or measured values for the proton library spectra including those of Na₂O, MgO, Al₂O₃, SiO₂, and S. This proton library consists of the collected intensities from analyzing standards of chemically pure and homogeneous fine-grained simple compounds (NaCl, MgO, Al₂O₃, and SiO₂) and elemental sulfur. There is no proton signal from the oxygen within these oxides. The proton intensity is proportional to the concentration of the proton emitters: Na, Mg, Al, Si, and S.

In the Foley *et al.* (2003a) calibration, the α and proton data were merged and analyzed as one set of data and therefore we refer to their results as coming from the α -proton mode. The two modes are merged because some elements have lower and less distinctive intensities in the α mode and higher and/or more distinctive intensities in the proton mode and vice versa. For example, the sodium signal for the α mode is typically difficult to decipher from the large silicon signal in basaltic to andesitic samples, but is easily seen in the proton mode. Because of this, the accuracy of sodium measurement is better for the proton mode than for the α mode. The other element contributing to the sodium region of the protons is aluminum. In order to assure that sodium was calculated accurately from the proton mode, the Al/Si ratio in the alpha-proton mode was set from the X-ray data. The merging of the α and proton spectra was done for each calibration standard as well as each analyzed sample. A least-squares program was then used to calculate the

abundances in the unknown using the library, consisting of merged α and proton spectra from homogeneous fine-powdered oxides and/or elements. The least-squares program fits the analyzed spectrum with the intensities measured from the standards and converts the measured intensities to sample concentrations using equations given by Foley (2002). Alpha-proton mode error bars for the Foley *et al.* (2003b) Pathfinder analyses are computed from average

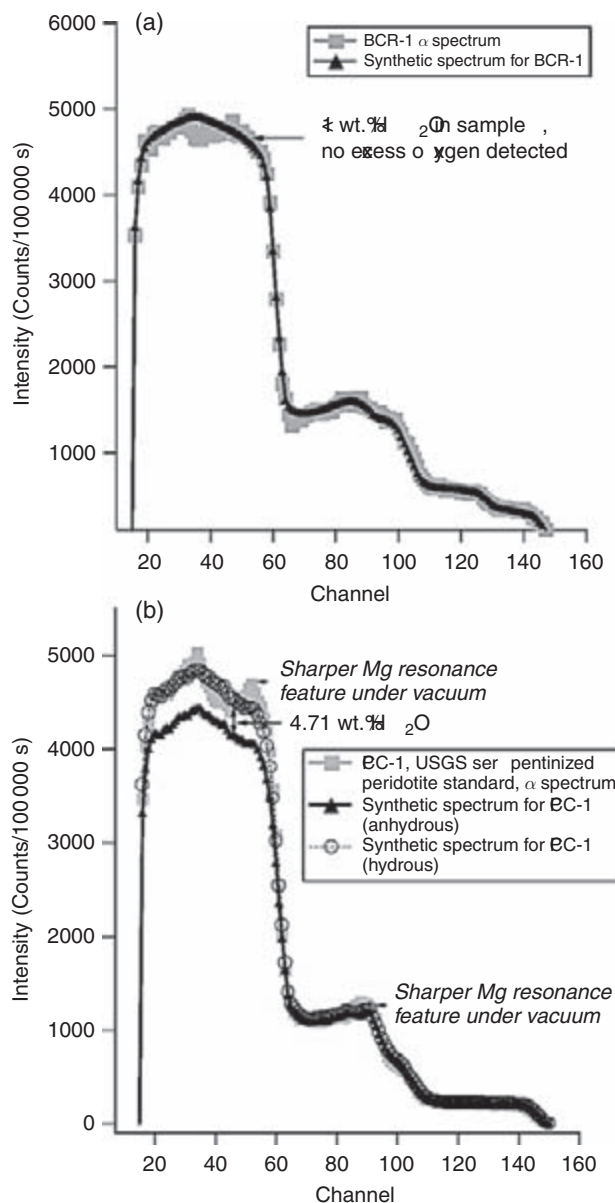


Figure 3.5. Series of α -mode laboratory spectra showing the detection of excess oxygen, present in samples having greater than 1 wt.% water. (a) The raw spectrum minus atmospheric signals for a basalt standard, BCR-1, and a spectral fit using the α program with the library calibration values assuming the oxidation states as listed in Govindaraju (1994). No excess oxygen was detected. (b) (1) The raw spectrum for a serpentinized peridotite standard, PCC-1; (2) the synthetic anhydrous spectrum from the α program with the library calibration values also assuming oxidation states as listed in Govindaraju (1994); (3) the α program fit which includes oxygen bound as water. There is a significant excess of oxygen signal when sample water is present.

relative percent deviations determined in the laboratory calibration and the counting statistical errors for each sample.

The raw α spectra for geostandards were compared with calculated α spectra assuming stoichiometric oxygen excluding mineral-bound water from their individual references. Also, the raw α spectra were compared with the α spectral fit from the α -proton program including all measured elements. This was done to observe the magnitude of the oxygen signal due to mineral-bound water in geostandards. Figure 3.5a shows the raw laboratory spectrum for BCR-1, minus atmosphere, compared with the α spectrum assuming stoichiometric oxygen (Govindaraju, 1994) excluding water. Because BCR-1 contains less than 1 wt.% water, the raw and the synthetic spectra for BCR-1 are very similar. Figure 3.5b shows the raw and synthetic spectra for PCC-1. Because PCC-1 contains 4.71 wt.% water (Govindaraju, 1994), the raw spectrum for PCC-1 is much higher in the oxygen region than the calculated α spectrum excluding water. A calculated spectrum including water matches the raw spectrum well.

The α -mode oxygen measurements, shown in Figure 3.6, yield an accuracy of 1 relative percent (1σ) both for geostandards containing <1 wt.% water and for samples containing abundant water, as described in detail by Foley (2002). Hydrogen is the only rock-forming element that cannot be detected directly by the APXS. However, its

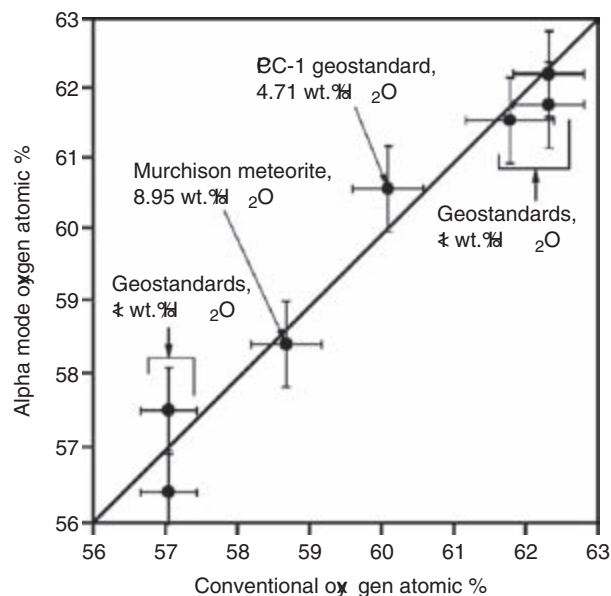


Figure 3.6. Laboratory α -mode bulk oxygen accuracy for geostandards and Murchison meteorite. Atomic percent of the α mode is plotted versus the atomic percent of the conventional oxygen concentration on hydrogen-free basis (because the alpha-mode cannot measure hydrogen). This plot shows geostandards containing <1 wt.% water including AGV-1, BCR-1, G-1, G-2, and DTS-1 all measured under Martian conditions, and samples containing water, as labeled, were measured under vacuum. The bulk oxygen measurement by the α -mode has a relative 1σ error of one relative percent calculated from the analyses of multiple geostandards. The errors for conventional values are average errors for total oxygen calculated by propagating the reported errors for each oxide and converting it into the total oxygen error.

Table 3.1. *Foley et al. (2003b) X-ray mode results ($\pm 1\sigma$)*

Soils	Na ₂ O*	MgO	Al ₂ O ₃	SiO ₂	P ₂ O ₅	SO ₃	Cl	K ₂ O	CaO	TiO ₂	Cr ₂ O ₃	MnO	Fe ₂ O ₃
A-2 Deploy	3.2 ± 0.7	8.7 ± 2.0	10.4 ± 0.8	40.9 ± 0.8	0.9 ± 0.2	6.0 ± 1.2	0.7 ± 0.2	0.50 ± 0.04	6.1 ± 0.4	0.7 ± 0.2	0.3 ± 0.1	0.5 ± 0.1	21.2 ± 0.9
A-4 Next to Yogi	3.2 ± 0.7	8.0 ± 1.9	10.6 ± 0.8	41.0 ± 0.9	1.2 ± 0.2	6.9 ± 1.4	0.8 ± 0.2	0.50 ± 0.07	5.6 ± 0.4	1.0 ± 0.3	0.4 ± 0.1	0.4 ± 0.1	20.4 ± 0.8
A-5 Dark Next to Yogi	3.2 ± 0.6	7.1 ± 1.7	10.4 ± 0.8	40.7 ± 0.9	0.6 ± 0.1	5.7 ± 1.1	0.8 ± 0.2	0.50 ± 0.05	6.1 ± 0.4	0.6 ± 0.1	0.5 ± 0.1	0.20 ± 0.06	23.7 ± 1.0
A-9 Disturbed Soil by Scooby	2.6 ± 2.4	6.4 ± 1.6	10.2 ± 0.9	41.7 ± 0.9	0.8 ± 0.2	6.6 ± 1.4	1.2 ± 0.3	0.70 ± 0.09	6.4 ± 0.5	0.8 ± 0.2	0.2 ± 0.1	0.1 ± 0.1	22.2 ± 1.0
A-10 Lamb	1.8 ± 0.7	7.5 ± 1.7	9.8 ± 0.7	41.3 ± 0.9	0.6 ± 0.1	6.4 ± 1.3	0.8 ± 0.2	0.40 ± 0.04	6.0 ± 0.4	0.8 ± 0.2	0.3 ± 0.1	0.4 ± 0.1	24.0 ± 1.0
A-15 Mermaid	2.7 ± 0.8	6.7 ± 1.6	9.9 ± 0.8	43.2 ± 1.0	0.6 ± 0.1	5.2 ± 1.1	0.8 ± 0.2	0.70 ± 0.07	5.5 ± 0.4	0.8 ± 0.2	0.3 ± 0.1	0.3 ± 0.1	23.2 ± 1.0
Indurated soil													
A-8 Scooby Doo	3.1 ± 0.8	6.4 ± 1.5	10.5 ± 0.8	45.0 ± 1.0	0.5 ± 0.1	5.5 ± 1.1	0.9 ± 0.2	0.80 ± 0.06	7.0 ± 0.5	0.7 ± 0.2	0.1 ± 0.1	0.3 ± 0.1	19.1 ± 0.8
Rocks													
A-3 Barnacle	3.2 ± 0.5	2.1 ± 0.5	12.8 ± 0.9	54.1 ± 1.1	0.7 ± 0.1	2.0 ± 0.4	0.5 ± 0.1	1.1 ± 0.07	5.7 ± 0.4	0.6 ± 0.1	0.10 ± 0.04	0.3 ± 0.1	16.7 ± 0.7
A-7 Yogi	4.9 ± 0.8	5.2 ± 1.2	11.2 ± 0.9	47.4 ± 1.1	0.5 ± 0.1	4.4 ± 0.9	0.8 ± 0.2	0.70 ± 0.06	6.6 ± 0.5	0.7 ± 0.2	0.10 ± 0.1	0.4 ± 0.1	17.1 ± 0.7
A-16 Wedge	4.9 ± 0.9	4.1 ± 1.0	11.5 ± 0.8	48.0 ± 1.1	0.6 ± 0.1	3.0 ± 0.6	0.6 ± 0.1	0.80 ± 0.07	6.9 ± 0.5	0.7 ± 0.2	0.00 ± 0.04	0.3 ± 0.1	18.6 ± 0.8
A-17 Shark	3.6 ± 0.8	3.9 ± 1.0	10.7 ± 0.8	53.9 ± 1.2	0.5 ± 0.1	1.7 ± 0.4	0.5 ± 0.1	0.80 ± 0.09	7.7 ± 0.6	0.5 ± 0.2	0.10 ± 0.1	0.4 ± 0.1	15.8 ± 0.7
A-18 Half Dome	4.0 ± 0.7	3.4 ± 0.8	12.3 ± 0.9	50.0 ± 1.1	0.6 ± 0.1	3.0 ± 0.6	0.7 ± 0.2	1.0 ± 0.08	6.0 ± 0.5	0.7 ± 0.2	0.10 ± 0.1	0.4 ± 0.1	17.9 ± 0.7

Key: All X-ray Na₂O* values are calculated from α-proton mode Na₂O/SiO₂ values except for A-9, disturbed soil by Scooby Doo, which is derived from X-ray. Errors are the statistical and laboratory combined error, at the 1σ level. Sulfur is assumed to have +6 oxidation state because of its high abundance, and because of the Viking soil analyses which support this oxidation state (Toulmin *et al.*, 1977). Fe is assumed to have +3 oxidation state in the soils and +2 oxidation state in the rocks based on IMP (Imager for Mars Pathfinder) red/blue ratios which indicate more oxidized iron in the soils than the rocks (McSween *et al.*, 1999).

Table 3.2. Brückner et al. (2003) X-ray mode results

Soils	Na ₂ O	MgO	Al ₂ O ₃	SiO ₂	P ₂ O ₅	SO ₃	Cl	K ₂ O	CaO	TiO ₂	Cr ₂ O ₃	MnO	Fe ₂ O ₃
A-2 Deploy							Not reported						
A-4 Next to Yogi	1.00	9.95	8.22	42.5	1.89	7.58	0.57	0.60	6.09	1.08	0.2	0.76	19.6
A-5 Dark Next to Yogi	1.05	9.20	8.71	41.0	1.55	6.38	0.55	0.51	6.63	0.75	0.4	0.34	23.0
A-9 Disturbed Soil by Scooby							Not reported						
A-10 Lamb	1.32	8.16	7.41	41.8	0.95	7.09	0.53	0.45	6.86	1.02	0.3	0.51	23.6
A-15 Mermaid	0.97	7.46	7.59	44.0	1.01	6.09	0.54	0.87	6.56	1.20	0.3	0.46	23.0
Indurated soil													
A-8 Scooby Doo	1.56	7.24	9.09	45.6	0.61	6.18	0.55	0.78	8.07	1.09	—	0.52	18.7
Rocks													
A-3 Barnacle	1.69	3.20	11.02	53.8	1.42	2.77	0.41	1.29	6.03	0.92	0.1	—	16.2
A-7 Yogi	1.19	6.71	9.68	49.7	0.99	4.89	0.50	0.87	7.35	0.91	—	0.47	16.7
A-16 Wedge	2.30	4.58	10.24	48.6	1.00	3.29	0.41	0.96	8.14	0.95	—	0.65	18.9
A-17 Shark	2.03	3.50	10.03	55.2	0.98	1.88	0.38	1.14	8.80	0.65	0.05	0.49	14.8
A-18 Half Dome	1.78	3.91	10.94	51.8	0.97	3.11	0.37	1.10	6.62	0.82	—	0.52	18.1
Ave. error (rel.%)	40	10	7	10	20	20	15	10	10	20	50	25	5

presence is inferred by excess oxygen above that which can be bound with all other detected elements in their highest oxidation states. Thus, one may infer the water content in samples for which the oxidation states of sample elements are known to within a resulting error of ~ 1 wt.% water.

Also important for understanding the volatile content of the Martian soils and rocks is measurement of sample carbon. Carbon is detectable by the α mode only if present above 0.3–0.8 wt.% (Foley *et al.*, 2003a,b and Brückner *et al.*, 2003, respectively). Under Martian conditions carbon, if present, will appear in channels 15–32 as a rectangle-like feature on top of the rest of the spectrum. Since no sample carbon was detected, it is assumed to be <0.3 –0.8 wt.% and therefore the accuracy of sample carbon measurement was not further quantified.

3.2.3 Application of calibration to Pathfinder data

In order to apply the fore mentioned calibration routines to the Pathfinder dataset, one difference between the laboratory and flight instruments (which are otherwise identical) had to be addressed. This difference is the presence of a thin alumina/VYNS (~ 1200 Å alumina/organic polymer) film held by a stainless steel grid in the laboratory instruments between the sources and the sample. This protective grid is used in the laboratory as a barrier to protect the instrument chamber and samples from curium contamination. The steel grid is thicker than the range of the α particles and it therefore prevents some α particles from reaching the sample, but causes an insignificant absorption of the 14–18 KeV X-rays from the curium sources. Therefore, relatively fewer α particles will scatter or undergo (α , p) in the presence of the protective grid. Absorption by the grid causes the α and proton spectral signals for laboratory standards to be relatively lower than those in the Pathfinder samples. Because all the standard intensities are reduced by the same relative amount, this does not affect the calculation of the absolute sample abundances for the α and proton modes. The X-ray mode Pathfinder abundances, however, are affected by the change in the proportion of α particles and X-rays striking the sample. Characteristic X-rays from the sample are excited by both α particles and X-rays from the curium sources, as previously discussed. With a decreased α beam, there is less characteristic X-ray production from the sample. The proportion of generation of sample X-rays by α particles and X-rays has been determined experimentally with the laboratory APXS by analyzing pure oxide targets with and without a 28 μm mylar foil over the curium sources. This mylar absorbs all of the α particles, and thus prevents them from interacting with the sample. By comparing the laboratory X-ray yield with and without the mylar foil, the ratios of the X-ray produced by α particles and the X-rays from the ^{244}Cm source were measured for many elements and inferred for others (Figure 3.7). The standard library utilized by Foley *et al.* (2003a), which contains the intensities corresponding to a certain atomic percent of each element, and the calibration curves of Brückner *et al.* (2003) were corrected to compensate for this instrument difference. The fraction of characteristic

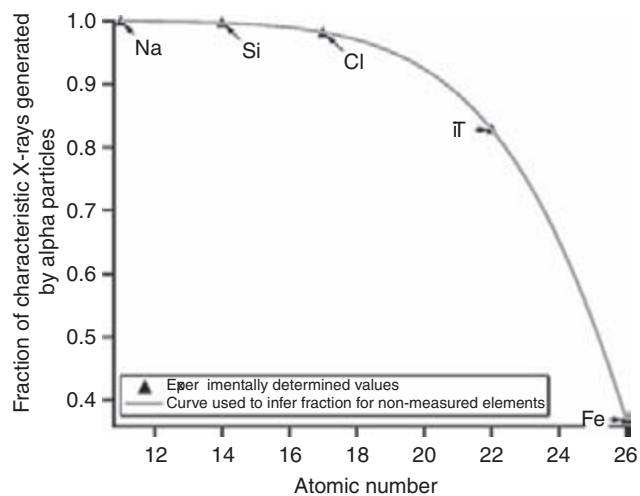


Figure 3.7. Fraction of sample characteristic X-rays generated by alphas for different atomic numbers. The plot shows that elements lower than manganese in atomic number have more of their characteristic X-rays generated by α particles, while elements higher than manganese in atomic number have more generated by X-rays. The curve used to infer the fraction for non-measured elements is an exponential fit to the data points.

X-rays generated by α bombardment was used to increase the reference library values and the calibration curve results by an appropriate amount. Since the steel grid reduces the intensity of α particles by 15% (its surface area) it reduces the amount of X-ray generation by α particles by 15%. The new library values and the calibration curve results are therefore increased by 15% of the fraction of characteristic X-rays produced by α particles for the Pathfinder sample analyses.

The initial Pathfinder data analyses (Rieder *et al.*, 1997b) were performed only with the X-ray mode of the instrument uncorrected for the absence of the protective grid on the flight instrument. This is the reason for the differences in the abundances computed by the earlier study by Rieder *et al.* (1997b) and those completed later by Brückner *et al.* (2003) and Foley *et al.* (2003b). All of the abundances in the X-ray mode are different from those initially derived. In particular, the differences are large enough that the inferred Pathfinder SFR composition was re-classified as basalt-andesitic to tholeiitic andesite (with a silica content of $\sim 57\%$) rather than purely andesitic (with a silica content of ~ 62 wt.%), which has significant implications for the understanding of the petrology of the Pathfinder rocks, as discussed in the following sections.

3.3 CHEMICAL RESULTS

Using the newly tested X-ray library modified for instrumental differences, the data from five rocks and seven soils at the Pathfinder site were re-analyzed with results given in Tables 3.1 (Foley *et al.*, 2003b) and 3.2 (Brückner *et al.*, 2003). The most prominent differences between these results and those of Rieder *et al.* (1997b) are lower abundances of

Table 3.3. Na_2O abundances for X-ray and alpha-proton modes

Soils	Na_2O X-ray abundances (wt.%) $\pm 1\sigma$	Na_2O α -proton abundances (wt.%) $\pm 1\sigma$
A-2 Deploy	5.5 ± 0.4	3.2 ± 0.7
A-4 Next to Yogi	4.8 ± 1.0	3.2 ± 0.7
A-5 Dark Next to Yogi	3.2 ± 0.9	3.2 ± 0.6
A-9 Disturbed Soil by Scooby	2.6 ± 2.4	2.6 ± 2.4
A-10 Lamb	2.0 ± 0.6	1.8 ± 0.7
A-15 Mermaid	1.8 ± 1.4	2.7 ± 0.8
Indurated soil		
A-8 Scooby Doo	2.6 ± 0.8	3.1 ± 0.8
Rocks		
A-3 Barnacle Bill	2.8 ± 1.6	3.2 ± 0.5
A-7 Yogi	2.2 ± 2.5	4.9 ± 0.8
A-16 Wedge	3.8 ± 1.0	4.9 ± 0.9
A-17 Shark	3.9 ± 1.9	3.6 ± 0.8
A-18 Half Dome	4.0 ± 0.8	4.0 ± 0.7

Source: Foley *et al.* (2003b).

silica and higher abundances of iron as well as new measurements of P_2O_5 , Cr_2O_3 , and MnO . The reasons for these differences between the preliminary Rieder *et al.* (1997a) results and these final X-ray results were described in Section 3.2.

All X-ray abundances in Table 3.1 from Foley *et al.* (2003b) were independently measured by the X-ray mode with the exception of Na_2O , which was measured by the α -proton mode. The α -proton mode values are more accurate than X-ray values for Na_2O because of larger counting statistical uncertainties and background uncertainties due to a light leak in the x-ray mode (as discussed further by Brückner *et al.*, 2003). Even with the higher statistical error, the X-ray results for Na_2O from Foley *et al.* (2003b) are within 1σ of the α -proton results given here (Table 3.3).

All of the chemical results from Brückner *et al.* (2003) (Table 3.2) were derived from the X-ray mode alone. A comparison of the X-ray results from Foley *et al.* (2003b) and Brückner *et al.* (2003) is shown in Figure 3.8. They agree within 1σ for MgO , SiO_2 , SO_3 , Cl , K_2O , some CaO , TiO_2 , Cr_2O_3 , and Fe_2O_3 . The Brückner *et al.* (2003) results for Na_2O are significantly lower than the X-ray or α -proton mode X-ray values from Foley *et al.* (2003b). This may be due to the difficulty in subtracting the background from the sodium region for the X-ray sodium region, and hence the higher possibility of systematic errors in the X-ray Na_2O values. The Brückner *et al.* (2003) abundances for P_2O_5 and MnO are both systematically higher than the abundances of Foley *et al.* (2003b) by ~ 1 – 2σ . These differences may be due to uncertainties in the calibration curves for these elements, which were uncorrected for matrix

effects, as discussed by Brückner *et al.* (2003). Specifically, these abundance differences may be due to differences in the handling of the asymmetrical X-ray peak contributions from the neighboring sulfur and iron. The Brückner *et al.* (2003) aluminum values are all systematically lower by approximately 2σ , while the values of calcium are higher for all Pathfinder samples than the X-ray results of Foley *et al.* (2003b). These differences are due to systematic differences in the calibration routines near the accuracy level of the measurements. All differences between the two calibration routines are within 1 – 2σ and these differences do not alter the bulk chemistry of the average soils or of the SFR (discussed later) enough to change the interpretations of their petrology.

The α -proton abundances for C, O, Na, Si, (K, Ca as a group), and Fe for the Martian rocks and soils have been obtained independent of the X-ray mode. Elements measured by the α -proton and X-ray modes are in agreement with one another, within error, verifying the accuracy of the measured abundances (Foley *et al.*, 2003b). The additional contribution of the α -proton mode is the determination of the concentrations of sample carbon and oxygen, which the X-ray mode cannot measure. Sample carbon was not detected in any of the Pathfinder APXS analyses, implying that the carbon concentration is below 0.3–0.8 wt.% (Foley *et al.*, 2003b and Brückner *et al.*, 2003, respectively), the approximate detection limits for carbon, in both the rocks and soils at the Pathfinder site. The bulk oxygen determination from the α mode has yielded some excess oxygen in some of the rocks, above that which may be accounted for by stoichiometric relationships with measured major elements. It is probable that this excess oxygen is bound to hydrogen, which is the only major rock-forming element not measured with the APXS. The absolute amount of excess oxygen is dependent on the choice of stoichiometry for both iron and sulfur, the only measured major elements which may have varying oxidation states which are not well-constrained. Using the abundances measured from the α mode, the amount of excess oxygen detected can be converted to an amount of mineral-bound water possibly present in the samples with different assumptions of the oxidation states of iron and sulfur. Table 3.4 lists the variation in inferred water content with assumptions of oxidation state. The probable range of water content for the soils, based on these analyses and visible and near-infrared spectra (McSween *et al.*, 1999; Bell *et al.*, 2000; Bridges *et al.*, 2001), is between -1.4 ± 1.7 and 1.0 ± 1.6 wt.%; none of which is significantly different from zero. The probable range of water content for the rocks based on the same assumptions is between 0.1 ± 1.3 and 4.3 ± 1.3 wt.%. The bulk α -proton abundances and the variation in the potential water content with oxidation state are discussed further by Foley *et al.* (2003b).

Since the X-ray mode is the most independent of the three modes, its elemental abundances are used with the sodium content from the α -proton joint mode to yield bulk sample abundances on a dry basis from the Foley *et al.* (2003b) analyses which may then be compared with other chemical analyses of the Martian surface to determine the petrology of the Pathfinder rocks and soils. Use of the Brückner *et al.* (2003) X-ray values yields comparable interpretations.

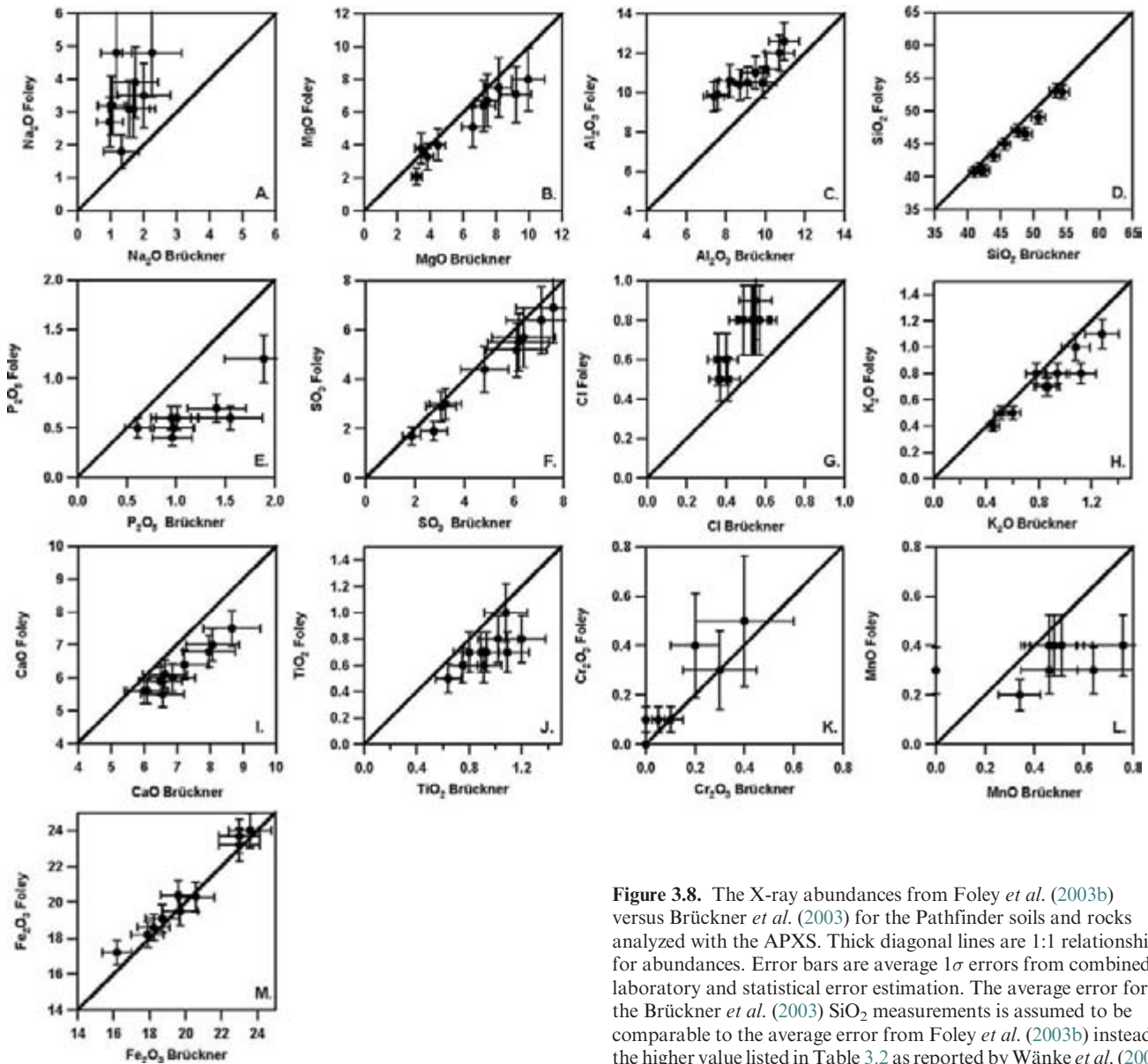


Figure 3.8. The X-ray abundances from Foley *et al.* (2003b) versus Brückner *et al.* (2003) for the Pathfinder soils and rocks analyzed with the APXS. Thick diagonal lines are 1:1 relationship for abundances. Error bars are average 1σ errors from combined laboratory and statistical error estimation. The average error for the Brückner *et al.* (2003) SiO₂ measurements is assumed to be comparable to the average error from Foley *et al.* (2003b) instead of the higher value listed in Table 3.2 as reported by Wänke *et al.* (2001).

3.4 PETROLOGY OF THE PATHFINDER SOILS AND ROCKS

3.4.1 Soils

The Pathfinder soils appear to be products of chemical alteration of original mafic material by fluids or gases rich in sulfur and chlorine. The lack of detection of carbon implies the absence of carbonate. If carbonates were once present in surface materials, they may have been dissolved by acidic weathering conditions during more recent epochs, as hypothesized by Wänke and Dreibus (1994) and Clark (1999). They have argued that carbonates should not be expected at the surface of Mars because of the high abundance of SO₃. Shergottites, the most abundant group of Martian meteorites, contain mantle-derived concentrations of ~200 ppm H₂O, ~100 ppm CO₂, and between 1200 and 5600 ppm SO₂. Terrestrial MORBs contain ~200 ppm H₂O

and similar concentrations of SO₂ and CO₂. On Mars, which is poorer in H₂O and CO₂ but similar or richer in SO₂, it is expected that SO₂ dominates the volcanic gases (as inferred from the meteorite volatile abundances summarized by Wänke and Dreibus, 1994). At least part of the SO₂ quickly transformed to SO₃ will together with water vapor produce sulfuric acid, which in turn will decompose carbonates and return CO₂ to the atmosphere. The sulfuric acid will also decompose olivine and form MgSO₄ and FeSO₄. Large deposits of sulfates have been observed by the Mars Exploration Rover (MER) missions *Spirit* (Gusev crater) and *Opportunity* (Meridiani Planum) at the equatorial regions of Mars (Gellert *et al.*, 2004; Rieder *et al.*, 2004).

Alteration of the Pathfinder soils is supported by the high FeO/MnO weight ratios of some soils and the high abundances of S and Cl in all soils. The average Pathfinder soil FeO/MnO weight ratio is 68 ± 15 , which overlaps the SNC values. Yet, some Pathfinder soils, like A-5, have FeO/MnO

Table 3.4. *Inferred Pathfinder water abundances $\pm 1\sigma$*

Soils	[H ₂ O wt.%] ^a	[H ₂ O wt.%] ^b	[H ₂ O wt.%] ^c
A-2	n.d.	1.6 \pm 1.7	-0.6 \pm 1.7*
A-4	n.d.	1.2 \pm 1.7	-1.0 \pm 1.7*
A-5	n.d.	-1.4 \pm 1.7*	-3.7 \pm 1.7*
A-10	n.d.	2.5 \pm 1.7	0.3 \pm 1.7*
A-15	n.d.	1.0 \pm 1.6*	-1.2 \pm 1.6*
Rocks			
A-3	2.0 \pm 1.3	0.3 \pm 1.3*	-1.9 \pm 1.3
A-7	7.1 \pm 1.4	3.4 \pm 1.4*	1.3 \pm 1.4*
A-8[†]	—	2.9 \pm 1.6	1.0 \pm 1.6*
A-16	4.2 \pm 1.3	1.5 \pm 1.5*	-0.8 \pm 1.4
A-17	5.7 \pm 1.3	4.3 \pm 1.3*	2.2 \pm 1.3
A-18	2.7 \pm 1.3	0.1 \pm 1.3*	-2.0 \pm 1.3

Key: The different columns are for varying assumed oxidation states of sulfur and iron.

^a S²⁻ and Fe²⁺,

^b S⁶⁺ and Fe²⁺,

^c S⁶⁺ and Fe³⁺.

Errors are calculated from statistical error and laboratory accuracy. n.d. means not determined; [†] indurated soil;

* probable oxidation state based on IMP data (McSween *et al.*, 1999; Bell *et al.*, 2000; Bridges and Crisp, 2000).

Some samples have * labels on both columns (3) and (4) because red/blue ratios from different IMP analyses yield contradictory results and may therefore be less reliable.

values as high as 135 ± 30 (obtained by the Chicago calibration, only). The Mainz group found at Meridiani Planum several soil samples with high FeO/MnO ratios of around 100 (Rieder *et al.*, 2004) that also contained high contents of the mineral hematite as determined by the Mössbauer Spectrometer (Klingelhöfer *et al.*, 2004). This FeO/MnO deviation for the Pathfinder soils may indicate that some of the Pathfinder soil is not derived by physical weathering of igneous rocks. This is further supported by the prevalence of correlated MgO, SO₃, and Cl, indicative of the presence of salts that may have resulted from weathering. Some ideas for the formation of Martian soil include chemical weathering of basaltic starting materials in a warmer and wetter ancient (3–4 Ga) climate (Banin *et al.*, 1992; Gooding, 1992; Burns, 1993), sporadic weathering of basalt at high temperatures during shock events (Morris *et al.*, 1995), or thermal alteration of palagonitic tephra by heating during penetration or emplacement of hot lava (Bell *et al.*, 1993).

The Martian Pathfinder soil appears to consist of nanophase iron oxides, silicate mineraloids (amorphous materials), and salts (Banin *et al.*, 1997 and references therein). Bell *et al.* (2000) and Morris *et al.* (2000) claim that these materials match the chemistry, near-infrared to visible spectroscopy data and the magnetic experiment data (Madsen *et al.*, 1999; Hargraves *et al.*, 2000) most consistently. The Imager for Mars Pathfinder (IMP) visible and near-infrared

Pathfinder imager operated in the 400–1000 nm range and observed the Pathfinder soils and rocks (Bell *et al.*, 2000 and references therein). The soil IMP data are most consistent with palagonitic weathering of SNC-like basaltic glasses (Bell *et al.*, 2000; Morris *et al.*, 2000). Morris *et al.* (2000) further suggest that glassy protoliths on Mars may be produced by volcanic fire fountaining and/or impact processes (with later enrichment in S and Cl). Comparison with rates of lunar glass production supports this as a viable possible source for the Martian soils (Morris *et al.*, 2000).

As summarized by Banin (2005), the Martian soil appears to be a product of the slow chemical and physical alteration involving gaseous and aqueous species within the Martian atmosphere and/or hydrosphere with Martian rocks. The soil compositional results from the Viking, Pathfinder, *Spirit*, and *Opportunity* missions have all been utilized to infer possible widespread processes affecting the Martian surface which include acid-fog reactions of volcanic emissions with bedrock (Banin *et al.*, 1997; Tosca *et al.*, 2004), and/or precipitation of salts from the evaporation of shallow seas (Squyres *et al.*, 2004) or seeping-up acidic groundwater (Burns and Fisher, 1990).

Some of these soil formation hypotheses may be tested through analyses of how such processes will affect the soils' chemistry. For example, changes in abundances due to acid-fog reactions for Shergotty were calculated by Bell *et al.* (2000), using the experimental data of Banin *et al.* (1997). In particular, acid-fog reactions leach out Ti, Fe, Al, and Mg and add volatiles (such as sulfur and chlorine) contained in the original acid-fog. However, there is no measurable difference between the Viking 1 soils, Pathfinder soils, and Shergotty Mg/Si or Ti/Fe values. This indicates that if weathering and/or acid-fog reactions were widespread on the Martian surface, then the starting material must have been more mafic than Shergotty (a typical Martian basalt). In support of some chemical alteration process, the IMP soil spectral data (based primarily on iron absorptions) independent of the APXS chemical composition are similar to spectra of Hawaiian tephra that have been aqueously and thermally altered (Bell *et al.*, 2000).

An additional model, proposed by Brückner *et al.* (1999), of major soil formation purports the mechanical mixing of Martian meteorites, Pathfinder SFR, and volcanic emissions. The Martian soils show a considerable Mg concentration from which it was inferred, based on Viking data, that the crust of Mars is mafic (Clark, 1993). The Martian meteorites also have mafic to ultramafic composition (see Chapter 17). In contrast, the rocks at Ares Vallis represent highly fractionated crustal material, rich in Si and K, but low in Mg, which holds regardless of the nature of these rocks, that is, igneous or sedimentary. The compositional difference between soils and rocks cannot simply be explained by physical weathering of these rocks, even considering weathering and interaction with volcanic gases SO₂ and HCl (Wänke *et al.*, 2001). Addition of material richer in Mg and Fe, but poorer in K and Cr as observed by the Martian meteorites, seems unavoidable. Taking the almost identical soil composition at the three landing sites (Viking 1 and 2 and Pathfinder) as representative for the whole

surface soil of Mars, Brückner *et al.* (1999) have shown that all elements fit into a two-component mixing model with the Pathfinder rocks (high K, low Mg contents) as one component and the Martian meteorites as the other component. Hence, it was concluded that large geologic units of Pathfinder rock composition as well as of basaltic (Martian meteorites) composition must exist on Mars and these units cover about equal areas. This hypothesis is consistent with the orbital Thermal Emission Spectrometer (TES) data (Bandfield *et al.*, 2000). The admixture of a Pathfinder type rock component is needed to especially account for the high K content of the soils.

3.4.2 Rocks

The full suite of X-ray, proton-mode, and alpha-mode measurements (including water abundance modeling) need to be evaluated to interpret the petrology of the Pathfinder rocks. Although the α -proton mode and the X-ray mode yield similar chemical abundances for the Pathfinder rocks on a volatile-free basis, the potential presence and abundance of water in some of the rocks brings into question the hypothesis that they are unaltered igneous rocks. If the Pathfinder rocks are indeed igneous, then their bulk chemistry must first be examined on an anhydrous basis, as is done for terrestrial igneous rocks (Philpotts, 1990). However, the amount of water estimated to be present in the Pathfinder rocks A-7 and A-17 is higher than that of any unaltered terrestrial mafic igneous rocks or SNC meteorites. A-7 and A-17 may instead be metamorphic or sedimentary rocks. Therefore, various petrogeneses of the Pathfinder rocks will be considered.

The Pathfinder rocks analyzed with the APXS were also examined with the rover and lander cameras having spatial resolutions of 0.7–1 mm per pixel at closest range (McSween *et al.*, 1999). Used in tandem, the two instruments may be able to determine the lithology of the rocks examined. However, the rocks have ambiguous textures. Some have lineations and/or flutes while some are bumpy and/or pitted (McSween *et al.*, 1999). The texture of some rocks resembles volcanic vesicles. However, these vesicles may also have been formed by chemical etching of the rocks to produce a pitted texture. A chemical etching process was described by Campbell and Claridge (1987) for some rocks in Antarctica. Furthermore, vesicles can also be produced by honeycomb weathering which commonly forms in sandstones by a combination of chemical salt weathering reactions and physical weathering (Robinson and Williams, 1994). The rocks also have abundant ventifacts (facets and polished fragments from sandblasting), which obscure the original rock texture (Bridges *et al.*, 1999). Thus, the textural observations from the rover camera images do not unequivocally determine the lithology of the rocks.

The rock images and the chemical analyses both support various amounts of soil cover on the rocks. Since the soil contains significantly more sulfur, the sulfur content was utilized to infer the composition of the Pathfinder SFR using linear regressions (Figure 3.9) as done previously (Rieder *et al.*, 1997b; McSween *et al.*, 1999). This SFR

composition may then be utilized to infer the potential lithology of the Pathfinder rocks.

Images from the Pathfinder landing site suggest that some of the Pathfinder rocks may be conglomerates, resulting from and indicative of intense fluvial weathering of the Martian surface (Rover Team, 1997; Ward *et al.*, 1999). One possibility is that the Pathfinder rocks are graywackes as suggested by McSween *et al.* (1999). Pettijohn (1975, p. 212) describes graywackes as dark gray sandstones with a significant matrix content in which either lithic fragments (lithic graywackes) or feldspars (feldspathic graywackes) dominate. Graywackes form one-fifth to one-fourth of all (terrestrial) sandstones, and are most common in Paleozoic and earlier orogenic belts. They are absent in undeformed sequences deposited on stable cratonic or shield areas. They are generally marine, and in many terrestrial samples are believed to be turbidite sands (Pettijohn, 1975, p. 230). As a note of caution, however, sandstones are normally classified on the basis of their texture and modal (visual mineral abundance) mineralogical composition (Pettijohn, 1975, p. 210). With only the normative (inferred mineral abundance from bulk chemistry) mineralogical composition and a rover view of the surface of the rock, classification of the Pathfinder SFR as sedimentary is problematic.

It is unlikely that some chemical weathering process or conglomeration of sediments produced abundances which are so consistent with an evolved igneous rock from an SNC parent composition (as illustrated by the work of Minitti and Rutherford [2000] described later on within this section). Furthermore, some Pathfinder rocks (e.g., Barnacle Bill, A-3, which has the lowest inferred water content) have spectral properties which match those of fresh basalt to basalt-andesite (Smith *et al.*, 1997; Ward *et al.*, 1999), and others (e.g., Shark, A-17, which has the highest inferred water content) which match those of weathered basalt or basalt-andesite (Smith *et al.*, 1997). The water content of some Pathfinder rocks, which is the only chemical data bringing into question the rocks' igneous origin, may thus be due to weathering of original evolved igneous rocks (basalt-andesites) involving little to no major chemical changes except for the addition of water and oxidation of iron. Mössbauer detection of ferric oxyhydroxides (hematites) and oxyhydroxysulfates (jarosites) at the Meridiani Planum *Opportunity* landing site as well as its detection of weakly and pervasively altered olivine within the plains and Columbia Hills of the *Spirit* landing site, respectively, support such a hypothesis (Klingelhöfer *et al.*, 2004; Morris *et al.*, 2006).

An important caveat of these interpretations is that all of these comparisons of the Pathfinder SFR assume that its composition may be accurately deduced using the linear regressions. However, there are four observations bringing into question the determination of the SFR chemistry in this fashion. First, while many oxides show good linear regressions against sulfate, some major elements such as calcium and aluminum show considerable scatter among the rock data. This implies that there is some chemical heterogeneity among the rocks. Second, the plot of the sodium versus sulfate shows that the rock trend with sulfate is different

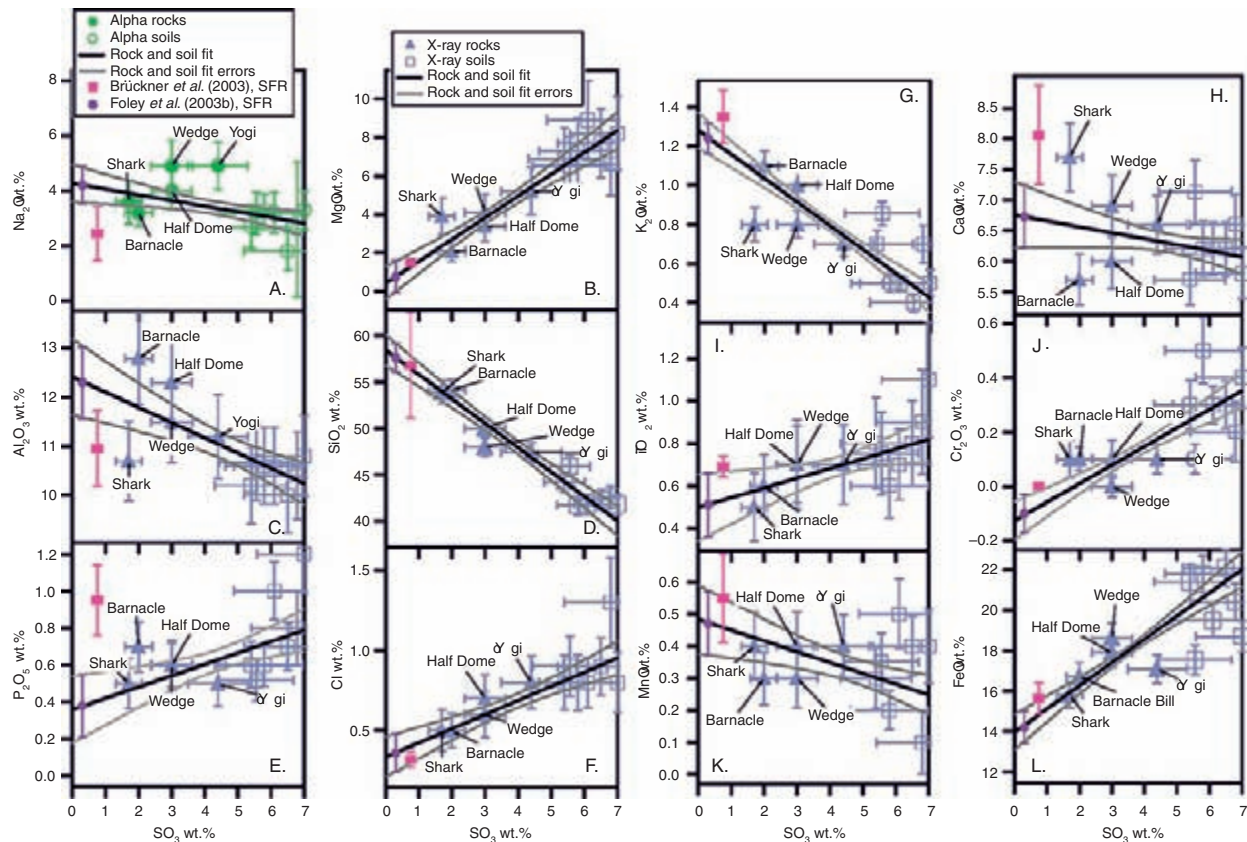


Figure 3.9. Linear regressions for oxide and element contents, calculated from data in Table 3.1, versus sulfate content for Pathfinder rocks and soils. All of the rocks have considerably less sulfur than the soils and linear trends to no sulfur are made showing that some soil-like component appears to cover the rocks by varying degrees. The linear regressions enable computation of the soil-free rock composition (SFR) and were computed using the technique of Williamson (1968) which takes into account the errors in both the ordinate and the abscissa for each oxide-sulfate pair. Some oxides, such as MgO and SiO₂, show good linear trends to low sulfate content in the rocks. However, other oxides such as Al₂O₃ and CaO, indicate some chemical heterogeneity among the rocks, and the FeO plot illustrates some chemical heterogeneity among the soils. (For a color version of this figure, please refer to the color plate section or to the e-Book version of this chapter.)

from the linear regression trend acquired with both rock and soil data. Specifically, the concentration of Na₂O in rocks increases with sulfate. This increase of Na₂O in the rocks with increasing sulfate may imply some sort of alteration trend (i.e., as the remnant of the evaporation of a fluid containing such salts rich in both sodium and sulfur). If so, then the SFR Na₂O abundance may be 2.4 wt.% attained from linear regression of the rocks alone. Third, there is chemical heterogeneity among the soils' iron content. While A-5, A-10, and A-15 are all high in iron content, A-2, A-4, and A-8 are substantially lower in iron content. This implies that the linear regression for the iron content of the rocks may be inappropriate. Fourth, the observation from the α -proton joint mode that the A-17 Pathfinder rock, which is also least covered with soil, contains 3.3 ± 1.3 wt.% water, assuming a 50/50 mixture of FeO and Fe₂O₃, is

inconsistent with the interpretation that all the rocks are completely unaltered igneous rocks. Hence, some linear regression trends as well as the water content of the rocks bring into question the validity of linear regression analyses to determine an SFR composition. There are, therefore, some significant differences from an ideal mix of purely unaltered igneous rocks with sulfate-rich more mafic soils. They are not, however, as evident as the overall patterns of good linear regressions for most oxides. Therefore, the deviations (from the linear fit and among the water contents) probably indicate some minor weathering reactions occurring on the rock surfaces that do not appear to drastically affect the derived composition of the Pathfinder SFR (as inferred from the quality of the linear fits, or the r^2 values, which are utilized to determine the error bars for the SFR composition in addition to the individual error measurements).

To derive the SFR composition, Brückner *et al.* (2003) fitted only the rock data and extrapolated the linear regression line to higher sulfur values. For all elements, except for Al, the soil data scatter around the rock regression line (Brückner *et al.*, 2003). This observation indicates that there is adhering soil on the surface of the rocks, however, not sufficient to cover the rock surfaces completely. A-17, the one rock with the lowest S content, comes close to the derived SFR composition. This implies that A-17 has the lowest soil coverage of all rocks. If A-17 had an alteration rind, then all other rocks would have the same type of rind, otherwise they would scatter much more. However, the existence of some type of alteration rind cannot be excluded. Keeping in mind the low penetration depth of alphas and